ROMA TRE
UNIVERSITÀ DEGLI STUDI

Department of science
Ph.D. in Material science, Nanotechnology and complex systems
XXXII DOCTORAL PROGRAM

Morphological alterations of a xerotolerant *Acinetobacter baumannii* under desiccation stress investigated by atomic force microscopy

Shadi Bashiri

Tutors
Prof.Giovanni Capellini
Prof.Paolo Visca

Morphological alterations of a xerotolerant *Acinetobacter baumannii* under desiccation stress investigated by atomic force microscopy

A thesis presented by
Shadi Bashiri
in partial fulfillment of the requirements for the degree of
Doctor of Philosophy
in Material science, Nanotechnology and Complex systems

Roma Tre University
Department of science

April 2020

"Some great thing which He designs to accomplish would have been too much without a little bitter in the cup."

Catharine McAuley

Abstract

Multidrug-resistant(MDR) *Acinetobacter baumannii* has recently emerged as a challenging problem and major cause of healthcare-associated infections (HAIs) because of its antimicrobial resistance and propensity to cause multi-facility outbreaks. The ability to develop antimicrobial resistance mechanisms and tolerance to desiccation are at the basis of the epidemiological success of *A. baumannii*. Therefore, desiccation tolerance is thought to contribute significantly to the persistence for an extended period of time and the spread of these bacteria in the healthcare environment. Despite the relevance of long-time desiccation tolerance of *A. baumannii*, the molecular and morphological basis of this phenomenon remains elusive.

Alternatively, desiccation resistance can vary between different strains of *A. baumannii* specimen. In this regard, it has recently been proven that the adapted strains to the hospital environment like *A. baumannii* ACICU cells can survive desiccation far better than the laboratory strains, however, most of the studies have been restricted to the laboratory strains such as *A. baumannii* ATCC19606. Considering the basic function of the bacterial cell membrane, as the outer layer of cell structure, that maintains the bacterial shape and protects the bacterial components against environmental stresses, it plays a significant role to tolerate desiccation. Thus, elucidating the structure and alterations of the cell envelope is important to unravel not only the complexities of cell morphology and maintenance of integrity but also how desiccation leads to cell damage and death.

Therefore, this Ph.D. thesis was aimed to study the consequences of desiccation-induced stresses on *A. baumannii* ACICU bacterial cell envelope under the simulated-hospital conditions. The following main questions were asked:

- What is the overall morphology of *A. baumannii* ACICU bacterial cells?
- Is there any relation between the cell morphology changes and cell desiccation survival?

- Which growth factors can significantly influence the shape of *A. baumannii* ACICU cells?
- What is the effect of different degrees of desiccation stresses and long-time storage on bacterial cell morphology?

To address these questions, the advanced Atomic Force Microscopy (AFM) technique was employed, which has produced a wealth of new opportunities in nanobiotechnology and has emerged as a key platform enabling the simultaneous morphological and mechanical characterization of biological systems. The evolution of the bacterial cell under different growth phases, distinct cultural growth conditions, and in various growth media as the effective parameters on cell morphology changes were assessed. Then different degrees of environmental stresses on the bacterial cell membranes were examined to discover the cell membrane changes and resistant mechanism of *A. baumannii* ACICU. Meanwhile, the desiccation survival of the cells before and after drying, during prolonged desiccation, and different storage conditions were examined. Furthermore, a new AFM approach (SFMSF) was implemented to explore the specified-bacterial cell over time.

The presented results in this thesis revealed growth phase-independent morphology for *A. baumannii* ACICU cells, displaying a coccus morphology. Conversely, the cell morphology was found to significantly depend on growth conditions concerning oxygen availability during cultivation. Taken together both results of morphology alterations and cell viability assessment demonstrated that the cells with minimal footprint and lower surface-to-volume ratio are more resistant to desiccation. The cell membrane pores and intracellular material leakage were observed as a sign of the cell death pathway. Additionally, deformation of the outer cell membrane, and reduction in cell volume was found to be dependent on the stresses caused by different drying methods. Moreover, it was observed that although the maintenance of the cells in water can help to retain their viability for long-time, osmotic stress causes cell membrane weaknesses.

Acknowledgments

First of all, I would like to give my special thanks to Professor Giovanni Capellini as my main supervisor for his outstanding support, his guidance, and for the time that he has spent for each stage of this project, which helped me to advance my thesis in the right direction. I would like also to express my gratitude to Professor Paolo Visca, for his fruitful discussions, expertise, and profound insight on this project.

I greatly acknowledge our group members, Prof.Monica De Seta, Dr.Luciana Di Gaspare, Dr.Luca Persichetti, and especially Michele Montanari for giving me all the necessary assistance in lab and university during these three years. I wish also to thank my coordinator Professor Fabio Bruni, who always was always helpful. I also appreciate the members of Professor Visca's team in the Department of Biology, Daniela Visaggio, and Massimiliano Lucidi for collaborating and sharing scientific experience.

Special thanks to my dear friends Heba, Parisa, and Nilofar who always wished the best for me and encouraged me to achieve my goals. My gratitude extends to my sibling Shahin, Shayan, and lovely Shima who are the most important persons of my life. I owe gratitude to my mother to educate me for nearly 30 years, all my achievements belong to you.

Finally, I would like to express my deepest thanks and gratitude to my beloved husband Mohammad, who supported me and stayed beside me to achieve this goal. I would never be able to achieve this goal without his support and encouragement; He is my partner in this work; therefore, I dedicate this success to my dear husband Mohammad.

List of abbreviation

3D	Three-Dimension
SPM	Scanning Probe microscopy
STM	Scanning Tunneling microscopy
TEM	Transmission Electron Microscopy
AFM	Atomic Force Microscopy
CM	Contact mode
NC	Non-Contact Mode
IC	Intermittent-Contact mode
TM	Tapping Mode
PFT	Peak Force Tapping mode
FD	Force Distance
FV	Force-Volume
HZ	Hertz

RMS	Root Mean Square
EC	European Clone
RH	Relative Humidity
ICU	Intensive Care Unit
MDR	Multi Drug-Resistant
LB	Luria Bertani
LA	Luria-bertani Agar plate
CAA	CasAmino acid
BSA	Bovine Serum Albumin
OD	Optical Density
CFU	Colony-Forming Units
PM	Periplasmic membrane
PG	Peptidoglycan
OM	outer membrane
LPS	Lipopolysaccharide
ECM	Extra-Cellular Materials
MDO	Membrane-Derived Oligosaccharides
VAP	Ventilator-Acquired Pneumonia
UTI	Urinary-Tract Infections
GIT	Gastro-Intestinal Tract
GIs	Genomic Islands
IS	Insertion Sequences

Contents

List of Tables

List of Figures

Chapter 1

Introduction

1.1 General background of microorganisms

Microorganisms are a group of several distinct classes of living beings that existed on Earth for billions of years. The organisms that constitute the microbial world, based on their similarity or the examination of their difference in the internal cellular organization, have been divided into two groups, namely prokaryotes and eukaryotes. The discriminative parameter is that eukaryotic cells have a distinct nucleus containing the cell's genetic material, the compartmentalization of the intracellular environment in intracellular organelles (e.g., nucleus, Golgi apparatus), while prokaryotic cells do not have a nucleus and have free-floating genetic material instead. All bacteria are included in the prokaryotic organism. However, changing the global environments, evolution, genetic exchanges, gave rise to fundamentally different cell wall formats in the bacteria to survive.

Gram staining classification

Historically, the bacteria are divided into two main groups based on their Gram-stain retention characteristics. In 1884, Christian Gram developed a cell-staining procedure for light microscopy to differentiate these two groups of bacteria, which was later named him. The entire perception of gram-positive and gram-negative bacteria based on their response to gram staining because of their chemical composition and structural the cell wall (Beveridge, 1999). In the Gram-staining procedure, after heat fixation on glass slide, the bacteria are

stained by solutions of carbol gentian violet and iodine (Lugol solution). Then ethanol is added until no further dye is eluted from the layer. Subsequently, the bacteria are re-stained with a diluted ethanolic fuchsine solution. The bacteria appearing dark blue to purple under the microscope are designated gram-positive, red one gram-negative. The difference in stainability between typical representatives of both groups depends on the structure of their cell walls. Fig. 1.1 represents the Gram-positive and Gram-negative response to staining along with electron microscopy image and schematic diagram of their cell wall structures (Dror, 1964). Most Gram-positive bacteria are bounded by a single cell membrane, generally featuring a relatively thick and resilient peptidoglycan layer in the cell walls, which do not allow the crystal-violet stain to be removed and, consequently, the Gram-positive bacteria appear purple under the microscope lenses (Fig 1.1a). In contrast, most gram-negative bacteria are surrounded by two different cell membranes separated by a thin peptidoglycan layer in the periplasmic compartment existing between the inner and outer membranes (Fig. 1 b) (Gupta, 1998; Sutcliffe, 2010). This thin layer does not retain the stain. Therefore, the decolorizing alcohol step of Gram staining washes the primary stain (crystal violet) from the cells afterward, the secondary stain (carbol fuchsin or safranin) colors the bacteria pink. Despite the vast majority of bacteria adhere to the color differentiation of the Gram stain, some bacteria do not obey this classification; these are called gram-variable bacteria, which cannot be easily differentiated by staining (Beveridge, 2001).Indeed, the staining response of gram-variable bacteria are also due to their cell wall composition and structure. Accordingly, advances in identifying gram-negative cell wall components by using a modern molecular technique well describe the specific gram-negative and gram variable cell walls. Gram-staining is widely used in clinics and microbiology laboratory to distinguish between monoderms (having one membrane, Gram-positive) and diderms (two membranes, Gram-negative); and confirmed by the molecular and microscopy techniques for enabling a thorough investigation of the cell structure, as we can see in Fig 1.1 c-f.

Gram-negative cell wall structure

The gram-negative cell wall is a remarkable structure, which protects the contents of the cell from harsh environments. On same cases of gram-negative bacteria, the cell wall is strong enough to withstand turgor pressure, tough enough to endure extreme temperatures and pHs and sufficiently elastic to expand several times their normal surface Area (Koch and Woeste, 1992).

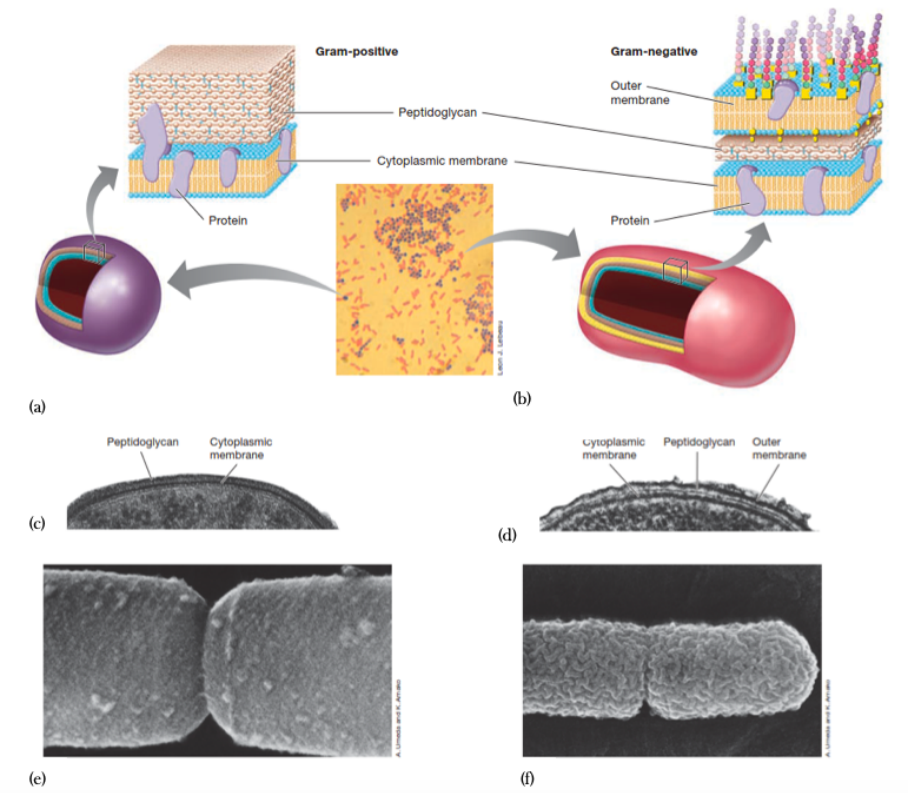

Figure 1.1: Cell wall of bacteria. (a,b) Schematic diagram of Gram-positive and Gram-negative cell wall. (c,d) and (e, f) showing transmission electron microscopy images (TEM) and scanning electron microscopy of a gram-positive and gram-negative bacterium, respectively. (Image adapted from Madigan et al., 2015)

As it is shown in Fig. 1.2, gram-negative bacteria have an outer membrane (OM) situated above a thin peptidoglycan layer. Sandwiched between the outer membrane and the plasma membrane, a concentrated gel-like matrix, in the periplasm, defines the periplasmic space, which contains the peptidoglycan (PG) layer (Beveridge and Graham, 1991). Since the periplasm is located above the plasma membrane (cytoplasm membrane), it is not part of the protoplast

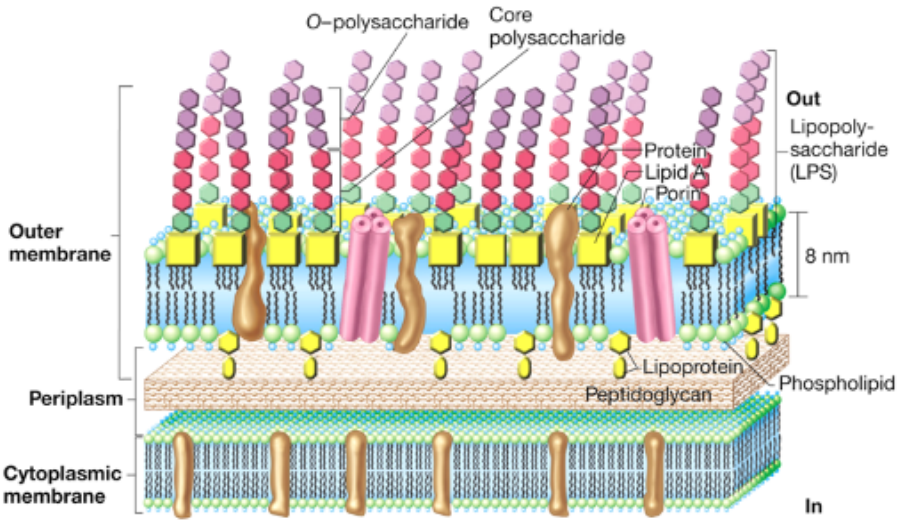

Figure 1.2: The gram-negative cell wall

and is not part of the "outer world" either since it is separated from the external environment by the outer membrane. Together with the plasma membrane and the cell wall containing the outer membrane, a peptidoglycan layer, and periplasm constitute the gram-negative envelope (Beveridge, 2001; Beveridge and Graham, 1991).

With the aid of electron micrographs, three or four electron-dense regions in the gram-negative cell envelope are shown in Fig. 1.3. Moreover, sometimes the outermost region of gram-negative cell walls can be presumably formed by the S-layer as a fourth layer (Fig. 1.3 b). The following parts describe the structure and composition of gram-negative cell walls in detail.

Outer membrane The cell surface of Gram-negative bacteria plays a myriad of roles in the physiology of these organisms, including transport of molecules in and out of the cell, interaction with and sensing of the extracellular environment, and protected from external stresses (Silhavy et al., 2010). As shown in Fig. 1.2, the bacterial cell surfaces are composed primarily of lipids, lipopolysaccharide, carbohydrates, and proteins, the diversity in the molecular composition and arrangement of these structures has vast implications for vir-

ulence in pathogenic bacteria.

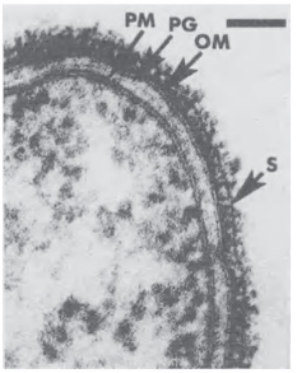

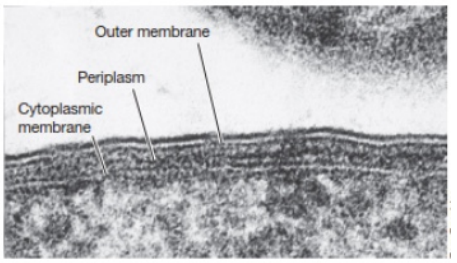

Figure 1.3: (a): Transmission electron micrograph of gram-negative cytoplasmic membrane and wall (Medigan et al., 2015) and (b): Electron micrograph of the gram-negative cell envelope (Beveridge, 1999). A gram-negative cell wall structure PM: Periplasmic membrane; PG: Peptidoglycan; OM: outer membrane; S: S-layer

Lipopolysaccharide Lipopolysaccharide (LPS) is the first barrier of many gram-negative bacteria and the major component of the outer leaflet of the outer membrane (OM). LPS exhibits a complex structure encompassing three domains; a highly conserved lipid-A embedded within the membrane is attached to a core oligosaccharide, which linked to a heterogeneous O-antigen side chain (Raetz and Whitfield, 2002). As seen in Fig. 1.3. (b), the outer

membrane comprises phospholipids, proteins, preferably contain polysaccharides, and linked polysaccharides to complex form (LPS). Besides the importance of LPS on rendering strength to the gram-negative cell, the biological activity of LPS as an immune molecule result in toxicity to the animals. The toxicity of gram-negative cells is associated with the LPS layer, in particular, Lipid A.

Periplasm The periplasm is a gel-like matrix because of the high concentration of proteins, which is located in a space between the cytoplasmic membrane and the outer membrane. The periplasm contains the peptidoglycan layer and many different classes of proteins depending on the organism. The proteins which function in transport are called periplasmic binding proteins.

Peptidoglycan The peptidoglycan is an electron-dense, rigid structure with varying thickness, as shown in Fig. 1.1 (c, d) and 1.3, The peptidoglycan (murein) is a polymer consisting of sugars and amino acids that forms a mesh-like layer outside the plasma. According to the most accepted model, the basic structure of peptidoglycan consists of glycan strands arranged parallel to the cell surface, which is cross-linked by peptide bridges and thus form a stable net-like layer. Gram-negative cell walls mainly contain only one such layer (thickness 2-2.5 nm), while the gram-positive ones possess several of them arranged in layers that are connected to each other (thickness 30-40 nm). In the case of gram-negative bacteria, the thickness of the layer corresponds to the height of one turn of the polysaccharide helix, which is necessary for complete cross-linking.

Membrane Structure The cytoplasmic membrane surrounds the cytoplasm. If the cytoplasmic membrane is damaged, the integrity of the cell is destroyed, the cytoplasm leaks into the environment, and the cell dies. The cytoplasmic membrane is structurally weak and confers little protection from osmotic lysis, but it is an ideal structure for the major function in the cell. The cytoplasmic membrane is only 8 - 10 nanometers wide, but is still visible in the transmission electron microscope (refer to Fig. 1.3 a). The outer surface of the cytoplasmic membrane faces the environment, and in gram-negative bacteria interact with a variety of proteins that bind substrates or process larger molecules for transport into the cell. The inner surface of the cytoplasmic membrane is in contact with the cytoplasm and interacts with proteins and other molecules in this milieu. Bacterial proteins are mainly produced in the cytoplasm, where they

have transport to the respective destination sites cytoplasm, cytoplasmic membrane, periplasmic space, outer cell membrane, or secretion in Gram-negative bacteria; (cytoplasm, cytoplasmic membrane, cell wall inclusive periplasm-like space, or secretion in Gram-positive ones).

The general structure of the cytoplasmic membrane is a phospholipid bilayer. Phospholipids are composed of both hydrophobic (fatty acid) and hydrophilic (glycerol–phosphate) components. The cytoplasm is a solution of salts, sugars, amino acids, nucleotides, and many other substances. The hydrophobic portion of the cytoplasmic membrane is a tight barrier to the diffusion of these substances. Although some small hydrophobic molecules pass the cytoplasmic membrane by diffusion, polar and charged molecules do not diffuse but instead must be transported.

Cell shape classification

Bacterial species also can be classified based on their shape or morphology. The Microscopy examination by revealing the cell shape and size can be a useful technique to identify different bacteria (Medigan et al., 2015). Diversity in bacterial cell morphology is the consequence of adaptive pressures optimizing bacterial fitness. Although cell shape rarely has phylogenetic relevance, it affects many biological aspects of bacteria, including nutrient acquisition, motility, dispersion, stress resistance, and interactions with other organisms. The basic morphology of the bacterial cells is classified in coccus for their spherical shape, bacilli for their rod-shaped and spirochetes for their spiral shapes. There are some other cell shapes that immediately recognizable by their unusual cell shapes such as spirochetes, appendages, bacteria, or filamentous bacteria. It became increasingly clear that the peptidoglycan as one of the essential components of the cell wall plays a significant role in maintaining the shape, mechanical stabilization of the form of the cell, and protecting against the osmotic pressure (Cabeen and Wagner, 2005). Furthermore, the availability of nutrient or growth state may cause morphological changes, indicating that bacteria can manipulate morphology to their advantage. The general classification systems of bacterial were addressed until now. As the subject of this thesis is" the morphological investigation of desiccation tolerance of *A. baumannii* ", which is gram- negative and diderm bacteria, we described in detail the gram-negative bacterial cell structure and composition. The remaining part of this chapter will outline the importance of pathogenesis and virulence of *A. baumannii* as a Multi-Drug-Resistant (MDR) bacterium, which leads to the nosocomial infections by its peculiar capability of desiccation tolerance.

Accordingly, the targets of desiccation damage into the bacterial cell and their resistant mechanisms will be addressed.

1.2 General background of *Acinetobacter baumannii*

Acinetobacter spp was initially described by Beijerinck in 1911 and assigned the name Micrococcus calcoaceticus (Howard et al., 2012). The organism shared characteristics with Moraxella spp and was classified in the same group for some time; however, significant differences were identified and led to the designation of this organism as Achromobacter spp (Peleg et al., 2008). Hence, in 1954 the name Acinetobacter was first proposed by Brisou and Prevot (1954) from the Greek word "Akinetos" that literally translates to "non-motile" or unable to move (Almasaudi, 2015). This name was suggested in order to separate the motile species within the genus Achromobacter and grouping the non-motile species under the new genus, Acinetobacter. Nevertheless, more recent studies have shown that some strains belong to the Acinetobacter genus can display surface, or twitching, motility (Antunes et al., 2011).

Natural habitat

The natural habitat of Acinetobacter spp has been investigated extensively in the past few years. They can be isolated after enrichment from the soil, water, vegetables, animals, and human body lice (reviewed by Peleg et al., 2008; Giamarellou et al., 2008; La Scola and Raoult, 2004). *A. baumannii*, in particular, have been isolated from animal specimens (Francey et al., 2000; Vaneechoutte et al., 2000) and body lice specimens obtained from homeless persons (La Scola and Raoult, 2004). The presence of Acinetobacter spp in these different habitats led to the consideration of this genus as a ubiquitous organism in nature (Fournier and Richet, 2006).

In general, the results indicate the wide distribution of *A. baumannii* may provide insight into its potential natural habitat as well as providing a route for the dissemination into the hospital setting. The hospital environment possesses the moist conditions and temperature allowing for the development *A. baumannii*, *A. pittii* (formerly known as geno.sp.3), and *A. nosocomialis* (formerly known as geno.sp. 13TU) to disseminate (Nemec et al., 2011; Peleg et al., 2008; Dijkshoorn et al., 2007). Despite that, among all *Acinetobacter baumannii* complex species, which cause nosocomial infections, only *A. baumannii* displays a high capability to resist desiccation stresses; and can persist on inanimate surfaces for prolonged durations up to several months.

Furthermore, the hospital environment provides a large number of hosts that *A. baumannii* can infect. Acinetobacter spp are easily grown on common solid and liquid growth-media. On solid agars, they have a smooth, grayish-white colony that could sometimes be mucoid and have a diameter of 1.5 to 3 mm after overnight incubation (Peleg et al., 2008). Most species in this genus grow well in temperatures ranging from 25 °C to 45°C , with optimal growth at 37 °C for species implicated with human infections.

The genus Acinetobacter

Acinetobacter is a genus belonging to the family Moraxellaceae, which has undergone extensive taxonomic changes ever since the first time it was discovered in 1911 (Peleg et al., 2008). This genus comes from a wide variety of environments and has various roles in ecological and clinical environments. The *Acinetobacter baumannii* complex species is difficult to distinguish by conventional phenotypic methods (since) the members of this genus can adapt to most substrates and thus results in confusion in the interpretation of biochemical tests (La Scola et al., 2006). Moreover, the Acinetobacter genus share several characteristics among one another. They appear by Gram staining as Gram-negative coccobacilli that could be in diploid formation or chains of variable length. However, they are difficult to de-stain, and therefore could be mistakenly observed as Gram-negative or Gram-positive cocci (Peleg et al., 2008). After identification of the first genus of Acinetobacter in 1911, many common characteristics were found between those bacteria. In 1968, it became widely accepted to group them under the current genus name, Acinetobacter, after an extensive review of their phenotypic characteristics. Interestingly, around that time, the first clinical isolate of Acinetobacter was isolated from the Intensive Care Units (ICUs) in 1969 (Stirland et al., 1969). Due to more advanced molecular methods such as DNA-DNA hybridization performed by Bouvet (in 1986), 12 genospecies identified which had more than 70% DNA-DNA relatedness (Peleg et al., 2008).

Currently, 51 species within this genus have been identified and given valid or provisional names (Al Atrouni et al., 2016a). Among them, the *A. baumannii* species is the most clinically relevant because it is the most frequently identified (MDR) isolate, followed by A. pittii and A. nosocomialis that is also clinically relevant, but to a lesser extent compared to *A. baumannii* (Dijkshoorn et al., 2007). More recent genome-wide analysis has shown *A. baumannii* is well separated from the other members of the Acb-complex and those of the complex from the remainder of species in the genus.

1.3 *A. baumannii* importance

The genus known as Acinetobacter has undergone significant taxonomic modification over the last 30 years. Its notable representative, *Acinetobacter baumannii*, is a non-fermentative, gram-negative, non-motile, oxidase-negative (coccobacillus) bacillus and aerobic that classified as a diderm bacteria. *A. baumannii* has emerged as one of the most troublesome pathogens for health care institutions globally that display ever-increasing rates of multidrug resistance. As such, it is identified as one of the most resistant bacteria to all classes of antimicrobials and multi-drug-resistant (MDR), forcing clinicians to use last resort antibiotics such as colistin (Garnacho-Montero et al., 2015; Bassetti and Righi, 2015; Saun et al., 2017). The emergence of *A. baumannii* as an important nosocomial pathogen is multifactorial. The metabolic versatility and resistance to various environmental stresses allow this pathogen to survive for extended periods in hospital settings. Besides, the number of virulence factors affords the bacterium the ability to adapt to and successfully infect the host (Dijkshoorn et al., 2007; Antunes et al., 2011; Roca et al., 2012; Weber et al., 2016). In summary, both desiccation tolerance and multidrug resistance may contribute to the maintenance of the species in the hospital setting and may partly explain its propensity to cause prolonged outbreaks of nosocomial infections (Gayoso et al., 2014; Zeidler et al., 2019).

Nosocomial infections

A nosocomial infection is defined as infections that occur within forty-eight hours after hospital admission, three days after discharge, or thirty days after surgery. It is estimated that one in ten patients admitted to a hospital is affected by a nosocomial infection (Inweregbu et al., 2005). Patients in ICUs are particularly susceptible to nosocomial infections, mostly due to mechanical ventilation, invasive procedures, and their immunocompromised status (Chatterjee et al., 2016). *A. baumannii* has been associated with high mortality rates of nosocomial infections from research dating back to the 1970s. This still true today since this pathogen is causing a wide range of infections, especially among critically ill patients. Despite the well-documented cases, the origin of this infection remains elusive due to the absence of a well-defined natural source of *A. baumannii*. Nosocomial infections caused by *A. baumannii* include pneumonia, ventilator-acquired pneumonia (VAP), bloodstream infections, skin, soft tissue infections, wound infections, urinary tract infections (UTI), and rarely gastrointestinal tract (GIT) infections (Zarrilli et al., 2009) provided in Fig.

1.4 (A). Patients at risk of developing *A. baumannii* infection are those with immunosuppression, prolonged hospitalization, critically ill patients in (ICUs), and resident in nursing homes (Dijkshoorn et al., 2007; Fishbain and Peleg, 2010). As shown in Fig. 1.4 (B), the primary mode of transmission through hospital staff coming in contact with patients and hospital equipment.

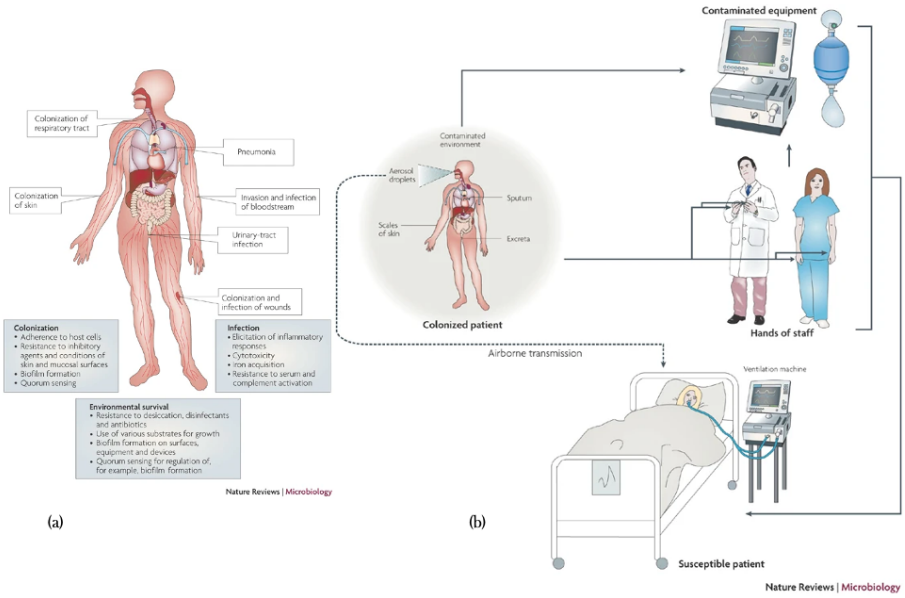

Figure 1.4: (a) *A. baumannii* host infections and colonization and (b) the increasing threat in hospitals multidrug-resistant *A. baumannii*, Image adapted from (Dijkshoorn et al., 2007)

The utmost *A. baumannii* nosocomial infection reported when its outbreak strains were traced back to dust filters found on respiratory ventilators and hemofiltration devices. The ability of *A. baumannii* to survive under such conditions may foster the resistance and virulence characteristics of this bacteria, which has allowed it to advance quickly as a nosocomial pathogen (Dijkshoorn et al., 2008).

Desiccation tolerance

Desiccation resistance is defined as the ability of the bacteria to maintain its viability under dry conditions or low water availability. This capability has enabled *A. baumannii* to become a successful opportunistic pathogen in the nosocomial environment. Compared to other Gram-negative pathogens commonly found in the nosocomial environment, *A. baumannii* clinical strains generally display better ability to survive desiccation in laboratory tests. In particular, the high desiccation resistance, which is unusual for gram-negative bacteria, has been reported for *A. baumannii* strains to survive on dry and inanimate surfaces from a few days to months. (Jawad et al., 1996 ; Wendt et al., 1996 ; Jawad et al., 1998 ; Antunes et al., 2011 ; Giannouli et al., 2013 ; Chapartegui-Gonzalez et al., 2018). This ability promotes persistence and spread in healthcare facilities such as bed rails, pillows, mattresses, tables, and medical equipment (Fournier and Richet, 2006; Zeidler and Muller, 2019). However, desiccation tolerance is highly strains-specific and can be variable among the *A. baumannii* strains (Nocker et al., 2012). Accordingly, previous studies have demonstrated that *A. baumannii* strains isolated from clinical or environmental sources exhibit significantly higher desiccation resistance than the laboratory strains (Jawad et al., 1998; Giannouli et al., 2013).

How much water is in a bacterial cell? Water is essential for all living organisms as it is crucial for many biomolecular processes, including protein folding and stability, enzyme-substrate interactions, and the maintenance of cell structure. Independent measurements made since the 1950s on different forms of bacteria have all provided somewhat similar values of the water in the cells. For example, it has been broadly reported that the protoplasm of E. coli contains 70 % water and 30% solids (Potts, 1994).

The water inside and outside the cells This water can be distributed among several structurally distinct cell compartments and namely the cytoplasm, the periplasm, and, if present, the capsule or extracellular investments. Living cells can achieve a dynamic state that is characterized by temporal and transitory shifts in the net concentrations of intracellular water, salts, lipids, macromolecules, trace metals, and cofactors (Potts, 1994). It can be argued that bacterial cells, while not bags of enzymes, are membrane-bound bags of water (Potts, 1994). These “bags of water” also contain the different proteins, one or more chromosomes in several millimeters in length when uncoiled, many different mRNAs, and ribosomes. While there is no notion of how these com-

ponents dispersed throughout the aqueous solvent, these findings point to the importance of water in the cell. Hence, removing the water from the cell can affect the cell viability and create severe challenges to the bacterial cells. Therefore, the bacteria that can survive against such harsh environmental conditions, desiccation, are collectively named Xerotolerant bacteria (Lebre et al., 2017).

Targets of desiccation damage

Desiccation or lack of water induces many biochemical, physical, metabolic, and physiological stresses to the bacterial cells. This condition can cause a cell viability loss that is related to damage to the cell-wall and cytoplasmic membrane. (Janning et al., 1994). Since not all the cells in a population respond to water deficit in the same way, the physiological status of the bacterial cell at the time of drying, slow or rapid, and also during drying seem to be a potential source of the variation in the desiccation sensitivity (Potts, 1994). Apparent changes associated with desiccation at the level of the bacterial aggregation may lead to a change in the surface area of a bacterial community, its shrinkage, a change in texture, precipitation of salts, change in shape, and change in color through oxidation of pigments. At the level of the single cell, the shrinkage of capsular layers, increase in intracellular salt concentrations, crowding of macromolecules, changes in volumes of cell compartments, reduced fluidity (increased viscosity), damage to external layers (e.g., pili, membranes), acquisition of static charge, and change in physiological processes (Potts, 1994).

In this regard, Figure 1.5 demonstrates the effects of desiccation briefly in a bacterial cell. Desiccation decreases turgor pressure and biochemical changes that can damage cell membranes by generating cell shrinkage and mechanical stress, which linked to the rapid loss of cytoplasmic volume (Mortel and Halverson, 2004; Scoffoni et al., 2014). It can also cause denaturation of intracellular proteins and conformational changes to DNA (Potts, 1994; Wolfe and Bryant, 1999). Other challenges faced by desiccating the cells are loss of enzyme activity, the formation of molecular aggregates, the accumulation of reactive oxygen species (ROS) that causes oxidative stress, consequently, cell death (Kranner and Birtic, 2005).

Contributing factors to desiccation tolerance

Desiccation tolerance is a multifaceted trait involving mechanisms range from cellular protection to repair of desiccation-induced damage, and many physiological and environmental factors can influence its impact on bacterial survival.

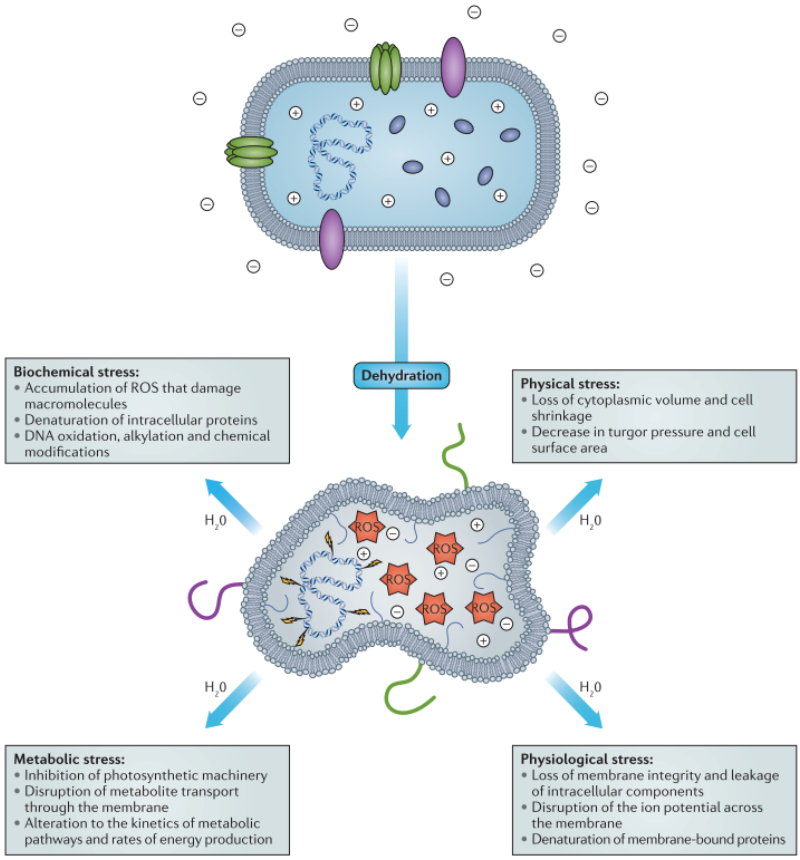

Figure 1.5: The effects of desiccation (lack of water) on the physiology and biochemistry of bacterial cells (Lebre et al., 2017)

To date, few factors contributing to the extraordinary desiccation resistance of this organism have been identified. Besides the fact that the biofilm-forming strains survive longer on dry surfaces (Espinal et al., 2012; Orsinger-Jacobsen et al., 2013; Gayoso et al., 2014), RecA, a protein involved in DNA repair, (Aranda et al., 2011) as well as the acylation of lipid A, a component of the *A. baumannii* outer membrane, (Boll et al., 2015) have been reported to be involved in desiccation resistance. Additional studies have suggested that BfmR,

as part of the two-component regularity systems, in addition to controlling the stress responses of *A. baumannii* during stationary phase and long-term drying, plays an essential role in the morphology and biofilm formation of this organism on abiotic surfaces. Together, these findings demonstrated the regularity link between the *A. baumannii* ability to persist in the environments and pathogenicity (Tomaras et al., 2008; Farrow et al., 2018). While these studies have provided valuable insights into desiccation tolerance associated-factors, they do not provide a comprehensive understanding of the *A. baumannii* protection-repair strategy. Further investigations are necessary not only to explore the crucial factors that influence bacterial survival entirely, but also to decipher the *A. baumannii* mechanisms of desiccation tolerance.

Mechanisms of desiccation tolerance

In response to desiccation, bacteria have developed a variety of mechanisms to mitigate the damage from drying. Some species can differentiate into dormant forms such as endospores or cysts, which are incredibly desiccation-resistant, but this strategy requires a significant expenditure of time and resources (Lebre et al., 2017). Other species have developed mechanisms that either help protect sensitive cellular components from damage or that sequester water in an attempt to avoid dehydration. These mechanisms include the alteration of membrane composition or LPS modification to help stabilize membranes during drying, and the accumulation of compatible solutes such as trehalose, which can protect cytoplasmic and membrane constituents (Potts, 1994; Farrow et al., 2018).

Further studies demonstrated that the bacteria react to changes in the environment, specifically to air-drying, by entering a reversible form of dormancy (Jones and Lennon, 2010; Rittershaus et al., 2013), EPS and biofilm formation (Anderson et al., 2011; Flemming et al., 2016), modification of cell membrane (Brown et al., 2000; Mortel and Halverson, 2004), accumulation of compatible solutes (Santos and Costa, 2002; Zeidler and Muller, 2019), as well as metabolic and molecular adaptation (Lebre et al., 2017). Despite the well-documented investigations, the morphological and molecular mechanisms of desiccation resistance remain poorly understood.

Chapter 2

Experimental setup

History of atomic force microscopy

Atomic-force microscopy belongs to the great family of scanning probe microscopy (SPM) with resolutions of the order of fractions of a nanometer. Scanning tunneling microscopy (STM) was the first technology to enable true 3D topographic imaging at atomic resolutions, invented in 1981 by Binnig. A major limitation of the STM is the necessity of the sample to be conductive. A few years later, in 1985, Binnig and Rohrer developed an atomic force microscope based on the same design as their STM to overcome this limitation. It had the properties of surface imaging and surface force measuring down to the nano-scale, but this time, contrary to the STM, the instrument was not restricted to one type of surface. It could be used in different environments going for the ultra-high vacuum to the liquids, to study any kinds of surfaces, including biological samples. Together, STM and AFM can be considered the main innovations behind the birth of nanotechnology. The AFM technique contours surface of the recording of interaction forces between a very sharp tip at the end of a flexible cantilever and the sample surface with piconewton sensitivity. With the right choice of parameters, it has enough resolving power to visualize single atoms, hence its name.

2.1 AFM in biology

Progress in Nanobiotechnology strongly relies on the development of scanning probe techniques, particularly atomic force microscopy (AFM) (Muller

et al., 2008). Indeed, the invention of AFM is a milestone in the history of nanotechnology (Gerber and Lang, 2006) and created new opportunities in physics, chemistry, biology and medicine. The unique flexibility of AFM to image, probe and manipulate materials made it the most versatile instruments in Nanoscience and nanotechnology, and stimulated numerous discoveries and technologies (Gerber and Lang, 2006).

The possibility to operate in liquid environments and at ambient temperature moved AFM towards biology, and led to the analysis of biomolecules and cells at (sub-) nanometer resolution (Horber and Miles, 2003). Since its invention, AFM has become one of the keys enabling technologies for studying materials and biological research at the nanoscale (D. Y. Abramovitch, et al., 2007; Viljoen et al., 2020). The advantages of AFM allow to measure the interaction force accurately at high resolution in a physiological environment and most media, including air, water and solutions without the need for fixation or staining and adapted to work over a vast temperature (Gerber and Lang, 2006; Horber and Miles, 2003).

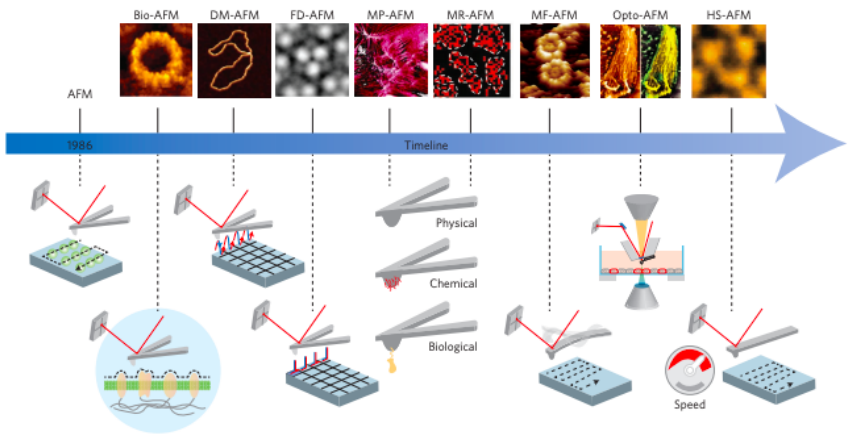

Figure 2.1: Timeline of key inventions, starting from the birth of AFM in 1986 to the latest AFM imaging modes in molecular and cell biology (Dufrene et al. 2017)

The first AFM image of living cells obtained in 1991. Additionally, AFM has also been used to image many other biological objects, including single

DNA molecules, purified proteins and membrane proteins in reconstituted or native membrane (Y. Dufrene, et al., 2017). Over recent decades, variety of AFM modes have been developed to address the wide complexity of biological systems, which can range from nucleic acids and proteins in cells and tissues, a variety of AFM modes have been created over the years (Fig.2.1)

Besides imaging, AFM enables mechanical manipulation and measurement of samples. The probe can also be used to push into or pull away from the surface. This has been used to investigate the role of forces for everything from tissues down to single proteins to characterize the micro-scale stiffness. Over the past few years, AFM has been used widely to measure the mechanical properties of soft biological tissues and cells. Moreover, nonmechanical analysis of cells is becoming increasingly important in cancer research (Dufrene et al., 2017).

2.2 Working principle

The principle behind the atomic force microscopy is the measurement of the interactive force between a tip and the sample surface using special probes made by an elastic cantilever with a sharp tip on the end (Fig. 1.6). The force applied to the tip by the surface, results in bending of the cantilever. A laser beam is focused on the back of the cantilever measuring the cantilever deflection, and detecting the laser reflection by a photodiode detector, make it possible to evaluate the tip–surface interactive force. The displacement of the reflected beam corresponds to amount of cantilever deflection during scanning. The sample is placed on a piezo scanner which is capable of three-dimensional movement in response to an applied voltage. The cantilever deflection is converted to an electric signal, which is used to adjust the distance between the sample and the cantilever.

The three basic concepts that one must be familiar with in order to understand the operation of an AFM are piezoelectric transducers (piezoelectric scanners), force transducers (AFM probe), and feedback control. Basically, the piezoelectric transducer moves the tip over the sample surface, the force transducer senses the force between the tip and the surface, and the feedback control feeds the signal from the force transducer back in to the piezoelectric, to maintain a fixed force between the tip and the sample.

Piezoelectric transducers Typically, the scanners used for moving the probe relative to the sample in an AFM are constructed from piezoelectric

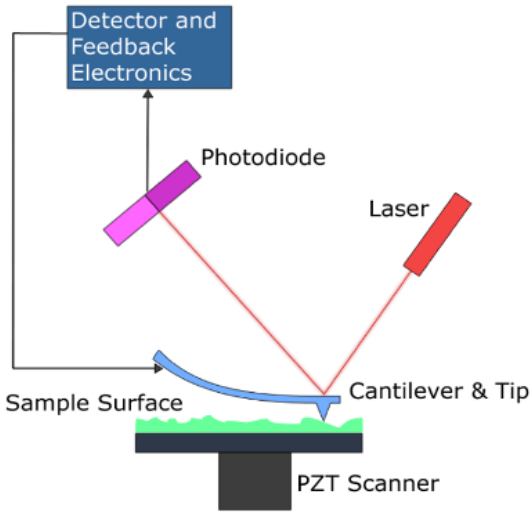

Figure 2.2: A schematic representation of an AFM

materials. This is because such piezoelectric materials are readily available, easily fabricated in desirable shapes, and cost effective. The piezoelectric materials are used for controlling the motion of the probe as it is scanned across the sample surface by converting the electrical potential into mechanical motion. The relative position of the tip over the sample is thus controlled by the application of voltage to the electric contacts of the piezo, resulting in extension, squeezing or bending of the piezoelectric material. Piezoelectric scanners can be designed to move in the three dimensions by expanding in some directions and contracting in others.

Force transducers The force between an AFM probe and a surface is measured with a force transducer. Usually, a flexible cantilever which ended by a small sharp tip located at its free end, is used as a sensor. The shape of the tip is generally either a pyramid or a cone, but can also be a ball when the AFM tip in the shape of either pyramid or cone, comes into contact with the surface, Forces acting between the AFM tip and the sample surface result in deflections of the cantilever Depending on the forces, a torsion and/or a bending of the cantilever take place while scanning a sample. Force transducers

may be constructed that measure forces as low as 10 piconewtons between a probe and a surface. Typically, the force transducer in an AFM is a cantilever with integrated tip (the probe), and an optical lever.

Feedback control The reason an AFM is more sensitive than a stylus profiler that simply drags a tip over the sample surface, is that feedback control is used to maintain a set force between the probe and the sample. As illustrated in Figure 1.6, the control electronics take the signal from the force transducers, and use it to drive the piezoelectric so as to maintain the probe–sample distance, and thus the interaction force at a set level. Thus, if the probe registers an increase in force (for instance, while scanning the tip encounters a particle on the surface), the feedback control causes the piezoelectric to move the probe away from the surface. Conversely, if the force transducer registers a decrease in force, the probe moves towards the surface.

Probes

The atomic force microscope sensing the surface using special probes made of cantilever with a sharp tip on the end and measure the interaction force between it and the surface being scanned. The cantilever sensitivity and the sharpness of its tip play a significant role and affect the resolution of the AFM, combined with other factors such as step size and the number of scanning lines.

The body of the cantilever is usually manufactured from silicon or silicon nitride and the back of the cantilever is coated with different materials such as aluminum or gold to enhance the reflectance of the laser beam to the detector area.

Cantilevers are produced in different shapes, either rectangular or V-shaped, and integrated by a tip microfabricated at the free end, while in some applications there is no need for a tip at all. In order to make handling simple, the cantilevers are attached to a cantilever substrate or chip.

Typically, the length of the cantilever ranges from 100μm to 200μm and the width from 10μm to 40μm , while the thickness is in the range from 0.3μm to 2μm.

The curvature radius of AFM tip apex is of the order of $1 \div 50$ nanometers depending on the type and on the technology of manufacturing. The interaction force F of a tip to the surface can be estimated from the Hooke law:

$$F = k.\Delta Z \tag{2.1}$$

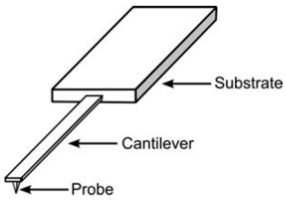

Figure 2.3: Illustration of AFM cantilever, probe and substrate (Eaton and West.2010).

Where k is the cantilever elastic constant; δZ is the tip displacement corresponding to the bending produced by the interaction with the surface. The k value is largely depends on the cantilever material and geometry. Moreover, in the oscillating mode, the cantilever resonance frequency which can be obtained as follows:

$$\omega_{ri} = \frac{\lambda_i}{l^2}\sqrt{\frac{EJ}{\rho S}} \tag{2.2}$$

Where l is the cantilever length; E the Young's modulus; J the inertia moment of the cantilever cross-section; ρ the material density; S the cross section; λ a numerical coefficient (in I the range $1 \div 100$), depending on the oscillation mode.

$$K_{tri} = \frac{D_0 \bar{d}}{2L^3}\left(1 + 4\frac{d^{-3}}{b^3}\right)^{-1}\sqrt{\frac{EJ}{\rho S}} \tag{2.3}$$

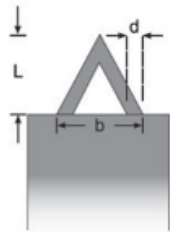

Figure 2.4: AFM triangular cantilever (Eaton and West.2010)

Probes with triangular cantilever have higher stiffness and, hence, higher resonant frequencies. They are usually used in oscillating AFM techniques.

Cantilever specifications include resonant frequency, spring constant, and the Q-factor and have a large influence on the resulting data quality. To obtain high-resolution images, it is important to choose the most appropriate tip and cantilever depends on the sample and the AFM operation mode.

The shape of the cantilever and its dimensions, together with the manufacturing material, determine its spring constant, where the shorter and the thicker the cantilever is, the higher its resonant frequencies and spring constant. In general, cantilevers with a high resonant frequency and spring constant are suitable for imaging biological samples using non-contact- or intermittent contact–mode AFM, whereas cantilevers with the lowest possible spring constant are most suitable for contact-mode operation.

In contact mode, to be able to feel the surface with atomic resolution, the stiffness of an AFM cantilever should be much smaller than the spring constant that maintains the atoms confined together on the surface.

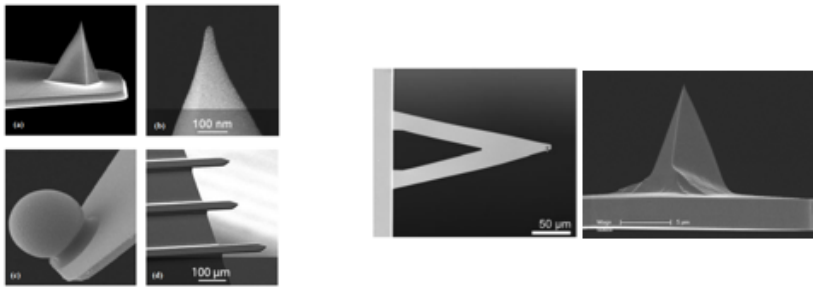

Figure 2.5: AFM probe shapes

In general, soft cantilevers are used in contact mode to avoid damage to the sample. On the other hand, stiff cantilevers are preferred for imaging in dynamic mode to overcome capillary forces. Ideally, cantilevers of high resonant frequency and low spring constant are preferred. The Q-factor is a measure of the sharpness of the resonance spectrum and is defined as:

$$Q = f_0/\Delta \mathrm{f} \tag{2.4}$$

Where f_0 is a resonant frequency, δf is frequency bandwidth within which the amplitude drops to $1/\sqrt{2}$ times the peak value. Cantilevers with higher Q-factors are more sensitive to deflections of the probe, resulting in an improved signal-to-noise (S/N) ratio for the detection signals, which leads to improved AFM image quality.

Force-curve

Besides imaging, the other key capability of AFM is to measure the surface mechanical properties such as stiffness and adhesion via force distance curves. A typical force distance curve has a full cycle containing an approach curve and retract curve. Force–distance curves are measured by monitoring the deflection of the cantilever as it approaches, touches, and withdraws from the sample. By default, therefore, they are measured in contact mode. The cantilever starts from a free level position in 'A' and moves towards the surface. At position 'B' the cantilever is attracted to the surface without a real load on it. This surface area is called the 'snap in' region.

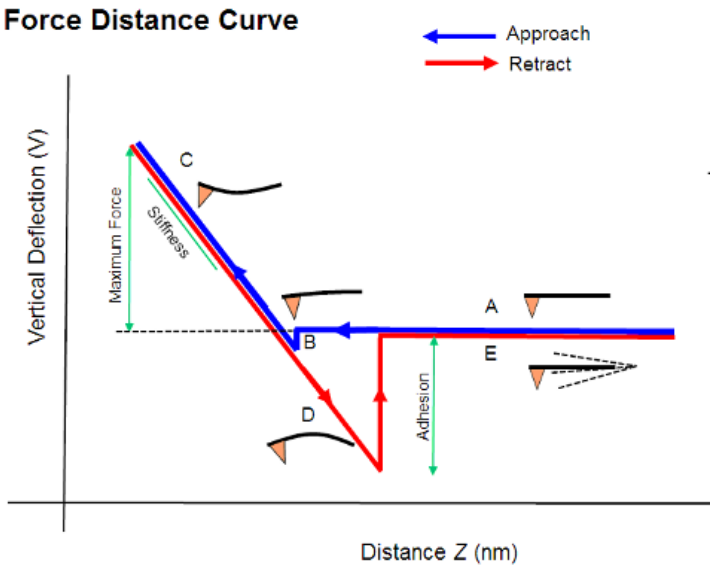

Figure 2.6: Scheme of Force-distance curve

While the cantilever is moving further into the sample, it starts to bend with an increasing the loading force. When the cantilever reaches the maximum predefined loading force, the approach curve ends and the retract curve starts. The cantilever moves in a reversed direction to move away from the sample. Due to the adhesion, the tip may not leave the surface as it is attracted to the surface at position 'B'.

The cantilever remains in contact with the surface until the maximum adhesion force is reached and the tip is detached from the sample. With a quantitative calibration of detector sensitivity (nm/V) and cantilever spring constant k (N/m), using Hooke's Law (F=-kx) the measured cantilever deflection can be converted to the fore. Therefore, a quantitative output of the maximum loading force, adhesion force, snap-in force, and stiffness (with further calculation) can be achieved by applying the force distance curve mode. (Eaton et al., 2010; Voigtlande, 2015)

2.3 AFM operation modes

After the invitation of AFM, a variety of operating modes of AFM include contact mode, tapping (intermediate) mode, and non–contact have been developed. They are distinguished according to different operating force ranges as shown in Figure 1.11. Contact mode and tapping mode are two most widely used AFM modes in the ambient environment. The methods that the AFM can acquire images can be considered as: Contact mode (C-AFM) -non contact mode (NC-AFM) and Intermittent-contact mode (IC-AFM) which has been known as tapping mode.

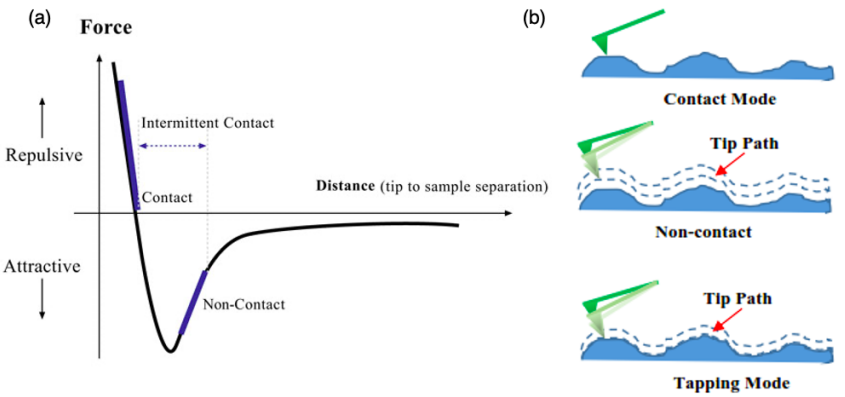

Figure 2.7: (a): diagram of the potential energy between probe and sample, (b): AFM operation modes.

To describe the operating AFM modes, the main interaction forces between

the tip and the sample, coming from the Lennard-Jones potential:

$$u(r) = u_0 \left[-2 \left(\frac{r_0}{r} \right)^6 + \left(\frac{r_0}{r} \right)^{12} \right] \tag{2.5}$$

Here the first term describes the long-range attractive Van-der-Waals forces and the second term takes into account the short-range repulsion due to the Pauli Exclusion Principle. The parameter r0 is the equilibrium distance between atoms, the energy value of the minimum.

Contact mode

As indicated by its name, the contact mode (C-AFM) corresponds to the state that tip is in contact with the sample surface under repulsive forces. The topographic image of the surface can be produced by operating in the constant force mode or constant height mode. In the constant force mode, the force between the tip and the surface is simultaneously measured and kept constant via a feedback loop controlling the vertical position of the sample relative to the tip. Thus, the scanner responds instantaneously to topographical changes by keeping the cantilever deflection constant. For the constant height mode, the measured data are the cantilever deflection, whereas the relative distance between the tip and the surface is kept constant via the feedback loop. The deflection of the cantilever is thus directly used to reconstruct the topography of the sample. A constant height mode can be employed for atomically smooth surfaces. Cantilevers used in contact-mode have relatively small stiffness, allowing to provide high sensitivity and to avoid the undesirable excessive influence of the tip on the sample) Mironov, 2007).

Non-contact Mode

In the non-contact (NC-AFM) mode, also called dynamic mode, Attractive Van der Waals forces acting between the tip and the sample are detected, and topographic images are constructed by scanning the tip above the surface in the distance about 10 to 100 nanometers with no contact. The dominant forces in the non-contact (NC) mode substantially weaker than the forces used by contact mode, therefore the tip must be given a small oscillation. However, it makes NC mode suitable for soft materials to avoid damaging the sample. In this mode, the cantilever vibrates near its resonant frequency, depending on its spring constant, with amplitude around hundreds of angstroms (Å). The separation between the tip and the sample surface is monitored by the feedback

loop, either using a constant frequency or a constant amplitude technique. However, this mode provides less resolution and the scanning is relatively slower than the contact mode. In general, the fluid contaminant layer is substantial, which are thicker than the range of the Van der Waals force gradient, therefore, attempts to image the true surface with non-contact AFM fail as the oscillating probe becomes trapped in the fluid layer or hovers beyond the effective range of the forces it attempts to measure.

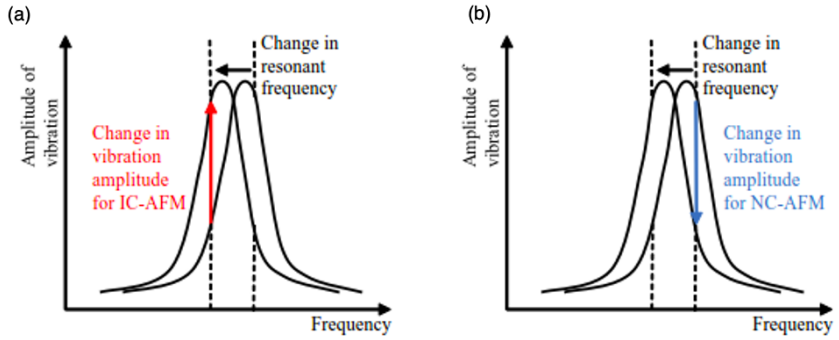

Figure 2.8: Response curve of oscillating the cantilever close to the sample surface in (a): in intermittent mode (IC-AFM), and (b): Non-contact mode (NC-AFM)

Intermittent-contact (Tapping mode)

Intermittent-contact (IC) or tapping mode works like NC mode where the cantilever is near the sample surface and vibrates at its resonant frequency, however, at the bottom of the vibration the cantilever touches or hits (taps) the sample surface which does not happen in NC mode. In tapping mode (or intermittent contact mode), the cantilever tip is oscillated at larger amplitudes, thereby crossing into both the attractive and repulsive force regions of the tip-sample interactions. In order to explain Tapping Mode operation, it can be useful to examine the dynamics of the operation. Assuming air damping is the dominant factor, the movement of the cantilever can be described using the (sinusoidal) driven damped harmonic oscillator mode:

$$m^* \frac{\partial^2 z}{\partial t^2} + b\frac{\partial z}{\partial t} + k_z = F_0 \tag{2.6}$$

with m* being the effective mass of the cantilever, z the displacement of the lever, b the damping coefficient, k the spring constant, and F_0 the driving force ($F_0 = kA_0$). With the natural frequency:

$$\omega_0 = \sqrt{\frac{k}{m^*}} \quad \text{and the relaxation time } \tau_0 = \frac{m^*}{b} \tag{2.7}$$

We can write the amplitude of the lever as:

$$A(\omega_0) = \frac{A_0}{\sqrt{\left(1 - \left(\frac{\omega_d}{\omega_0}\right)^2\right) + \frac{1}{(\omega_0 \tau)^2}\left(\frac{\omega_d}{\omega_0}\right)^2}} \tag{2.8}$$

The separation between the tip and the sample is controlled in the same way as in the NC mode. This potent mode overcomes problem associated with friction, adhesion and electrostatic forces and has many advantages; it is suitable for larger scan sizes than the NC mode, it is faster than NC mode and less damaging to the sample than the contact mode, therefore it is widely used. The lateral resolution is better compared with both contact and NC modes.

Peak force tapping mode

During scanning in contact mode or Tapping Mode, the probe applies vertical and lateral forces to the cell surface. The vertical force is needed to feel the surface, but the lateral forces are usually unwanted as they often cause obscuring in the image because of dragging and pushing of flexible surface structures.

Also, the vertical forces have a lower resolution because the minimum force is required to bend the cantilever is sufficient to deform very soft structures lead to uncertain height and shape. Even in tapping mode (TM), reduction and localization of the vertical interaction require the use of small amplitudes, which results in lateral dragging through the spatially extended, soft structures, presented by the cell surface.

In the past years, there have been major breakthroughs in developing new quantitative AFM-based imaging techniques. Among these, quantitative imaging and peak force tapping (PFT) methods allow researchers to image the structure and the physical properties (e.g., Elasticity and adhesion) of the sample simultaneously at high speed and high resolution by controlling vertical forces in the range of some tens of Pico-Newton (PN). In PFT, the tip is oscillated in the vertical direction with an amplitude of 100-300 nm and at a frequency of

0.25, 0.5, 1.0, or 2.0 kHz. The z piezo is driven with a sinusoidal rather than a triangular waveform in conventional force-distance (F-D) curves for each image pixel.

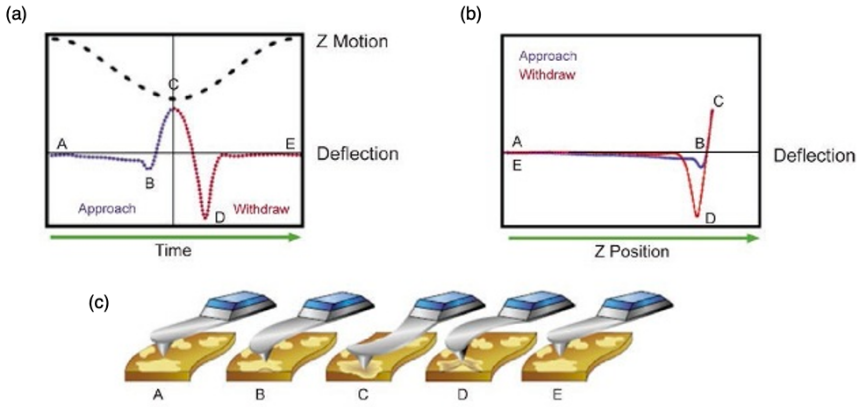

Figure 2.9: Scheme of peak force tapping mode (a) the heartbeat curve, (b) force-curve of peak force mode, (c) tip approach to the surface (Image adapted from Bruker, 2011)

This oscillating system allows direct force control of damaging lateral forces, which is very useful for the structural imaging of soft samples. In addition, individual force curves can be analyzed to generate adhesion and mechanical maps to a much better resolution than in conventional Force-Volume (FV) imaging (at best 64 pixels × 64 pixels). A remarkable feature of PFT is that F-D curves are recorded at frequencies that are 3 orders of magnitude higher than in FV imaging.

As a result, the imaging speed is similar to that of topographic imaging (8 min for a 512 × 512 pixel image), which is much faster than conventional FV imaging (80 min for a 64 × 64 pixel image).Images are reconstructed by using the z-piezo position at the moment the tip touches the surface (zero-force image).The combination of sinusoidal modulation and background subtraction conducted for each probe–sample interaction provides PFT with highly sensitive force control, which allows the use of low imaging forces. The maximum probe–sample interaction force (peak force) of each curve is used to control vertical forces.

PFT is also capable of operating at frequencies of up to 1 kHz of live cells as compared with the force-volume, which has shown a maximum frequency of ∼100Hz. As FV uses a triangular motion to move the probe in and out of contact with the sample surface, Because of the short delay in the feedback loop it has difficulty maintaining low set points or imaging forces at higher frequencies.

So, it is possible that force-curve mode distorts or effectively change the apparent structure of the cell surface. PFT mode has been successfully applied to image various delicate biological samples like cells (Berquand et al., 2010; Heu et al., 2012; Pletikapic et al., 2012), membrane proteins (Medalsy et al., 2011; Alsteens et al., 2012), vesicles (Hardij et al., 2013), and amyloid fibrils (Adamcik et al., 2011). In the present work, we used PFT, which allows reduction of both vertical and lateral forces in order to achieve unrivaled resolution of microvilli on live epithelial cells (Schillers et al.,2016; Alsteens et al.,2012).

ScanAsyst mode

ScanAsyst uses the PFT mechanism, which decouples cantilever response from resonance dynamics, to automatically adjust all critical imaging parameters. Because the peak force feedback directly controls the interaction force, there is no distinction for peak force for soft or hard parts of the sample. A real-time feedback loop constantly monitors and adjusts the gain to keep the data quality within a predefined noise level (unlike manual gain adjustment where usually one gain is used for a whole image).

ScanAsyst optimizes the gain according to the current sample condition at different locations. The algorithm also optimizes the set-point to the minimum force required to track sample surfaces, controls the scan rate, and can automatically lower the z limit if necessary. This results in extremely high-quality images without user adjustment of imaging parameters and without the normally problematic AFM user interfaces exhibiting numerous and often confusing parameters. In addition, ScanAsyst also sets the actual scan speed and the z-limits

Chapter 3

Material and methods

Bacterial strain

The *A. baumannii* ACICU strains (Iacono et al., 2008) as a prototype of the MDR strains used in this study belong to European Clone (EC) II isolated from the hospital. Three single colonies of A. baumannii ACICU strains were harvested from the agar plates and suspended in Luria Bertani (LB) rich medium.

3.1 Bacterial strain preparation

All the experiments of this work were performed following the same cultural conditions, except when specified in the text. Briefly, *A. baumannii* ACICU were grown in Luria-Bertani broth (LB) and incubated overnight at 37°C in a tube with vigorous shaking (i.e., 250 rpm). After the incubation, bacterial culture was refreshed 1:100 and re-incubated at $37°C$ based on the experiment purposes we focused on. The bacterial growth was monitored during time by measuring the absorbance at 600 nm ($OD_{600} = 1$) to obtain the growth curve.

Growth phase-dependent

To investigate the morphological feature variations depending on the growth phase, the overnight bacterial culture was refreshed 1:100 in a flask containing LB medium and re-incubated at $37°C$ under vigorous shaking (i.e., 250 rpm). The bacterial growth was measured as absorbance at 600 nm for up to 48 hours. Based on growth curve obtained, an aliquot of bacterial culture was

collected at different time points assigned to different growth phases (i.e., at 3, 6, 14, 24, and 48 hours of incubation at $37°C$), washed twice with sterile distilled water and diluted to reach a final $OD_{600} = 1$ (corresponding to ca. $5x10^8$ CFU/ml). Twenty μl of the bacterial suspension (corresponding to ca. 10^7 CFU for each glass slide) was then spotted on a microscope glass slide (Thermo ScientificTM SuperFrostTM Microscope slides 76 $\times$26 mm, with 1 mm thickness) and air-dried under the laminar flow hood. The prepared bacterial samples, then measured with AFM in ambient conditions. Cell viability was monitored by viable count on LB agar plate (LA) before and immediately after air-drying.

Growth conditions-dependent

Flask-shaking bacterial cells

The overnight *A. baumannii* ACICU bacterial culture was refreshed 1:100 in a 350 ml flask containing 50 ml of LB medium and incubated at $37°C$ under vigorous shaking (i.e., 250 rpm).

Tube-static bacterial cells

The overnight bacterial culture was refreshed 1:100 in a 15 ml tube containing 5 ml of LB medium and incubated at $37°C$ in the static condition. In both conditions, bacterial growth was monitored for two days by measuring the absorbance at 600 nm ($OD_{600} = 1$). Based on the growth curves obtained, the bacterial cells were collected at time points which are assigned to the logarithmic and stationary growth phases. Likewise, A. baumannii ACICU cells grown in flask under shaking after 3 h and 14 h of inoculum, while the cells grown in static conditions were harvested at 14 h and 30 h after inoculum. In each growth condition, bacterial cells were washed twice with sterile distilled water and diluted to reach a final OD_{600}=1. Twenty μl of the bacterial suspension was spotted on a microscope glass slide and air-dried under the laminar flow hood. The cell viability assessment before and after air-drying besides the AFM measurement was performed for the prepared bacterial samples.

Bacterial cell suspended in different mediums

In order to study the nanoscale surface variations of *A. baumannii* ACICU cells in different media, the bacterial culture was washed twice with sterile distilled water and diluted to reach a final $OD_{600} = 1$ in different media such

as LB, Casamino acid (CAA), Saline solution (0.9% NaCl), sterile distilled water and 1 mg/ml Bovine Serum Albumin (BSA) solved in water. Then, 20μl of the bacteria re-suspended in the aforementioned liquids were poured on a microscope glass slide and directly imaged by AFM in the first minutes of air-drying in their environments.

3.2 Drying methods

Given that A. baumannii strains have emerged as a desiccation-resistant bacterium, we aimed to investigate the changes in morphology and survival of these cells subjected to various environmental stresses, using different drying methods; freeze-drying, air-drying, and maintenance of water that will be explained in the following sections. For this purpose, the overnight bacterial culture was refreshed 1:100 in a flask containing LB and re-incubated at 37$°C$ under vigorous shaking (i.e., 250 rpm).

The bacterial growth was obtained by measuring absorbance at 600 nm, and cell viability and live-dead cell counts were performed at different time points. According to the acquired results, the bacterial cells with maximum viability and cell density were detected after 6 hours of growth in the LB medium. Therefore, bacterial cells were harvested 6 h post-refresh, washed twice with sterile distilled water, and diluted to reach a final $OD_{600} = 1$. For each sample, twenty μl of the bacterial suspension (corresponds to ca. 10^7 CFU) was collected to prepare the samples and dried under different drying methods for cell viability assessment and AFM measurements. The dried bacterial samples after preparation were stored in a 16-liter vacuum bell containing 50 g of silica gel with an average temperature of 20 $\pm$ 0.6 $°C$ and average relative humidity of 13 $\pm$ 6%. Moreover, we designed our experiment for a two-month examination of the samples dried under various drying methods. Therefore, to have an identical experimental condition, twelve samples were prepared for each drying method and measured at 1h, 6h, 24h, 48h, 72h, one-week, two-week, one-month, and two-month after desiccation.

Freeze-drying

Twenty μl of the bacterial suspension (corresponds to ca. 10^7CFU) was spotted on twelve microscope glass slide/ coverslip for AFM/viable counts measurements, then all of them immediately pre-frozen at -80°C for 15 minutes. Next, all the samples were put into the freeze-dryer instrument to freeze at

-50°C and dry under vacuum until the complete drying (water evaporation) approximately for 30 minutes. Finally, all the glass slides placed in covered Petri dishes and were stored in a 16-liter vacuum bell containing 50 g of silica gel with an average temperature of 20 ± 0.6°C and average relative humidity of 13 ± 6%, recorded by digital thermo-hygrometer at each time points. The coverslips were also placed in a covered Petri dishes and stored similarly in a sealed vacuum chamber with a same amount of silica gel.

Air-drying

Likewise, twenty μl of the bacterial suspension (corresponds to ca. 10^7 CFU) was spotted on twelve-microscope glass slides and coverslips, and dried under laminar flow laminar hood for about 20 minutes. All the air-dried glass slides and coverslips placed in a covered Petri dishes and were stored in a 16-liter vacuum bell containing 50 g of silica gel with an average temperature of 20 ± 0.6 °C and average relative humidity of 13 ± 6%, recorded by digital thermo-hygrometer at each time points.

Maintenance in water

The hydrated bacterial cell preparation was similar to air-dried *A. baumannii* ACICU cells prior to drying under a laminar flow hood. In other words, after the bacterial culture were washed with distilled water and adjusted to OD_{600} = 1, the bacterial suspensions were kept in two separate Falcone tubes for AFM measurements and viable count assays, for a two-month examination. At each determined time points, twenty μl of the bacterial cell was collected and spread on glass slides to measure in ambient conditions.

3.3 Bacterial storage conditions

To evaluate the desiccation survival of A. baumannii ACICU cells under simulated hospital conditions, we used saturated salt and silica gel compounds to control humidity for long-term storage of bacterial samples. To do this, the overnight bacterial culture was refreshed and re-incubated in flask containing LB at 37°C under vigorous shaking (i.e., 250 rpm). The bacterial cells were collected at different time points (i.e., at 3 h, 6 h, 14 h, 24 h and 48 h of incubation at 37°C), then washed twice with sterile distilled water and diluted to reach a final $OD_{600} = 1$. Twenty μl of the bacterial suspension corresponds

to ca. 10^7 CFU was spotted on a microscope glass slide and dried under the laminar flow hood.

Storage with silica gel

The air-dried *A. baumannii* ACICU cells were placed in a covered Petri dishes and stored in a 16-liter vacuum chamber containing a 50 g white silica gel to provide the humidity below 30% inside the chamber. A digital thermos-hygrometer was recorded a relative humidity inside the chamber 15 ±4% RH and temperature of 20 ± 2°C during the three months experiment.

Storage with salt

To storage the air-dried cells with salt, the bacterial sample were placed in a covered Petri dishes separately and maintained in a 16-litre vacuum chamber containing a $CaCl_2 \times 6H_2O$ saturated salt in an open glass beaker for three months. A digital thermos-hygrometer was recorded a relative humidity inside the chamber 23± 4% RH and temperature of 20 ± 2°C during the experiment.

Long-term storage with salt (Jawad et al. protocol)

The bacterial sample was prepared according to Jawad et al., 1998 protocol to study the morphology changes during long-term desiccation under simulated hospital conditions. In this way, the bacterial culture was grown in LB medium in falcon tube and incubated with vigorous shaking at 37°C. *A. baumannii* ACICU cells harvested after 18 hours by centrifugation (5,000 g × 5 minutes) and washed twice with sterile distilled water and diluted to reach a final $OD_{600} = 1$. Twenty μl of the bacterial suspension was spotted on a microscope glass slide and air-dried under the laminar flow hood. Then bacterial samples were put in a petri dishes and maintained by the presence of a saturated salt solution ($CaCl_2 \times 6H_2O$) for 31% RH in tight transparent plastic box.

Desiccation survival of bacteria was assessed by cell viability counts during two months storage as described in the following sections (i.e., at 0h, 6h, 24h, 48h, 72h, one-week, two weeks, and two months).

3.4 Desiccation survival assays

The desiccation survival assay is described as a procedure that followed to determine the length of time that bacterial strains could survive on glass coverslips when kept at 31% relative humidity (RH). For this purpose, the cell viability assessment is carried out by counting the viable cells (colony forming units CFU) before air-drying, immediately after air-drying, and at different time of storage under dry conditions.

Cell viability before drying

Bacterial desiccation survival was determined by viable counts for original bacterial cultures prior to placing on the coverslip. To do so, the aliquot of overnight bacterial culture was harvested, centrifuged and washed twice with distilled water. Then the bacterial suspension was diluted to reach $OD_{600} = 1$ corresponds to ca. 5×10^8 CFU/ml. For cell viability twenty μl of the bacterial suspension (corresponding to ca. 10^7 CFU for each glass slide) placed on LB agar plate (LA) to monitor the viable counts which consider as bacterial survival before desiccation.

Cell viability after drying

To evaluate desiccation survival of bacteria immediately after air-drying, twenty μl of the bacterial suspension, adjusted to $OD_{600} = 1$ was spotted on the coverslip and allowed to dry under a laminar flow hood.

After the complete drying of bacterial cells on the air, within half an hour, the samples were re-hydrated by distilled water and placed on the LB agar plate (LA) to determine the viable counts after air-drying.

Cell viability during prolonged desiccation

Prolonged desiccation survival of air-dried *A. baumannii* ACICU cell is measured by cell viability assessment for the stored cells under dry conditions in the presence of either saturated salt or silica gel to control humidity below 31% RH. With this aim, the air-dried coverslips at different storage times (i.e. 6h, 24h, 48h, one-week, two-week, and three-week, one-month, two-month and three-month after desiccation) were re-hydrated in distilled water and placed on the LB agar plate (LA) to monitor the viable counts.

3.5 Sample preparation for AFM measurement

The bacterial samples were prepared for AFM measurements in two different methods depending on experiment goals. Twenty μl of diluted bacterial suspension adjusted to $OD_{600} = 1$ was spread on a microscope glass slide (Thermo ScientificTM SuperFrostTM Microscope slides 76 $\times$ 26 mm, with 1 mm thickness). Then dried bacterial samples with different drying methods were stored in a sealed chamber to measure at determined time points. For the bacterial cells which were required to measure immediately after desiccation or even before complete drying, the bacterial cells were kept in a Falcone tube in a liquid state (i.e. hydrated cells and re-suspended cell in different mediums).

According to measurement time points, an aliquot of bacterial suspension was placed on a glass slide and allowed to dry in room conditions. Immediately after water evaporation under an optical microscope of AFM, the imaging was carried out.

Atomic Force Microscopy (AFM) measurement

Atomic force microscopy measurement was performed using a Dimension ICON AFM (Bruker, Santa Barbara, USA) set to Peak Force Tapping mode. We used the ScanAsyst-Air Bruker tip in the present study by a nominal spring constant of 0.4 Nm^{-1} and sharpened silicon tip with a nominal radius of 2 nm. The AFM images are recorded at room temperature, mimicking the hospital environments ranged from 20–24 °C. The oscillation frequency and oscillation amplitude of the cantilever are set to 1 kHz and 150 nm, respectively.

The obtained AFM images were analyzed and processed with the free Gwyddion Software (http://gwyddion.net). The bacterial cells scanned in different size from 3 μm $\times$ 3 μm for single cells to the maximum 98 μm $\times$ 98 μm in large scale. The tip scan rates varied from 0.4 to 1 Hz depending on the bacterial cell preparation conditions. For each measurement, height sensor and peak force error images were recorded simultaneously. The height sensor image specifies biophysical cell parameters, while the peak force error image emphasizes the bacterial cell morphology. Multiple images were recorded at each measurement to validate our observations.

AFM calibration and setup

ScanAsyst^{TM} is the first automatic image optimization technology of atomic force microscopy (AFM), with the core technology of Peak Force Tapping mode.

This technique by performing a very fast force curve at every pixel and using the peak of each force curve as an imaging feedback signal, enables users to rapidly obtain high-quality images. Moreover, direct control of the force as an advantage of ScanAsyst mode allow us to operate the small force during the measurement which helps protect delicate samples from damage and tip wear.

Together, these capabilities make ScanAsyst the most powerful and productive way to use AFM for imaging of any samples in either air of fluid (Su et al., 2012). Hence, in this work the ScanAsyst TM was applied to examine the bacterial cell morphology exposed to the air with a simple calibration before each measurement, explained as follows:

Mounting a tip on the cantilever One of the crucial requirements for accurate measurement is choosing a suitable probe with an appropriate cantilever holder depending on the imaging mode and sample property. With the intention of minimizing the imaging force to the bacterial cell, we used the ScanAsyst-Air tip of the silicon nitride cantilever by enough stiffness for appropriate deformation of the sample that retains high force sensitivity.

Laser alignment After mounting the ScanAsyst probe with a V-shaped cantilever on cantilever holder, we placed them together under the AFM scanner. Then the laser beam was aligned on the back of the cantilever by the control knobs whereas the laser spot was visible on it. Then laser spot was adjusted to the center of the photodetector in order to obtain the maximum sum, ranged from 4.5 to 5 Volts for the silicon nitride cantilever, and to verify the laser spot on the probe

Approach to the sample surface After focusing on a tip and setting the cross-lines on the V-shaped cantilever, we loaded the sample under scanner place by using the scroll-joystick or Bioscope software. During approaching, in the close distance between the scanner and sample to avoid a tip broken or cell damage, the scanner speed was reduced or auto finding surface was used to reach the sample. With the aid of the optical, we searched a sample surface to find the interest area of study, including a number of bacterial clusters or cells. Before engaging, we calibrated the probe and deflection sensitivity by thermal tune process to define the set point for measurement. The laser spot again readjusted to the center of a photodetector which may have drifted. The thermal tune calibration and readjusting the laser spot are routinely conducted after a few imaging.

Determination of scan parameters

After all the above steps, we engaged to the region of interest and set the initial scan parameters such as scan size, aspect ratio, sample/line, either ScanAsyst auto control or feedback gain/ peak force set point. Normally we used the scanned the clusters in size about 20 μm with the scan rate of 1 Hz and sample/line of 512 to image the sample. These parameters can be influenced to some extent of the sample type and preparation method.

Search find procedure (SFMSF)

By using a diamond pen, we drew the perpendicular-lines on the corners of the glass slides as a reference a bit far from the edges. Glass slides were cleaned with ethanol and dried with pure nitrogen to remove the fingerprints and remaining glass particles. Next, we dispread an aliquot of bacterial samples over each reference region and allowed them to dry under the laminar hood. Each region/reference was labeled as A, B, C and D from the top left side of the glass slide respectively.

Search : In order to find the reference marks, we employed the optical microscope of AFM to reach one of them in a corner of the glass slide. Given that in which reference region we are (A, B, C or D), we searched the area of interest containing several clusters with an appropriate size around those lines (horizontal, vertical or inner part of crossed-line).

Find : After specifying the desired cluster with the aid of an optical microscope of AFM, prior to engaging we utilized the manual navigation controls with a determined speed which allows us to adjust the tip to the intended position, for counting the steps and movement direction from the reference mark to the desired cluster. All the required information was recorded for the next measurement, including the reference label, the number of steps, direction of movement, even by attention to either vertical-line or horizontal-line of the reference, accompanied by optical images of the region of interest.

Measurement : Considering the subsequent measurement of the selected cluster it is essential to record the scanning parameters to have accurate analysis, such as the scan size, aspect speed, samples/line, feedback gain, and peak fore set point.

Storage : After the measurement, we stored the samples in a controlled condition in terms of humidity and temperature, the sealed chamber containing silica gel or salt, for re-measuring at different time intervals.

Find : To re-find our desired cluster we pursued the recorded information. To do so first the tip must be adjusted to the reference region (A, B, C or D) then, according to the number and direction of the steps with the same movement speed the determined cluster will be found. Pursuing the imaging parameters, the same as possible to the first measurement and recording optical images beside the accurate information about finding the cluster are strongly recommended. This method enables us to pursue the morphological changes of the specific clusters over time. Although the examination of the different clusters giving us some statistical information about their behavior in response to drying, it does not provide a detailed insight into the response of each cell or bacterium exclusively.

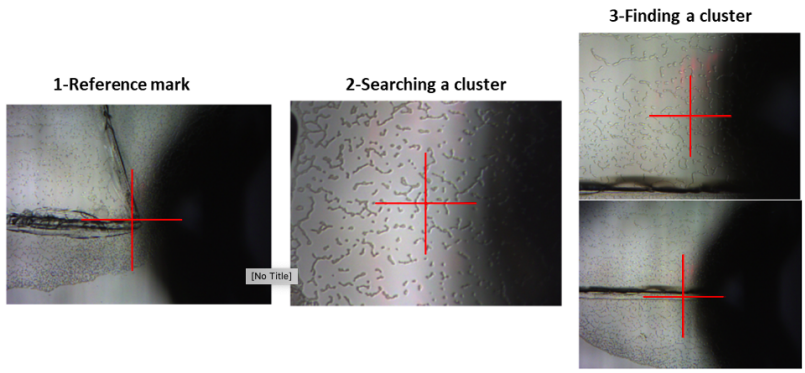

Figure 3.1: SMSF procedure for pursuing a cluster at different time intervals.

Figure 3.1 describes the SFMSF procedure to pursue a specified bacterial cell morphology changes during the time. As an example, one referenced mark on a glass slide is shown while the crossed-line is located on the edge of the reference as a start point for searching. After finding the intended cluster (step 2) the location can be determined by measuring the distance of the cluster from the reference edges or center of as indicated in figure 3.1 (step 3).

3.6 Post-processing of AFM-acquired images

Image leveling process

All acquired images of AFM, particularly the height images which are required for statistical analysis were initially processed by Gwyddion software. To do this several stages were applied in this order: removing the strip noises, removing the horizontal lines, leveling in flatten base, removing the background (in case of cell roughness analysis), fitting the plane to zero value, and finally selecting the appropriate color spectrum to display the bacterial cell and features.

In following we will show a two essential stages of leveling the AFM height images. As demonstrated in figure 3.2, flattening the images enables us to visualized interesting bacterial substances and intercellular materials around the cells (see the inset) and provide real value of cell parameters. The red arrows point to the cell profile distance from the substrate before and after flattening the image.

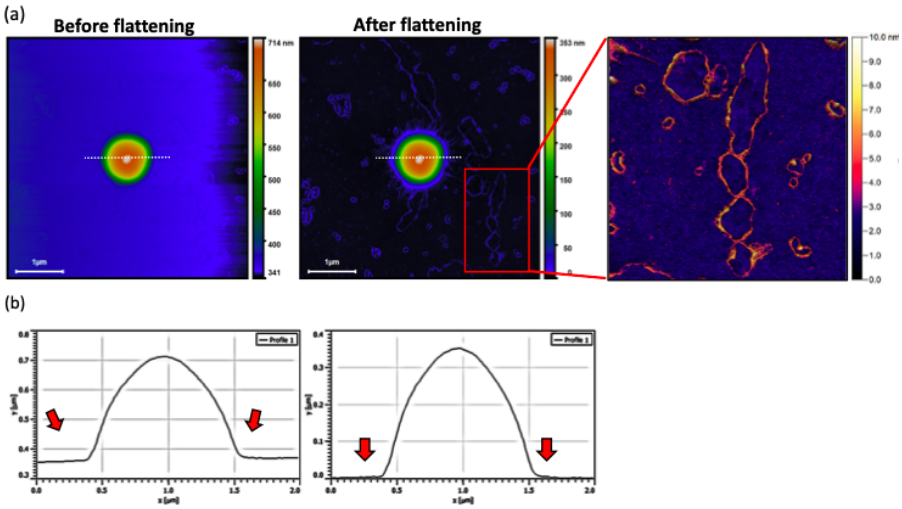

Figure 3.2: The first level of image flattening of air-dried *A. baumannii* ACICU (a) and the respective cell profile before and after leveling (b).

There are several leveling modes that can be selected and applied depending

of the obtained image as shown in figure 3.3, the image distortion or tilt can be remove by plane leveling.

The effect of growth medium like BSA in figure 3.3 can be reduced considerably to avoid unreal cell height, arising from the substances exists on the substrate and the distorted substrate (see the arrows). All the above surface leveling modes are applied to all the obtained images to make them ready for analyzing.

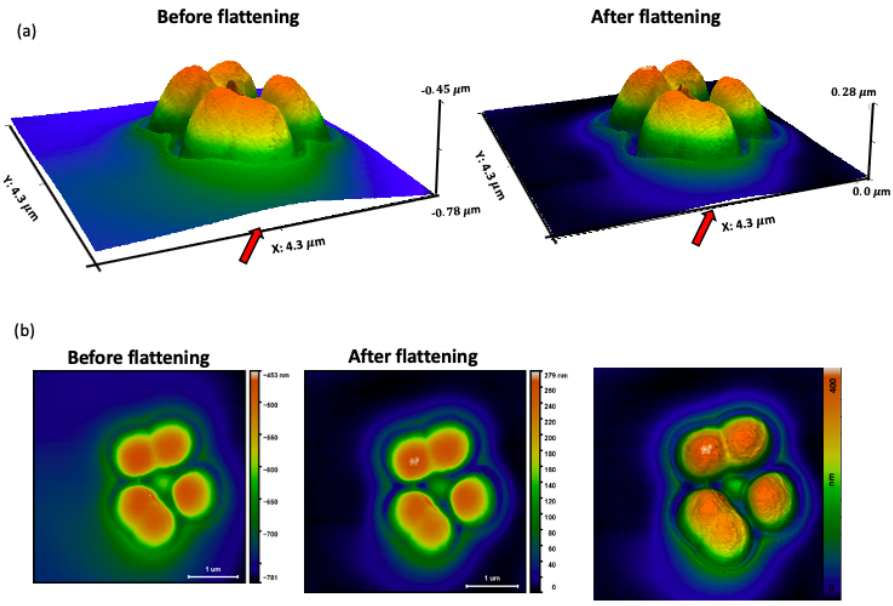

Figure 3.3: A 3D images of air-dried *A. baumannii* ACICU in Bovine Serum Albumin (BSA) medium to distorted cell surface before and after leveling (a) with a 2D image after processing (b).

Figures 3.2 and 3.3 represent the importance of image leveling in terms of cell morphology clarity and precise data analysis.

Determination of biophysical parameters of cells

Cell dimension After leveling the AFM height images, in order to measure the real biophysical parameters of cells, we performed a metrological analysis of the cell dimensions, volume, surface area, and surface roughness. For instance, we indicated the *A. baumannii* ATCC 19606 cell dimensions by plotting the lines over the cell surface as shown in figure 3.4.

The elongated horizontal axis is assigned to the cell length (L), which represented in white color, and the short horizontal distance, in red color, is considered as the cell width (W) in figure 3.4.

Since the AFM images are flattened, so the vertical axis in each of the length and width profiles represented the cell height (H), demonstrating by the blue dashed-line in profile1 of figure 3.4.

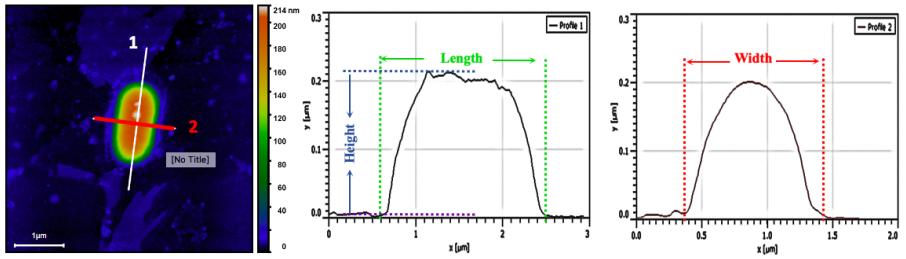

Figure 3.4: Characterization of *A. baumannii* ATCC19606 cell length (white solid-line) corresponds to the distance of green lines in figure 3.4, cell width (red-solid line) represented by profile 2 and bacterial cell height.

Notably, Cell surface depression and pore depths were measured from the highest protruding rim, the cell surface, relative to the lowest concave edge according to the plotted line.

Cell volume and surface area Thanks to Gwyddion software, enabled us to measure the cell-volume and cell-surface by applying a mask to the entire cluster, over a single-cell and even on the individual cell in a cluster. The ratio of cell surface to volume give us many important information about the biological properties of the bacteria.

Figure 3.5 shows different size of the mask on bacterial cells from the entire cluster to even doubling cells (C2). In fact, the cell-volume represents somehow

the space occupied by the intracellular materials, which can be interpreted as a set of curves, each belonging to one pixel in the XY plane.

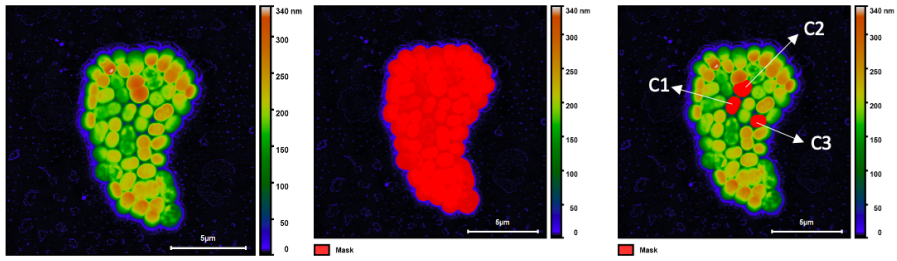

60 Cells in total	
Volume (µm³)	12.0
Surface (µm²)	68.3

	C1	C2	C3
Volume(µm³)	0.188	0.312	0.188
Surface(µm²)	1.060	1.217	0.876

Figure 3.5: Measuring the cell volume and surface by applying the mask with Gwyddion software.

Cell surface roughness The surface roughness was obtained by measuring the root mean square (RMS) of flattened images in the scale of 400 nm×400 nm for at least ten different areas of each cell and made an average on them. Figure 3.6 demonstrates the flattening and removing the background of bacterial cells to obtain the cell roughness. Because of the small size of the cells and depression in *A. baumannii* ACICU cells, it was essential to remove the background and flatten the image to obtain a real cell surface for roughness measurement.

The procedure of removing background of bacterial cell image is indicated in figure 3.6 along with the surface roughness before and after a background removal.

Statistical analysis : All the AFM data are reported as an average of at least 25 to 50 cells, analyzing ± standard deviation error (SD), unless otherwise indicated.

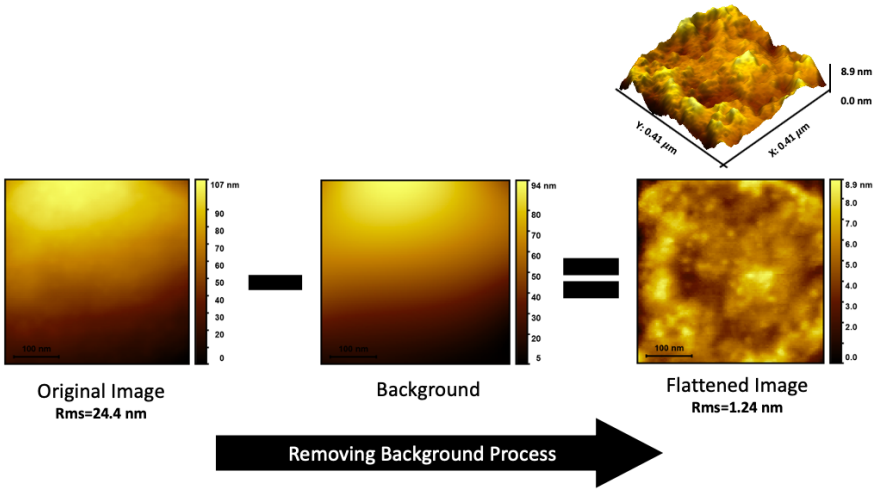

Figure 3.6: The AFM background removal of bacterial cell surface in order to measure the cell roughness (Rms)

Chapter 4

Growth factors-dependent *A. baumannii* ACICU morphology

In the first chapter, we introduced *A. baumannii* as a gram-negative bacterial pathogen with a peculiar ability to survive on dry surfaces, which contribute to a range of nosocomial infections. With particular attention to the targets of desiccation damage, we reviewed the structure of the gram-negative cell wall and its components in addition to the amount of cellular water distribution. Considering the basic function of the cell wall, which is the main barrier against the environment1 and confers the bacteria their shape, it is clear that cell morphology alteration may be correlated to the cell survival (Harding et al., 2017). Indeed, it has demonstrated that the bacterial cell morphology, can be influenced by many environmental features (Jacobs et al., 2012) such as transition under the growth phases (Soon et al., 2011), growth and re-hydration mediums (Morgan et al., 2006), nutrient levels (James et al., 1996), bacterial culture conditions (Gupta et al., 2016), and significantly by desiccation methods (Potts, 1994), which in turn cause multifaceted stresses to the bacterial cells (Van Teeseling et al., 2017).

Interestingly, it has been observed a large variance of the desiccation resistance among different *A. baumannii* strains, with isolates adapted to the hospital environment being more resistant than laboratory strains (Giannouli et al., 2013), such as the prototype of the International Clone II *A. baumannii* ACICU that has been selected to study the effect of desiccation and osmotic stress (Iacono et al., 2008). However, most of these morphological investigations have been conducted on *A. baumannii* ATCC19606 strain, with no data

on *A. baumannii* ACICU reported, insofar.

In order to bridge this literature gap, in this section, we employ the ultra-fine resolution and physical sensitivity of the AFM technique (Scheuring and Dufrene, 2010; Viljoen et al., 2020) to characterize the *A. baumannii* ACICU bacterial cell morphology as a function of their growth phases, growth conditions, and preserving media. We then search for a correlation between the cell shape changes and these biophysical parameters and how the shape impacts its clonogenic capability. We subsequently investigate the effect of desiccation stress on the cell morphology and survival capability, as a function of their growth phase and conditions. Finally, we shall see how the bacteria morphology is influenced by the preserving medium.

4.1 Growth phase-dependent morphology

It is well-established that the growth phase is associated to physiological and metabolic states of the bacterial cell, from the cell division in the logarithmic phase to nutrient starvation in the stationary phase (Cabeen et al., 2005; Rodriguez et al., 2008). Owing to the dynamic nature of the outer cell membrane and its components that continually developed during cell growth, there exist dependencies between cell shape to the velocity of their growth and division. Nonetheless, the morphology of *A. baumannii* ACICU at different growth phases and their response to desiccation have yet to be thoroughly characterized and understood. Hence, we aim to explore the effect of growth phases on *A. baumannii* ACICU cell morphology, we have used AFM technique operating in peak force TM mode in ambient conditions similar to those found in hospital environment (relative humidity below 30% and temperature of $22°C$). The cell viability assays (Colony Forming units, CFU) were carried out before and after air-drying to determine cell survival to examine the response of cell morphology changes to desiccation.

Bacterial growth curve

In order to determine the different growth phases of *A. baumannii* ACICU bacterial cell, we initially obtained the bacterial growth curve. To do this, the bacteria were grown in LB medium under vigorous shaking in a flask at $37°C$, as explained in section 3.1. We monitored the evolution of bacteria for 48 hours by measuring the optical density (OD) absorbance at the wavelength of 600 nm. As shown in Figure 4.1A, we observe the occurrence of an early logarithmic (t_{growth} <1 h), logarithmic (1 h <t_{growth} <4 h), late-logarithmic (4

h<t_{growth}<6 h), stationary (6 h<t_{growth}< 32 h), and death phase (t_{growth}>32 h), under our experimental conditions. Accordingly, we assigned the bacteria to the logarithmic, late-logarithmic, stationary, late-stationary, and death-phase after 3, 6, 14, 24, and 48 hours of growth, respectively, highlighted by different color bands.

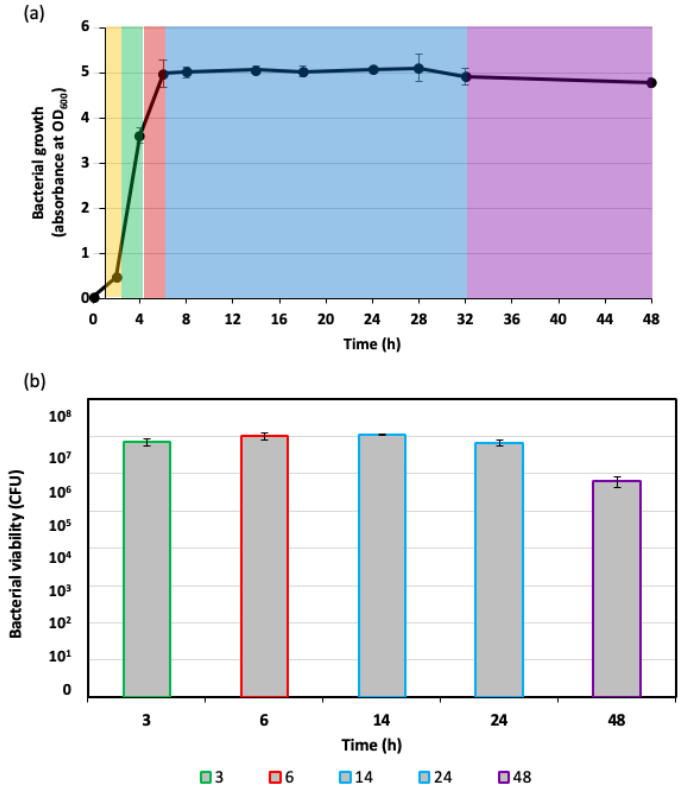

Figure 4.1: Growth curve of *A. baumannii* ACICU (a): indicating different growth phases in color; lag phase (yellow), logarithmic (green), late-logarithmic(pink), stationary (blue) and death phase(purple). The bacterial cell viability, according to each growth phase, was obtained employing the counting form colony units (CFU) by the relevant color of each phase (b).

We also assessed the bacterial cell viability at defined growth phases by

counting the number of colony-forming units (CFU) before air-drying, to examine the effect of growth phase on the survival of bacterial cells. Given the cell viability protocol, described in section 3.4, it is worth recalling that the viability of the cells at each growth phase was assessed using twenty μl of bacterial suspension adjusted to $OD_{600} = 1$, corresponding to 10^7 CFU. As indicated in Figure 4.1B, we observe nearly constant viability (approximately 10^7 CFU) in all the growth phases for the cells analyzed immediately after their extraction from the growth medium, except for those collected during the death-phase. Taken together, both growth curve and cell viability results suggest that this condition can be considered as an optimal condition for *A. baumannii* ACICU growth.

Morphological changes of the cell during growth

To investigate the cell morphology at different growth phase, we harvested an aliquot of bacterial broth culture for each growth phases and washed them with distilled water. Then a droplet of bacterial suspension was placed on a glass slide and allowed to dry under the laminar flow hood (see section3.1).
We performed the AFM measurements in ambient conditions (with relative humidity below 30% and 20-22°C temperature) using the peak force technique in ScanAsyst mode. (See sect. 3.2 for details). The height and peak force images are primarily used for carrying out the quantitative analysis and displaying surface morphology changes, respectively. In Figure 4.2 we show the AFM height and peak force images of *A. baumannii* ACICU cells at different phases of growth. The color bar in the height images represents a different height of bacterial cells (brown color for a low zone, like substrate, blue, and white colors for high zones), and is adjusted to the range of 0-540 nm in all the images to facilitate the cell height comparison.

From Figure 4.2, we observe a tendency of all investigated samples to condensate in clusters, with only a few sparse individual bacteria, probably due to the driving force of the evaporating water (similar to the coffee-stain mechanism). At the first look, the AFM height images show that *A. baumannii* ACICU cells in the logarithmic phase feature typically a larger height (blue color) as compared with cells belonging to other growth phases. After passing through the logarithmic phase, the height of *A. baumannii* ACICU cells decreased and remained nearly constant in the later growth phases. Moreover, we realize sizably larger cells in the logarithmic growth phase by visual examination of bacterial morphology in peak force images.

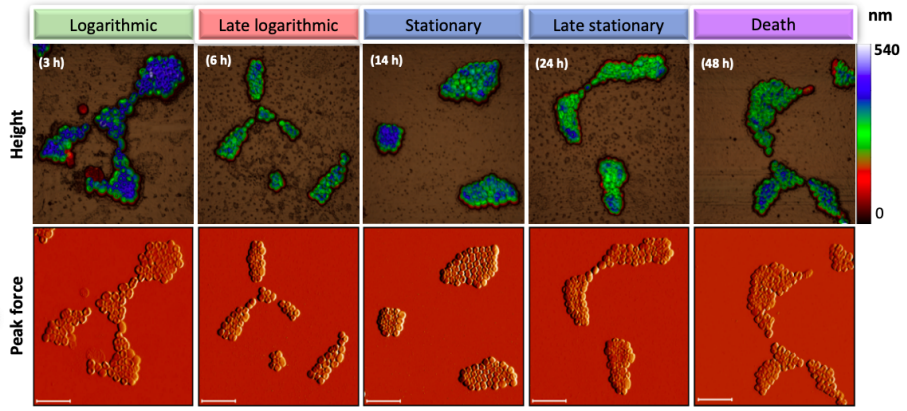

Figure 4.2: The AFM height and peak force error images of *A. baumannii* ACICU cell morphology at different growth phases. The color bar of height images is set to the 540 nm, and the scale bar is 5 μm.

Statistical analysis of cellular parameters To gain insight in the cell morphology, we have performed a statistical analysis of the bacteria length, width, surface, height, and volume. It is worth noting that the latter two quantities cannot be measured by means of other "standard" microscopy technique such as electron or light microscopy. The advance ability of AFM to provide three-dimensional data and images, enabled us to characterize all above biophysical parameters of *A. baumannii* ACICU bacterial cell as are summarized in Table 4.1.

The length and width parameters presented in this table were measured by a tool embedded in the Gwyddion software. For this purpose, cell length and width profiles are obtained by drawing a line respectively along the elongated and shortened horizontal axes. Likewise, the height of the cell was measured using the maximum vertical distance of the length (or width) profile to the substrate. More information on cell morphology is given by applying a mask over the individual cells in the cluster, providing cell-volume (3D) and cell-surface (2D) data from the entire cell.

As reported in Table 4.1, we realize that all cellular parameters decrease during bacterial growth. For all parameters, this decrease does not occur uniformly, nor at the same rate. To further address the cellular parameters changes, Figure 4.3 depicts the variation of cell surface area (as a function of L

Table 4.1: Cellular dimensions of *A. baumannii* ACICU at different growth phases

Growth phase	Cellular dimensions					
	Length (μm)	Width (μm)	Height (μm)	Volume (μm^3)	Surface (μm^2)	Surface/Volume (μm^{-1})
Logarithmic	1.29 ± 0.15	1.08 ± 0.11	0.397 ± 0.11	0.350 ± 0.06	1.090 ± 0.19	3.14± 0.40
Late-logarithmic	1.06 ± 0.14	0.90 ± 0.11	0.335 ± 0.04	0.201 ± 0.03	0.761 ± 0.16	3.79± 0.61
Stationary	0.96 ± 0.17	0.79 ± 0.10	0.375 ± 0.04	0.226 ± 0.06	0.677 ± 0.17	3.02± 0.31
Late-stationary	1.06 ± 0.18	0.88 ± 0.12	0.308 ± 0.06	0.203 ± 0.05	0.768 ± 0.18	3.86± 0.63
Death phase	1.15 ± 0.18	0.96 ± 0.13	0.316 ± 0.04	0.260 ± 0.04	1.008 ± 0.18	4.01± 1.12

& W) and the length-to-width ratio at different growth phases. In this figure, we can see that the cell surface changes occur in two different stages, divided by a dashed line. Initially, the cell surface decreases as the cell pass through the logarithmic phase and reaches the minimal surface and footprint in the stationary phase. Subsequently, the cell experiences an increase in the surface area at the late-stationery and death-phases. Furthermore, we notice that all the investigated *A. baumannii* ACICU cells show a coccus morphology in all samples, with an oval surface projection featuring an average length-to-width ratio of L/W=1.2 ± 0.02, which is growth-phase independent.

If the overall cell morphology is not observed to change, nonetheless, cells in the logarithmic phase have a larger volume, height, and surface. In contrast, the cells at the stationary phase characterized by a similar height, a sizably smaller volume and footprint. This indicates a more spherical coccus shape for the stationary cells, given the minimal surface to volume ratio observed, as compared to those of bacteria in the other growth stages.

In light of the CFU counts results above discussed, we can then argue that the cells having the minimal surface are associated to a higher resistance to desiccation. This observation is in line with the report of Madigan and his colleagues, suggesting that smaller cells can tolerate adverse conditions far better than the large cells (Madigan et al.,2015). Our findings confirm that the *A. baumannii* ACICU cells generally feature a coccus shape and particularly appear to be more spherical coccus morphology in the stationary growth phase. However, it is important to notice that we sporadically detected 4 μm-long rod-shaped cells in the logarithmic-phase stage, in agreement to other studies reporting a bacillus-like morphology for cells belonging to the rapid growth

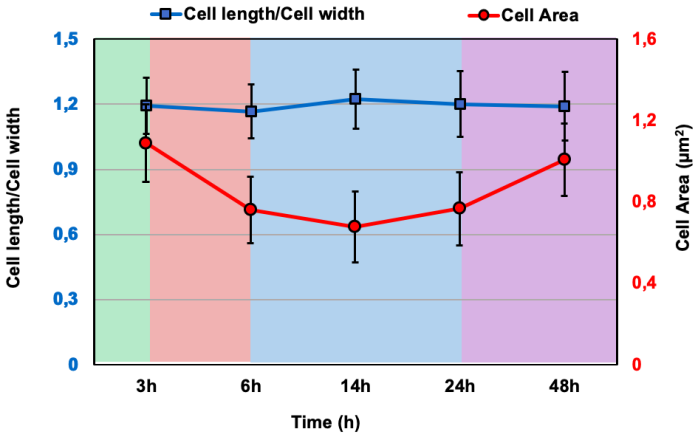

Figure 4.3: Statistical analysis of *A. baumannii* ACICU cell-surface variation during its growth phase.

phase (Public Health Image Library, 2012).

Figure 4.4 indicates an example of elongated-cells in the late-logarithmic phase indicated by black arrows. From the high magnification 3D rendering of a rod-shaped cell given in the inset, we can observe a sizeable lower height and a far larger footprint as compared to the surrounding coccus cells. To estimate the population of rod-shaped cells over the growth, we carried out quantitative analysis on more than twenty independent clusters for each phase. Based on the image analysis, the abundance of elongated-cells observed in the logarithmic growth phase $< 0.3\%$, increasing to $\sim 1.5\%$ in the late-logarithmic growth phase.

Interestingly, we detected no rod-shaped cell in the samples collected at incubation time longer than 6 h. After the logarithmic growth phase, the elongated *A. baumannii* ACICU cells surprisingly disappeared and not found in the stationary growth and dead phases. This phenomenon, disappearing the rod-shaped cells, might be explained by the fact that for a given amount of nutrients available to support growth, a larger population of small cells than of the large cells is possible, which in turn cause evolution (Madigan et al.,2015).

Our observations regarding the evolution of *A. baumannii* ACICU cells during the growth are in agreement with the studies on other *A. baumannii* strains, reporting the appearance of rod-shaped (bacillus) cells in exponen-

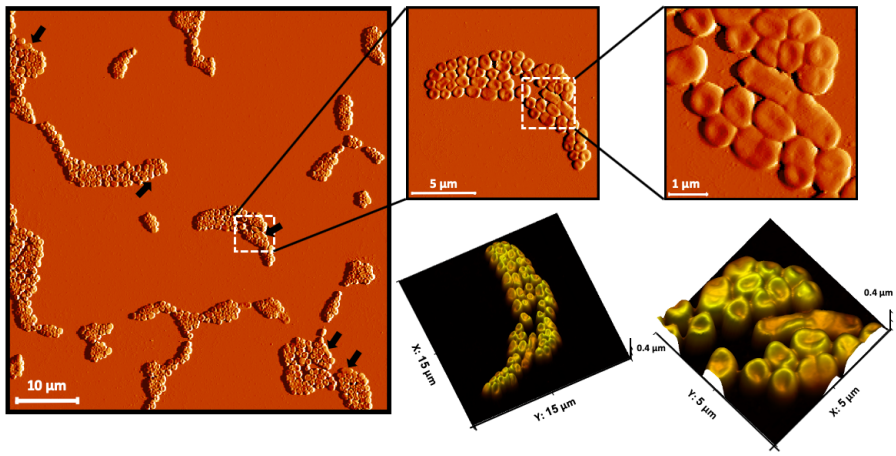

Figure 4.4: The population of rod-shaped *A. baumannii* ACICU cells at the late-logarithmic growth phase. The black arrows point out to the rod-shaped cells, whereas the white square shape zoomed the rod-cell in a high order of magnitude. Rod-shaped morphology displayed in peak force error and 3D images.

tial phase and more coccus shape in stationary growth phases (Potts, 1994; Madigan et al., 2015; Public Health Image Library, 2012).

Growth phase-dependent desiccation survival

The stresses that bacteria experience during the incubation and those stresses imposed by water removal from the cell, both contribute to a lesser resistance of bacteria against desiccation. In this section, we therefore evaluate the *A. baumannii* ACICU cell viability before and after air-drying at different growth phases by CFU counts, to analyze the effect of growth phase on desiccation survival of bacterial cells. The CFU measurements after desiccation allow to correlate the viability to the morphology results, simulating the exposure to air drying of the cells on the glass plate during the AFM scans.

We harvested the bacteria cell at different growth phases, washed them with distilled water, and adjusted to $OD_{600} = 1$. Twenty μl of bacteria suspension, corresponding to 10^7 CFU, was used for cell viability assessment before air-

drying, and the same amount of bacterial suspension was dried in the air to perform the cell viability after air-drying. Figure 4.5 demonstrates the survival rate of *A. baumannii* ACICU cells before and after air-drying as a function of the growth phase.

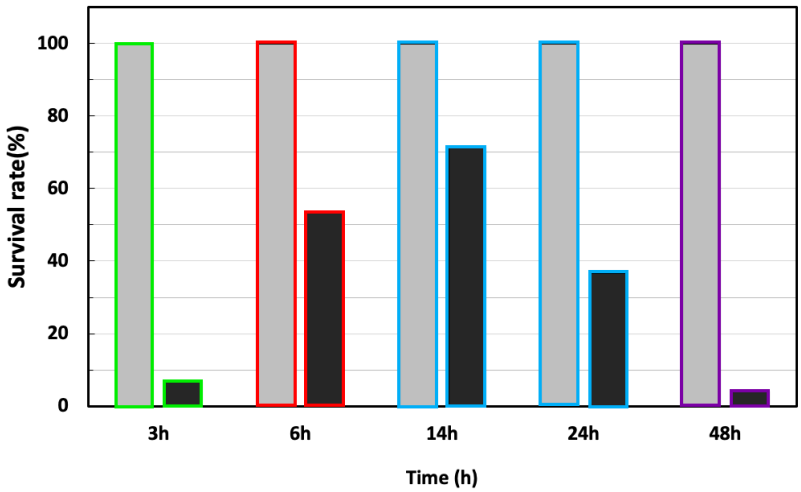

Figure 4.5: Desiccation survival of *A. baumannii* ACICU at different growth phases: before air-drying in the gray column, and immediate after air-drying in dark-gray.

As we discussed earlier (See figure 4.1), the viability for cells before air-drying at all growth phases is nearly constant and close to the maximum viability (i.e., 10^7 CFU), except for those cells belonging to the death-phase. The latter showed a one-log decrease in cell viability before drying. Therefore, in order to make a more tangible comparison between cell viability before air-drying and after air-drying, we calculated the percentage of viable cells after air-drying relative to the initial cell viability, i.e., $.10^7$ CFU, as demonstrated in Figure 4.5.

We observe from Figure 4.5 that the survival of the logarithmic phase cells after drying is significantly reduced so that the desiccation-induced stress causes a reduction of more than 90% in their viability. Conversely, we notice a slight decrease in the survival of the cells in the stationary phase after air-drying, with only a 30% loss of viability due to water-removal stress. These

results indicate that the logarithmic phase cells are highly susceptible to drying while the stationary phase cells show much better desiccation resistance than all other phases. Our findings are in accordance with the studies on other *A. baumannii* strains, stating that the cells in the logarithmic phase are more susceptible to desiccation (Farrow et al., 2018; Ziedler et al., 2018). As the growth phase causes structurally and physiologically changes in the cell, it may also enhance desiccation resistance. Hence, in the light of CFU results, we focus on the morphological analysis of AFM to find a correlation between the cellular evolution process and the survival of desiccation during growth. Given the cells at the stationary phase have a minimal footprint with the lowest surface-to-volume ratio and also indicate the maximum survival rate, we can conclude that the smaller cells can tolerate desiccation better, suggesting the shrinkage of the cells as a resistance mechanism to withstand desiccation.

Summary Observations showed that *A. baumannii* ACICU bacteria predominantly appeared as a coccus morphology with a length-to-width ratio of 1.2. In the logarithmic phase, the cells were found to be larger in size and height compared with other growth phases, however, bacterial cells became smaller as they reached the stationary phase, thereby occupying the lowest cell surface. On the other hand, analyzing the desiccation survival showed that the cells in the stationary phase are able to survive considerably against multi-faceted drying stress while logarithmic cells are highly susceptible to desiccation, reducing their cell viability by one log in CFU counts immediately after air-drying. Overall, the characteristic alterations of *A. baumannii* ACICU cell morphology during the growth, together with cell viability assessment, propose that the bacterial cell can enhance its ability to tolerate desiccation by reducing the cell surface. This finding, in turn, implies that factors that are important for desiccation tolerance in *A. baumannii* ACICU are regulated in a growth phase-dependent manner

4.2 Growth condition-dependent morphology

Bacterial cell morphology may also be influenced by other factors like temperature, oxygenation (Gupta et al., 2016), an abundance of carbon dioxide, light, pH (Morgan et al., 2006), relative humidity (Jawad et al., 1996), and the salt concentration (Carvalho et al., 2004) they experience during their growth (Chien et al., 2012). Indeed, shape drives the interactions between a bacterial

cell and its environment, and morphology modifications reflect the bacterial response to a given environmental change (Yang et al., 2016).

Consequently, after having discussed the influence of the growth phase on the morphology and resistance to desiccation of cells prepared in identical conditions, we now examine the impact on the cell morphology of bacterial culture conditions. Given the *A. baumannii* ACICU is an aerobic bacterium, we realize two extremely distinct growth conditions, in particular for what concerns the oxygen availability. To this aim, in addition to the vigorous flask-shaking used to prepare the bacteria discussed in the previous section, we investigate the cell viability and morphology of bacteria grown in tube-static conditions in which the amount of available oxygen is lesser than the flask-shaking ones.

Furthermore, as stated earlier, since most cellular changes during growth appear in the logarithmic and stationary phases, we design our experiments under different growth conditions focusing on these two phases. By doing so, we are not only able to monitor all cell changes in each growth condition but also allowed us to evaluate the effect of these two factors (i.e. growth phase and conditions) on cell morphology simultaneously. Hence, we initially need to obtain the growth curve of bacteria in order to harvest the samples at logarithmic and stationary growth phases.

Bacterial growth curve

We obtained the growth curves of the *A. baumannii* ACICU cells in flask-shaking and tube-static conditions using overnight bacterial culture broth. The bacterial suspension then refreshed 1:100 in a 15 ml tube containing 5 ml of LB and in a 350 ml flask containing 50 ml of LB and incubated at $37°C$ in static conditions or under vigorous shaking (250 rpm), respectively. The culture cell density was determined for 48 hours by measuring the absorbance of the cells at the wavelength of 600 nm ($OD_{600} = 1$) for both conditions.

The growth curve for flask-shaking conditions was previously shown in Figure 4.1A and discussed in detail in section 4.1. Figure 4.6, hence, displays the bacterial growth curve for the tube-static conditions in which each growth phase is characterized by a distinct color. It can be seen that the bacteria in tube-static conditions experience an exponential growth phase from 4h to 28h, describing logarithmic (4 h$<t_{growth}<$ 24 h) and late-logarithmic phases (24 h$<t_{growth}<$ 28 h). Conversely, the stationary growth phase, which lasts only 4 hours, occurs between 28 to 32 hours of growth (28h$<t_{growth}<$ 32 h). Hence, we harvest the cells in tube static/ flask-shaking conditions after 14h/3h and

30h/14h of incubation, corresponding to the logarithmic and stationary growth phases, respectively.

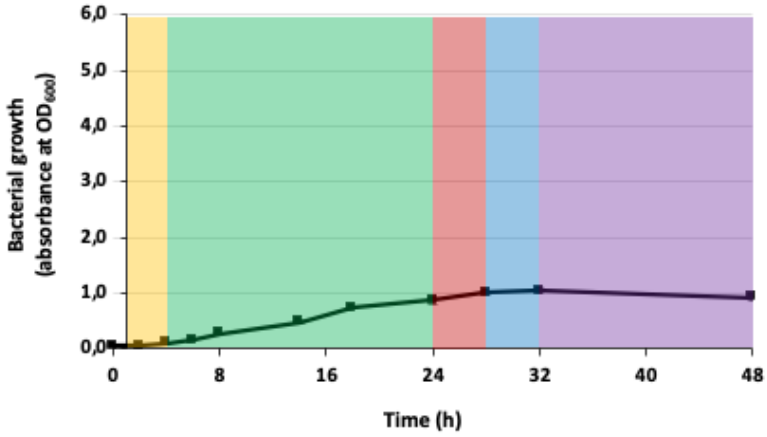

Figure 4.6: Growth curve of *A. baumannii* ACICU in static tube indicating different growth phases in color; lag phase (yellow), logarithmic (green), late-logarithmic (pink), stationary (blue) and death phase (purple).

The tube-static growth curve shows distinct dissimilarities from the flask-shaking growth curve, as immediately evident by comparison against Figure 4.1A. First, the obtained cell density for the bacteria, ca $OD_{600} = 1.5$, is 4× lower than that of the flask-shaking case. Furthermore, the cells in the tube-static conditions grow at a slower pace experiencing a rather long logarithmic phase of more than 24h, reaching the stationary phase after 30 hours of growth, i.e. at a time 5× longer. Given the higher cell density and the rapid transition of the cells from the logarithmic to stationary phase, these observations suggest the flask-shaking conditions as an optimal circumstance for *A. baumannii* ACICU cell growth.

Morphological changes under different growth conditions

We now move to the examination of the tube-static and flask-shaking prepared cells by employing the advanced AFM peak force technique operated in the

Scan-Asyst mode in the air. To validate our observations multiple images in different sizes are collected in several areas of glass slides. Figure 4.7 illustrates the AFM height and peak force images of *A. baumannii* ACICU cells grown under flask-shaking (panel A) and tube-static (panel B) conditions, for both logarithmic and stationary growth phases. At first glance, we notice the large decrease of cell height in tube-static conditions in comparison to the flask-shaking based on the color bar. We argue that this is not due to the death of the cells since we observe the opposite behavior in the flask-shacking ones, where the tallest cell observed belongs to the logarithmic phase characterized by a minimal survival rate after desiccation (see section 4.1).

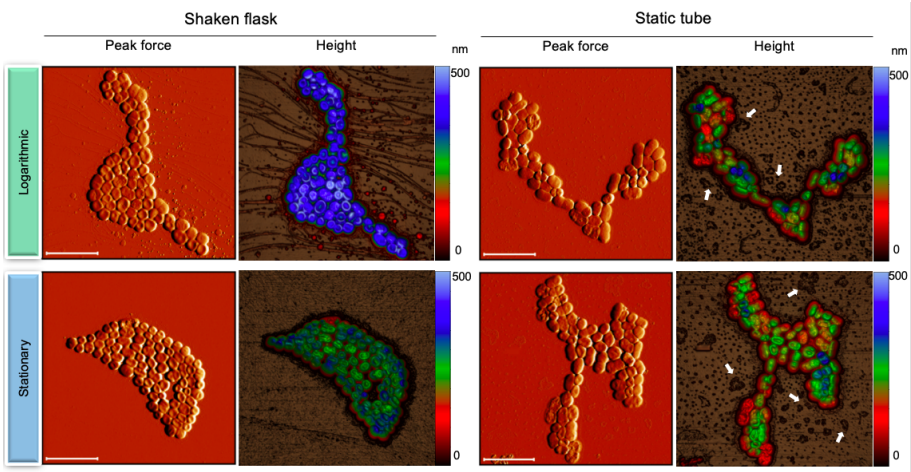

Figure 4.7: Comparison between *A. baumannii* ACICU bacterial cell at logarithmic and stationary growth phases, which grown in flask-shaking with average oxygen level (a) and grown in tube-static with low oxygen level (b). The height and peak force error images of AFM are employed by peak force scan-asyst mode.

On the other hand, further visual inspection of cells at different growth phases in flask-shaking (Figure 4.7A) and tube-static (Figure 4.7B) conditions expectedly shows that cell height decreases when entering the stationary phase. However, this reduction is more evident for the cells cultivated in flask-shaking. To give more insight into how the cell morphology changes under such cultivation conditions, we carried out a statistical analysis of bacterial cell biophysical

parameters, summarized in Table 4.2 for the tube-static and in Table 4.1 for the flask-shaking ones. The obtained results allow us to quantify in 2/3 the cell height reduction of the tube-static cells, 0.244±0.31, as compared to for flask-shaking, 0.397±0.11, in the corresponding logarithmic growth phase.

Moreover, quantitative analysis confirms our observations regarding a reduction of cell height during the transition from the logarithmic to the stationary growth phase, calculated as 8nm and 22 nm in tube-static and flask-shaking conditions, respectively. Another striking feature is the different shape characterizing the tube-static bacteria, which appear to be more elongated. From the quantitative analysis of the bacteria morphology (see Table. 2), we obtain a cell aspect ratio of L/W=1.6 implying elongated cells in tube-static conditions, which is comparable with those cells grown in flask-shaking with L/W=1.2, representing coccus cells (see table 4.1).

It is worth noticing that the morphology of the cells in the case of tube-static is also growth-phase independent. Moreover, closer scrutiny of the peak force images highlights the presence of a mild depression dividing the outer surface of the cells into two halves, as typical of diplococcus bacteria.

Besides, damaged and disintegrated rod-shaped cells with collapsed outer cell membrane can be observed in both phases of tube-static cells. In comparison, in the case of flask-shaking, the peak force images of the cells mainly indicate a coccus morphology with a slight depression in the central part of the outer cell membranes.

Table 4.2: Cellular dimensions of *A. baumannii* ACICU grown in static tube (ST)

Growth phase	Cellular dimensions					
	Length (μm)	Width (μm)	Height (μm)	Volume (μm^3)	Surface (μm^2)	Surface/Volume(μm^{-1})
Logarithmic	1.73±0.22	1.11±0.13	0.244±0.31	0.275±0.04	1.47±0.25	5.09±0.63
Stationary	1.67±0.30	1.05±0.12	0.232±0.25	0.263±0.05	1.56±0.32	5.50±1.28

All cell parameters in the tube-static conditions, similar to their counterparts in the flask-shaking, decrease with the bacterial transition from logarithmic to stationary phase except for the surface and surface-to-volume parameters that indicate the opposite trend. This is probably because the bacterium has spent a shorter time in the stationary phase and immediately enters the death phase, resulting in the cell collapse and subsequently increasing surface and surface-to-volume. Comparison between Tables 4.1 and 4.2 reveals that the

tube-static cells have larger lengths, width, and surface area than flask-shaking ones do, giving rise to a greater footprint for this set of cells.

On the other hand, in the case of the tube, the cells show a lower height and similar volume compared to the flask-shaking leading to a larger footprint and surface-to-volume ratio. In this respect, this value was calculated on average to be about 5.42 μm^{-1} in tube-static and about 3.02 μm^{-1} in flask-shaking conditions. In the following sections, we will argue that the larger footprint and surface-to-volume ratio may contribute to a lesser resistance to desiccation of cells prepared in tube-static.

The results of experiments show that the morphology of the bacterium can change under two factors of the growth phase and growth conditions. These changes can occur either in the cellular features or in the structure and shape of the cell. The cell analysis demonstrates that the bacterium basically retains its general shape when undergoing different growth phases, but this transition is necessarily accompanied by a decrease in cell height. For example, according to Tables 4.1 and 4.2, the decrease in height from the logarithmic phase to the stationary phase was measured from about 20 to 30 nm. On the other hand, cell changes under different growth conditions not only resulted in a much more pronounced decrease in height (about 150 nm decrease in tube length) but also affected the overall shape and structure of the cell.

As observed, the morphology of the cell alters from coccus in flask-shaking conditions to rod-shaped in tube-static. Consequently, these findings and observations indicate that bacterial growth conditions play a more determinant role in changing cell morphology than the growth phase does. It was therefore decided to get an insight into the cell surface features before studying the desiccation survival of the cells grown in tube-static and flask-shaking conditions.

Cell surface characterization In an attempt to scrutinize the impact of described growth conditions on cell surface features, we show in Figure 4.8, a high magnitude AFM peak force images (704 $\times$704 pixels per line) of prepared cells in the logarithmic and stationary phases by two incubation methods.

These images further highlight the difference in bacterial morphology obtained by flask-shaking and tube-static conditions. The visual inspection of the cell surface in flask-shaking (Panel A) evidence the presence of a smooth layer covering the bacteria and connecting them (see white arrows). This layer, which is absent in the tube-static case (Panel B), can be formed by polysaccharides and can play a role in enhancing the chance of survival of the bacteria under desiccation, protecting it from the harsh environment.

Instead, cells in tube-static conditions are found with two surface characteristics featuring a ripple structure and the cells with a smooth surface having pores on their outer cell membrane (see dashed circles).

These pores, to the best of our knowledge not yet reported in the literature, have an average depth of 20-30 nm and a similar diameter of about 100-150 nm, which are large enough to allow the leakage of intracellular material, such as proteins.

It is worth noticing that the observation of a very thin layer of materials left-over in the neighborhood of the tube-static cells, shown by black arrows in Figure 4.8, can be associated with the release of these intracellular materials. Panel C illustrates a high magnitude image of such materials releasing from the cells in tube-static conditions.

Cell surface roughness Additionally, we carried out the analysis of surface roughness (Rms) on at least twenty different bacterial cells in the area of 400 nm $\times$ 400 nm. The image processing for roughness measurements has been explained in section 3.6. Figure 4.9 displays representations of cell roughness in 3D-AFM height and the related probability density function (PDF) for both growth conditions. First, we identify small spherical particles with 30-40 nm in size in the case of flask-shaking (Panel A), pointed by arrows, which can be associated with cell proteins mostly found in the depression area of the cell outer membrane. The measured roughness shown in Figure 4.9 represents a normal distribution for all growth phases and conditions. Surface roughness for the cells prepared in flask-shaking conditions are distributed in a wide range from 0.5 to 4.5nm, with the mode in the class RMS=2 to 2.5nm and RMS=1 to 1.5nm for logarithmic and stationary growth phase respectively (a uniform class interval 0.5nm is used). On the other hand, for the roughness measured in tube-static cells characterized by a narrower range from 0.6 to 2.2 nm, the most probable value occurs in the class RMS= 1 to 1.2 nm for both growth phase. Furthermore, quantitative analysis shows that surface roughness decreases during cell evolution so that the average of this parameter varies from 2.23 nm to 1.94 nm for flask-shaking and from 1.22 nm to 1.11 nm for tube-static cells by the transition from logarithmic to stationary phase. Surprisingly, the acquired AFM images reveal a rougher topography with a ripple structure for tube-static cells on visual inspection (Fig. 4C). However, this apparent roughness is not reflected by quantitative roughness analysis, displaying a lesser surface roughness for tube-static cells compared to the flask-shaking conditions. This

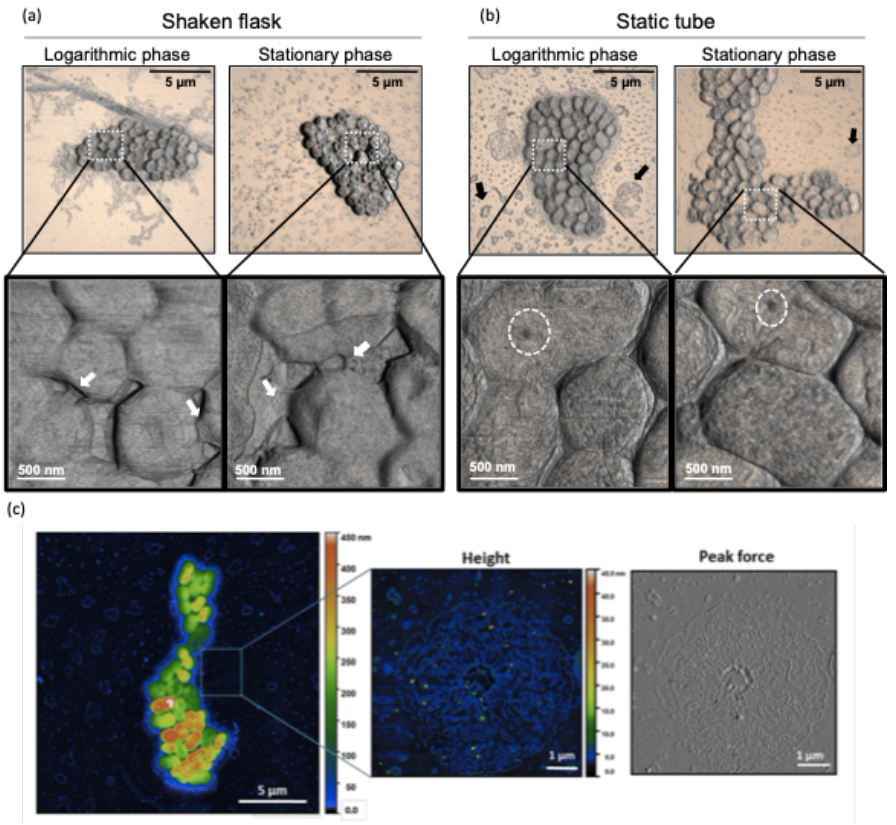

Figure 4.8: Cell surface alterations of *A. baumannii* ACICU strains depending on a different level of oxygenation during culture condition (a) in flask-shaking, (b) in tube-static, and intracellular materials surrounding the tube-static cluster (c).

contradiction between apparent surface roughness and quantitative measurement has also been reported for *A. baumannii* ATCC19606 by Soon et al. in 2009.

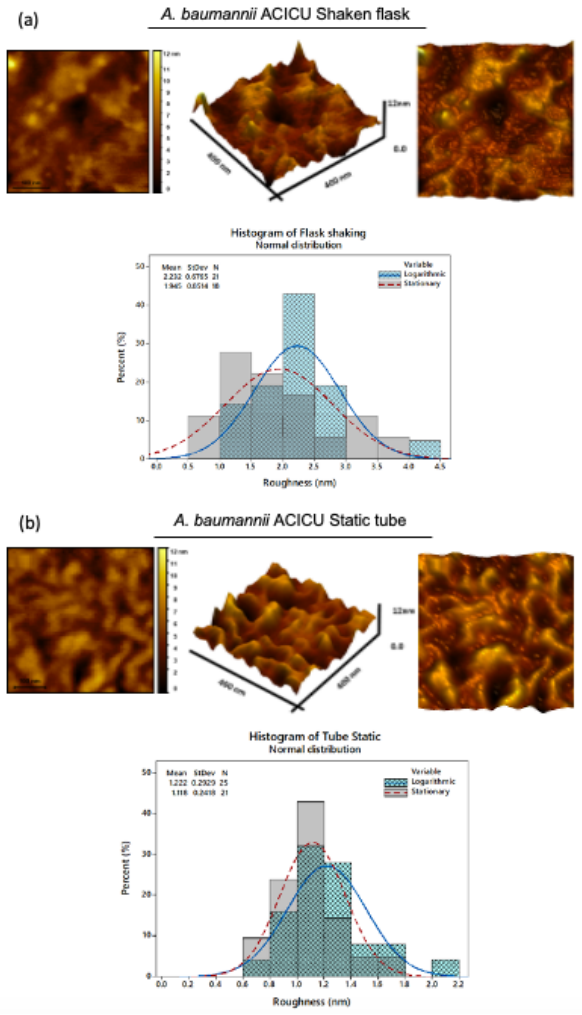

Figure 4.9: Cell surface roughness for the flask-shaking (a) and tube-static (b) growth conditions with the roughness distributions for both logarithmic and stationary growth phases.

Growth condition-dependent desiccation survival

To evaluate desiccation resistance of the *A. baumannii* ACICU cells grown in different conditions, we initially harvested the bacteria incubated in tube-static after 14h and 30h corresponding to the logarithmic and stationary phase in order to compare with the flask-shaking results obtained in section 4.1. In Figure 4.10, we demonstrate the cell viability assessment for the cells grown in both conditions before air-drying (in gray columns) and after air-drying (in black columns). As we demonstrated in section 4.1, for the flask-shaking conditions the bacterial cells in the logarithmic phase are found to be highly susceptible to desiccation, whereas the stationary phase cells tolerate desiccation much better (see Figures 4.5 and 4.10).

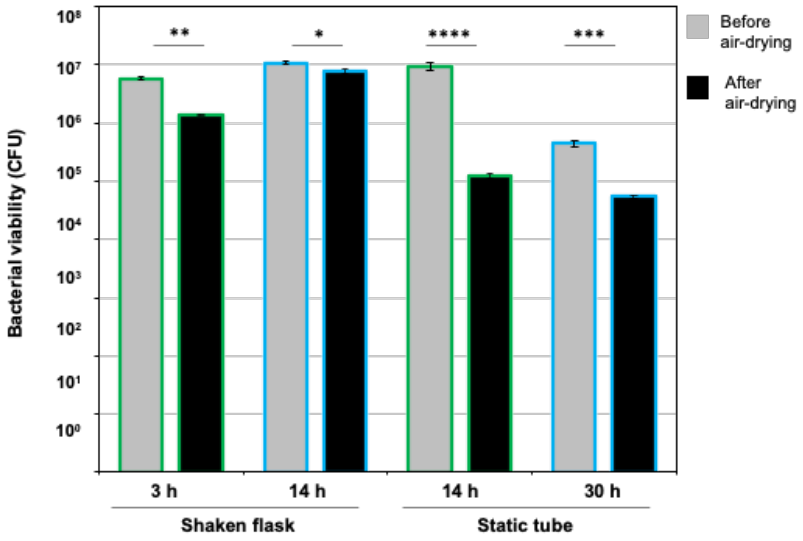

Figure 4.10: Desiccation response of *A. baumannii* ACICU cells grown in different culture conditions. Asterisks indicate statistically significant differences between before and after air-drying conditions (* P <0.05; ** P <0.01; *** P <0.001; **** P <0.0001).

For tube-static cells, the same pattern is observed (Fig. 4.10), where the cells display a decrease of 2- logs for logarithmic and one- log for stationary phase after air drying. It is worth noticing that the reduction of cell viability up

to ca, CFU=10^5 indicates a lesser resistance against desiccation which may be associated with the stresses that bacteria experience during the incubation. To better understand the effect of growth conditions on cell resistance to drying, we calculate the percentage of cell survival for tube-static conditions, similar to what shown in Figure 4.5 for flask-shaking cells.

The results reveal a desiccation-induced reduction of cell viability up to 99% and 88% for the logarithmic and stationary phases in the tube-static cells. These values can be compared with the corresponding viability of 90% and 30% for its counterparts in flask-shaking conditions. Interestingly, lesser survival desiccation of the tube-static cells is linked to their relatively larger footprint which correlates well with our observation stating that the stationary cells in flask-shaking have the highest desiccation resistance by occupying the minimal surface area. Given the significant decrease in cell viability after drying (up to ca, CFU=10^5), it is speculated that we may have observed dead cells in all cases except for those cells harvested at the stationary phase from flask-shaking conditions.

Summary Our results propose that the availability of oxygen in bacterial cultural growth plays an essential role in desiccation survival of bacteria, cell surface characteristics, and also changes in cell morphology. We notice that the *A. baumannii* ACICU cell morphology under different growth conditions can be altered significantly from coccus shape to rod-shaped cells depending on the high and low oxygen availability, respectively. It is found that bacterial cells grown in low oxygen levels(tube-static) undergo serious changes in their morphology such as decreasing cell height, cell elongation, and the emergence of cell membranes pores. Moreover, the inconsistency of apparent surface roughness with quantitative roughness value is another striking finding to report. Evaluation of desiccation survival shows that cells grown in low-oxygen availability are highly susceptible to drying, whereas those cells with adequate access to oxygen show better desiccation tolerance. We also demonstrate that a lesser desiccation resistance is linked to a larger cell footprint and surface-to-volume ratio. Eventually, comparing the cell morphology changes under the growth phases and different growth conditions reveals the latter as a predominant factor in cell modifications.

4.3 Bacterial mediums-dependent morphology

Recently, many studies have defined the effect of the growth medium, nutritional sources, and their relative protective agents on desiccation survival of the cells (Huang et al., 2015; Costa et al., 2000; Wang et al., 2019; Carvalho et al., 2004). Nevertheless, the role of different environmental conditions in bacterial cell morphology is still unclear. Therefore, here we intend to find out if various liquid solutions can change the morphology of *A. baumannii* ACICU cells or can even play a role in protecting the bacterial cells from environmental stress such as desiccation.

For this purpose, we use the overnight *A. baumannii* ACICU bacterial culture grown in LB under optimum growth condition, as described in the previous section 3.1. The bacterial suspension is washed twice with sterile distilled water and diluted to reach a final $OD_{600} = 1$ in different media such as LB, Casamino acid (CAA), Saline solution (0.9% NaCl), Bovine Serum Albumin (BSA), and sterile distilled water (see section 3.1). We employ the AFM peak force technique to scan the bacterial cell directly in their physiological conditions during desiccation. An aliquot of suspended bacteria in the above liquids is then poured on a glass slide and directly imaged by AFM technique in the first minutes of air-drying in such environments. Figure 4.11 displays the images collected by the AFM optical microscope immediately after water evaporation and before measuring the cells.

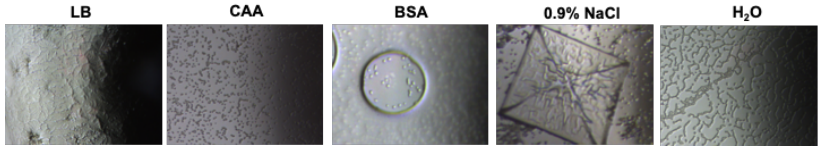

Figure 4.11: The optical images of the substrate surface (glass slide) covered by different liquid-solutions.

For cells suspended in the LB environment, leaf-like structures are formed on the sample substrate by drying in the air that sometimes is visible even with the naked eye. In the case of protein serum, a thin layer of BSA medium covers the cells so that the bacteria sink into it, except for the areas with bubbles shown in Figure 4.11. Drying in the air for the cells in saline solutions (NaCl 90%) is accompanied by immediate forming the huge salt crystals as soon as the water is evaporated. These large crystals are formed on the substrate

and visible without a microscope, making difficulties in cell measurement due to covering most cells and clusters (see a cubic crystal in Figure 4.11). In the case of CAA, we observe the cells mostly in single cells or small aggregation in contrast to the cells in distilled water, where the cells can be easily found in large clusters.

Cellular changes of drying bacteria in the physiological environment

In order to explore the protective role of different media on the morphology of *A. baumannii* ACICU cells, we performed the AFM measurements using scanasyst mode in the air immediately after water evaporation. The bacterial cells are monitored for 4 hours while drying in various physiological environments; the SFMSF approach (see section 3.5) is also used to follow the specified cell changes. It is worth noting that as the cells in the first minutes of imaging are not thoroughly dry, the scan rate must be decreased and adjusted to capture the cells accurately (to 0.4 Hz in our set-out). Figure 4.12, provides representative AFM height images of the drying process for two different *A. baumannii* ACICU cells in physiological LB medium.

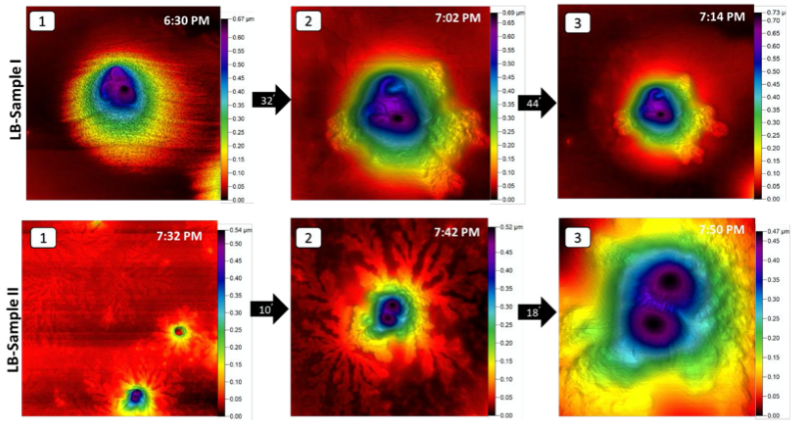

Figure 4.12: Drying process of *A. baumannii* ACICU in LB environments.

In the top panel, we observe the drying process of the bacterial cells in LB environments, surrounded by a mass of nutrients. One of striking results is

that by drying the cells, the mass of nutrients form leaf-like structures so that the bacterial cells are either trapped inside or covered by them. The panel below shows the distribution of leaf-like structures on the substrate with the cells placed at the center and top of these materials, making the cells appear taller. Cells are continually tracked for up to 4 hours, but no specific changes are detected due to the cell coverage by nutrients. Interestingly, we characterize the coccus morphology often without depression on the cell membrane for the cells suspended in LB. Given we prepare the overnight culture from the cells grown in LB medium under flask-shaking conditions, in section 4.1, this morphology was expected. The same measurement process was carried out for other liquid solutions, i.e., CAA, BSA, 0.9% NaCl, and sterile water. Similarly, the morphology of the cells in BSA and saline solutions not change over time, however, the latter prevent cells from being measured due to the creation of large salt crystals.

Morphology of suspended bacteria in different physiological environments

The morphology of *A. baumannii* ACICU cells in different physiological environments, along with the profile of cell changes in CAA and sterile water, is shown in Figure 4.13. What is evident from AFM height images is a remarkable difference in the height of the cells in various environments. The reason for the higher height of the LB and CAA cells can be attributed to the cells being placed on nutrients, whereas in saline solutions, the high cell height is due to the formation of crystals on the cell surface. Instead, the low height for the BSA cell caused by the BSA gel-like layer covering the sample substrate, rendering it inaccessible (see the red color around the cells). The lack of nutrients for the cells suspended in water result in low cell height, indicating the actual height of the *A. baumannii* ACICU cells.

By considering the alterations of *A. baumannii* ACICU cell morphology in various physiological environments relative to the cells suspended in water, we can recognize the protective role of liquid solutions in preserving the cells. As earlier stated, the cells in LB displayed a coccus morphology, most with an egg-shaped surface and some with depression in their outer membrane. Moreover, the nutrients formed a leaf-like structure and covered the cells during the drying process, as shown in Figure 4.12. In the case of CAA, the cells are observed in coccus and diplococcus morphology while surrounded by accumulated nutrients that formed capsules. The thick and long fibers among the cells are also detectable that seemed to connect the bacterial cells.

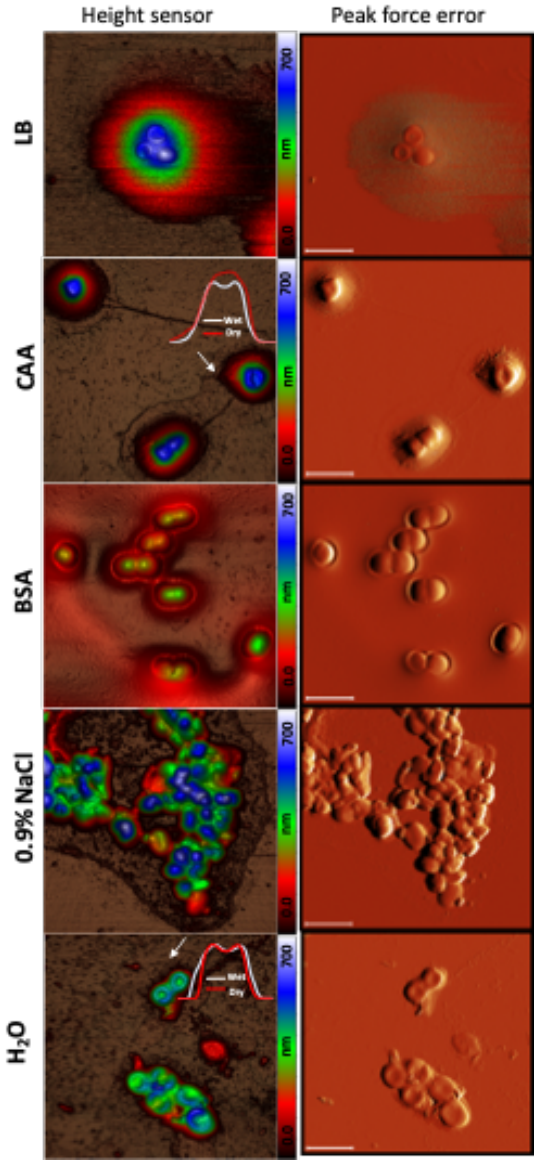

Figure 4.13: Morphology diversity of *A. baumannii* ACICU suspended in various liquid solutions.

Furthermore, we realize that the depression of the outer cell membrane restored after the cells were dried, which is evident in the cell profile before and after drying. This unexpected phenomenon was also characterized in other cells and might be related to the protective agents of CAA medium in capsules around the cells. Interestingly, we observed the phenotypic diversity of the cells in BSA protein serum, including diplococcus (in Figure 4.13), rod-shaped, and relatively elongated cells (from other images). Despite this diversity, all cells appeared with untouched morphology and without depression in cell membranes, whereas no changes were observed in their cellular features even after hours of drying. Measurement of the cells in saline solution (containing 0.9% NaCl) had a certain limitation for direct scanning the cells. Indeed, the formation of large salt crystals that had covered the sample substrate and cell surfaces caused difficulties in the imaging process. Examination of the *A. baumannii* ACICU cells suspended in sterile water, which suffered the lack of nutrients, showed the apparent depression in the inner part of their cell membrane with relatively low cell height. Moreover, during the desiccation process, the bacterial cells demonstrated a slight shrinkage in cell dimensions, as can be seen in the cell profile.

It is worth noticing that we observed the cells suspended in water in relatively larger clusters than the cells in LB, CAA, and BSA mediums that were mostly found either in single-cell or small aggregations. This finding is in accord with the study of James in 1995, who showed that the *A. baumannii* bacterial cells in low level of nutrients tend to aggregate in cluster form and remain firmly attached whereas in high nutrients show a dispersive behavior (James et al., 1996; Sutherland, 1998; Morgan et al., 2006).

Furthermore, in all LB, CAA, and BSA physiological conditions, we found the bacterial cells either in single-cell or small aggregations in contrast to the cells without nutrients (in water), which may be related to the higher nutrient-level. Taking to account all the above observations suggest that the most prominent morphological alteration in the absence of nutrients is the outer cell membrane depression, which is detectable in all cells suspended in water. Although the cells with depression in their outer membranes were randomly observed in other physiological conditions, all of the cells suspended in protein serum (BSA) displayed intact morphology. Particularly, it has been reported in the literature that Acinetobacter cells suspended in BSA survived longer on dry surfaces than cells suspended in distilled water (Jawad et al., 1996).

To the best of our knowledge, no attempt has been made yet to explore the *A. baumannii* ACICU cell morphology in protein serum (BSA) medium. However, further studies need to be carried out to investigate the protective

role of these mediums in cell morphology and desiccation survival. Another noticeable aspect of this experiment is the capability of AFM technique for operating in various environments, which has great importance and enables us to measure the bacterial cell directly in its biological conditions.

Summary Our observations are interesting in several aspects. First, by taking advantage of a particular ability of AFM, we successfully able to measure the bacteria cell in their environment. Second, we detect distinct morphology of *A. baumannii* ACICU cells suspended in protein serum (BSA) with an intact cell surface. The latter might be correlated with a different level of desiccation tolerance, as reported on literature by Jawad et al., 1994 a relatively better survival of *A. baumannii* strains in BSA protein serum.

The formation of the leaf-like structures surrounding the cells is another interesting result. The protective role of liquid solutions from cells against desiccation is characterized by comparing the morphology of the cells under different conditions with those suspended in water, which suffered from the lack of nutrients. An evident depression in the cell outer membranes is identified as the main effect of nutrient removal on bacterial cell morphology.

Chapter 5

The effect of desiccation-induced stresses on bacterial cell morphology

Desiccation expresses the removal process of water from cells that can occur either slowly or rapidly. The removal of the water from the bacterial cell, depending on the quantity removed, causes mild, moderate, severe water deficit (Potts, 1994). Therefore, desiccation imposes multifaceted stresses, including biochemical, metabolic, physical, and physiological stress on the bacterial cell that markedly impedes the function and survival of cells (Gayoso et al., 2013; Farrow et al.,2018; Lebre et al., 2017). Indeed, most bacteria cannot tolerate such stresses, however, a few of them can tolerate a water deficiency through the various physiological responses and resistant mechanisms, but our knowledge about the resistance mechanisms of the bacterial cell against desiccation stress is really poor.

It is documented in the literature that desiccation, in the level of the cell, leads to the shrinkage of capsular layers, changes in volumes of cell compartments, cell texture, and damage to external layers (e.g., pili, membranes). Given the important role of the bacteria cell wall in preserving the cell against desiccation and maintaining the cell shape, as the first barrier of the cell faced with the environment, it is becoming ever more important to understand how bacterial cells cope with desiccation.

A. baumannii has emerged as a global concern due to its peculiar ability to tolerate long-term desiccation on abiotic surfaces (Wendt et al., 1997; Jawad

et al., 1998, Giannouli et al., 2013), especially in hospital environments (Peleg et al., 2008; Rice, 2008). Studies over the past decades have provided important information on the desiccation survival of Acinetobacter species, most are focused on metabolic and biological features involved in bacterial desiccation tolerance (Jawad et.al, 1998; Giannouli et.al, 2013; Gayoso et al., 2013; Du et.al, 2017; Farrow et.al, 2018; Zeidler and Muller, 2018). Interestingly, it has been demonstrated that there is a large variance of the desiccation resistance among different *A. baumannii* strains; so that isolates adapted to the hospital environment, like *A. baumannii* ACICU strains as the prototype of the International Clone II, are more resistant than laboratory strains (Giannouli et al., 2013). So far, no studies have been conducted on the morphological changes of *A. baumannii* ACICU bacterial cells against desiccation.

Accordingly, in this chapter, we aim to scrutinize the morphological alterations of *A. baumannii* ACICU, as adapted bacteria to the environment, to desiccation with two main objectives. Firstly, we study the impact of different dissection procedures on the bacterial cell. Secondly, the prolonged desiccation effect on the bacteria that are exposed to such drying stresses will be addressed. We, therefore, designed a series of experiments in which bacteria are exposed to environmental stresses including osmotic (in water) and metric water stresses. To do this, the bacterial samples are prepared by keeping in water (hydrated), freeze-drying, and air-drying methods.

Bacteria maintained in water (hydrated sample) undergo osmotic stress and are exposed to air for a short time before conducting each measurement. On the other hand, freeze-dried and air-dried samples are subjected to desiccation, during which freeze-dried samples after the freezing process are dried slowly in a vacuum and the air-dried samples are dried in the ambient condition under a laminar hood and relatively faster. Additionally, to study the impact of prolonged desiccation, freeze-dried and air-dried samples are stored for two months in a sealed chamber with silica gel to control humidity and temperature, mimicking the hospital conditions. Conversely, the hydrated sample is maintained in water all the time and for each measurement, an aliquot of the sample is exposed to air given the experiment schedule.

We study the morphological changes of the bacteria being imposed such desiccation stresses by taking advantage of the AFM technique and evaluate their survival against desiccation in the light of cell viability assessment. Furthermore, we similarly examine the response of *A. baumannii* ATCC 19606 samples, as laboratory strains, to the same desiccation stresses in order to generalize and validate our observations.

5.1 Bacterial cell morphology under different degrees of desiccation

In order to investigate the morphology changes of *A. baumannii* ACICU under various drying methods, the bacterial cells are grown in the optimum condition, i.e. flask-shaking, and are harvested in the early stationary phase given our findings in section 4.1. Doing this allows us to study the response of cells that are relatively more resistant to desiccation. Then we prepare the samples using three different methods of drying, namely freeze-drying, air-drying, and maintenance in water (hydrated) that each imposes various degrees of environmental stress on the bacterium.

As described in section 3.2, briefly, the freeze-dried and air-dried bacteria are exposed to desiccation stress and respectively dry slowly under a vacuum and rapidly in the air, which in turn causes different degrees of drying stresses to these cells. Instead, cells maintained in water are mainly faced with osmotic stress and undergone drying stress for a shorter time. On the other hand, a review of the literature on the desiccation survival of *A. baumannii* strains, reporting that these cells can survive for 33 days on dry surfaces in simulated-hospital conditions (Jawad et al., 1996).

Therefore, we conduct our experiments in a two-month schedule and store all samples in a chamber containing silica gel to mimic the hospital environment by controlling the humidity below 30% at 22°C temperature.

To provide an identical experimental condition for all drying methods, as stated in the section 3.1, we prepare a separate sample at each time point of the measurements. After desiccation, the samples are placed in a covered Petri dish and stored for two months in a chamber equipped with silica gel to control humidity. Bacterial cells are captured using scan-asyst mode in the air with the scan rate of 0.4 Hz (for the hydrated sample) to 1 Hz (for the freeze-dried and air-dried samples) and a pixel number of 512 $\times$ 512 per line.

Figure 5.1 shows an example of morphological changes of *A. baumannii* ACICU cells at 1h, 6h, 24h, 48h, 72h, one week, two weeks, three weeks, one month, and two months intervals, under various drying methods. We recognize a decrease in the cell height for all samples over time, particularly, after two months of desiccation, given that the color bar is adjusted to a constant value. However, this reduction of height is not identical for all samples, as the bacteria are exposed to different stresses in each drying process.

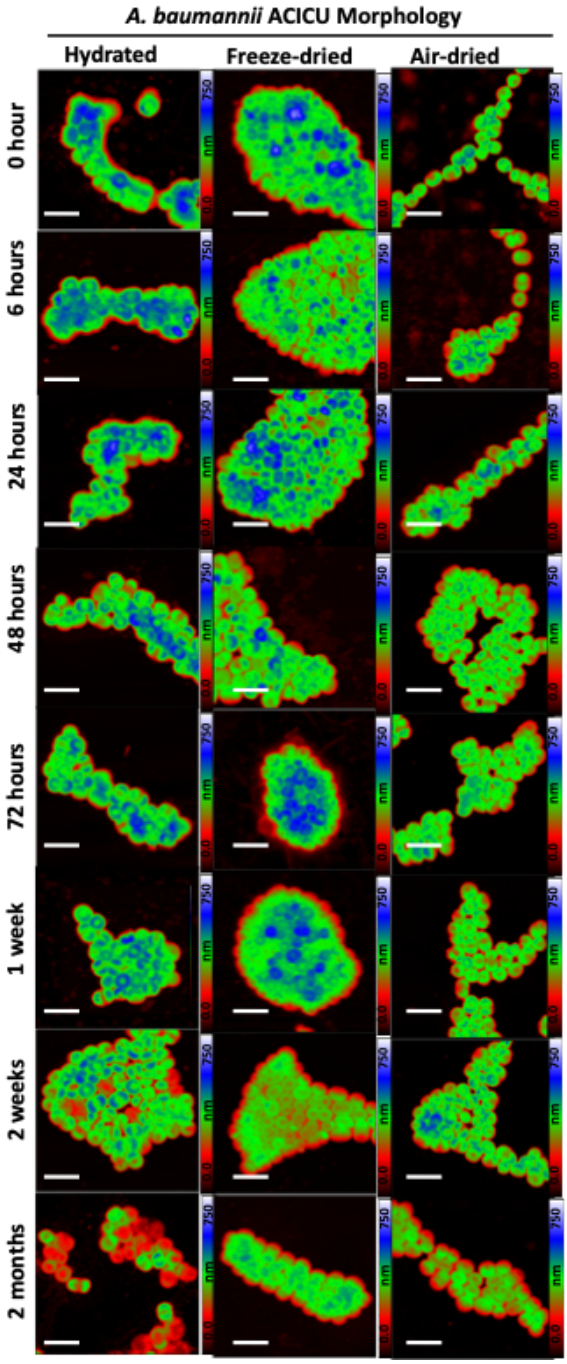

Figure 5.1: AFM image of dried *A. baumannii* ACICU morphology by maintaining in water, freeze-drying and air-drying methods during long-term desiccation.

A more detailed inspection of height variations shows that the hydrated cells have a higher height relative to the freeze-dried and air-dried cells at all measurement times, except for the sample that is measured after two months. We also notice that the freeze-dried cells form larger clusters compared to the hydrated and air-dried cells, which can be due to either slow drying under vacuum or freezing process. In addition, examination of peak force images, simultaneously captured for all the samples shown in Figure 5.1, reveals an intact morphology for the hydrated *A. baumannii* ACICU cells mostly having a mild depression in their outer membrane. In the case of freeze-dried cells, the presence of long and thick fibers around the clusters of cells can also be clearly detected (images will be shown later in detail).

Taken together all our observations from AFM height and peak force images, the most striking findings to address is strange and abnormal behavior of the cells after two months of drying. These cells having the intact morphology with considerably larger height throughout the drying period, suddenly show a sharp decrease in cell height and a damaged cell membrane after two months. Nevertheless, the visual inspection of the AFM images has not shown a significant change in the morphology and even height of the freeze-dried and air-dried cells after prolonged desiccation. First, we inquire about the morphological changes of *A. baumannii* ACICU cells under different degrees of drying stress to figure out how drying methods cause either damage to the cellular structure or alter it. Secondly, morphological alterations of these cells due to the prolonged desiccation needs to be examined by focusing on the cells in the first hours of desiccation and their changes after two months of storage. Eventually, the effect of various drying methods and prolonged storage under simulated hospital environments on desiccation survival of these cells will be evaluated by cell viability measurements.

5.2 The impact of environmental stresses on bacterial cell structure

To get a deep insight into the effect of drying methods on cellular structure, we compare the morphology of hydrated, freeze-dried, and air-dried cells at a specified time. The bacterial samples are selected after 24 hours of desiccation to draw a clear distinction between the hydrated cells and air-dried cells (see the materials and methods).

Figure 5.2 provides the visual inspection of the hydrated, freeze-dried, and air-dried cell morphology beside cell membrane deformation examination with

the AFM height and peak force images. From panel A, it is immediately evident that the hydrated cells display a larger height (blue color) compared to the freeze-dried and particularly to the air-dried cells (green-color).

We also realize the large depression in the air-dried cell outer membrane, however, given the height disparity in boundary cells, this structural deformation does not seem to be similar for all cells into the cluster. This discrepancy in the depression of the cell membrane between the central and boundary cells is also obvious in hydrated and freeze-dried samples. Hence, we perform a set of analyses on cell membrane deformations by drawing lines on the cell surface. Panel B illustrates the profile of the central and boundary cells, which are marked in panel A, relevant to hydrated, freeze-dried, and air-dried samples. It is worth noting that since the images are flattened, we can compare the cell length, height, and especially the depth of cell membrane depression among different dried cells.

The obtained results from Figure 5.2, clearly confirm our observations that the air-dried cells have a greater cell membrane depression than freeze-dried and particularly hydrated cells; that respectively measure at about 112 nm, 98nm, and 42 nm for the central cells. The boundary cells also follow the same trend as the central cells with more pronounced depression in their cell membrane.

Furthermore, by comparing the cell profiles it can be seen that the central cells reveal the symmetric depression in the center of the cell membrane, whereas the boundary cells are found with a tendency to stick to the inner clustered-cells. For more detail, in the area that boundary cells are in contact with the substrate, the lower cell height is detected, and on the other side where they are in touch with the inner clustered-cells, a more substantial height is observed. Another interestingly finding from the cell profiles is that regardless of the cell position, either central or boundary, the hydrated cells demonstrate a higher height above 500 nm, which is significantly higher than the air-dried cells with a height of less than 400 nm. On the other hand, freeze-dried cells by retaining their height similar to the hydrated cells (500 nm) and showing a deep cell membrane depression approximately 98 nm, which is comparable to the air-dried depression, display an intermediate behavior.

Taken to account all observations, there is a noticeable difference in cellular structures of hydrated, freeze-dried, and air-dried cells in terms of cell height and cell membrane depression as a consequence of various environmental stresses. Given that the hydrated cells are maintained in aqueous solution, they reasonably can retain more intracellular water. Therefore, such cells exhibit greater height and detect with mild depression in their outer cell membrane.

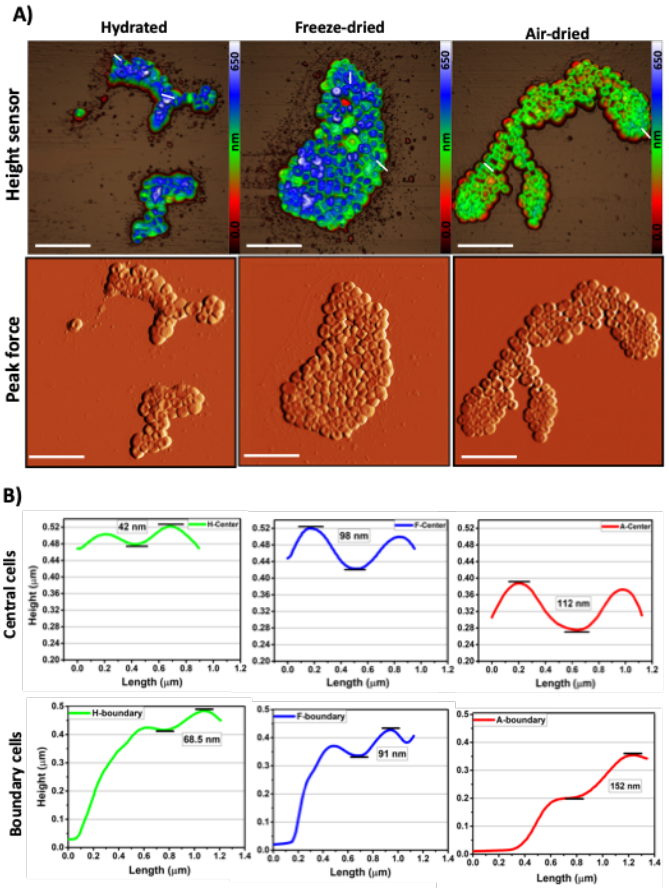

Figure 5.2: Desiccation impact on *A. baumannii* ACICU cell structure under various drying stresses through the freeze-drying and air-drying conditions, and for the hydrated cells under osmotic stress (A), the profile of cells in the center and boundary of the clusters with their outer cell membrane depression (B).

Before evaluating the effect of different drying methods on the desiccation survival of the cells, we first address the impact of long-term storage on the bacterial cell morphology under the simulated hospital environment.

5.3 The impact of prolonged desiccation on bacterial cells exposed to different environmental stresses.

A. baumannii ACICU

To further examine prolonged desiccation effects on *A. baumannii* ACICU cells that are prepared by various drying methods, we focus on the morphology alteration of the cells after two months of storage compared to the first hours of drying. Thus, Figure 5.3 illustrates the AFM height and peak force images for hydrated, freeze-dried, and air-dried cells at mentioned time points. From Figure 5.3, the hydrated cells are observed with larger height (in blue color) than freeze-dried and air-dried cells, as previously stated (see Figure 5.1). Subsequently, there is an apparent decrease in the height of all hydrated, freeze-dried, and air-dried cells after two-month of desiccation (Panel B). Surprisingly, despite that hydrated cells display a larger height consistently, their height decreases more further than other cells after two months. The hydrated cells, therefore, are observed as a group of cells that few of them appear with large height (blue color) and often with low height (red color), suggesting the collapse of the cells. This diversity in the cell height makes it difficult to visually compare the height of the hydrated cells with the freeze-dried and air-dried cells. Additionally, we detect leaf-like structures around clusters of hydrated cells, which can be associated with intracellular material leakage from the damaged cells. These leaf-liked structures are similar to what we observed around the *A. baumannii* ACICU cells that had been suspended in LB nutrients (see Figure 4.12).

Generally, we speculate that this stability in the morphology of freeze-dried and air-dried cells during prolonged desiccation may be due to the primary and rapid drying effect on the outer cell membrane whereas the vulnerability of the hydrated cells may describe the erosive impact of osmotic stress on their cell wall. It seems that maintaining the cells in water can cause weakness in the cellular structures such that they cannot morphologically tolerate desiccation stress much as freeze and air-dried cells. Subsequently, the hydrated cells lose their intracellular water further and dramatically over a prolonged time. To get a better understanding of the cellular changes, especially after long-time storage under dry conditions, we carry out statistical analysis for each sample summarized in Table 5.1. The average and standard deviation of the cell dimensions, volume, and surface parameters are calculated for more than 30 bacterial cells and reported at specified time points.

From the table above, we initially realize that the length and width of

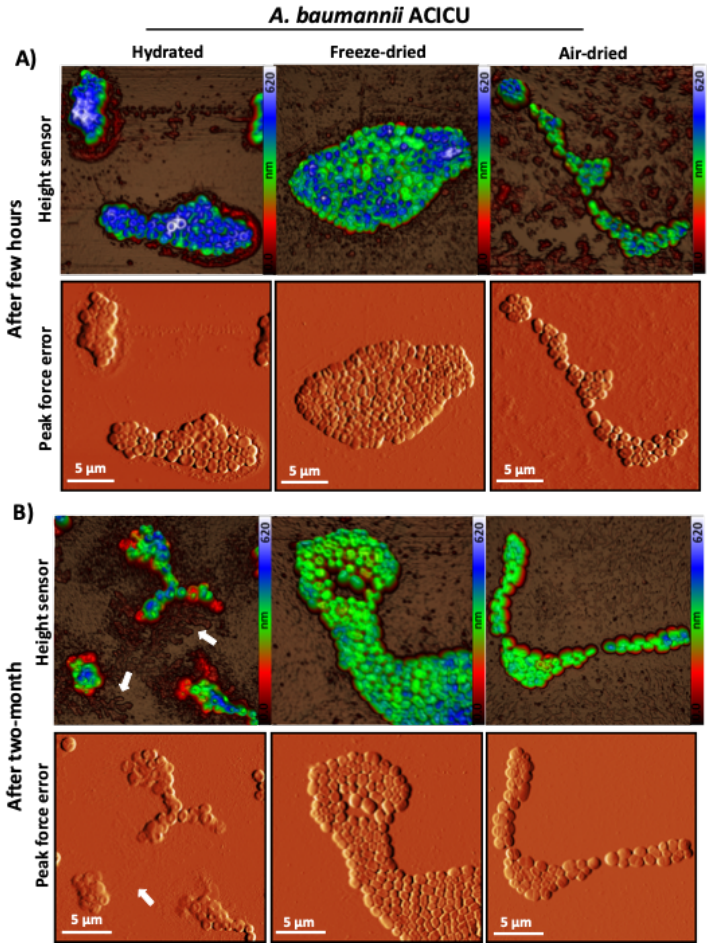

Figure 5.3: Distinction of hydrated *A. baumannii* ACICU morphology from the freeze-dried and air-dried cells subject to the long-term desiccation.

the cells in all drying methods are not changed during long-term desiccation, indicating a coccus morphology with the ratio of L/W=1.21 ± 0.05 for *A. baumannii* ACICU cells. A closer look at the data in Table 5.1 shows that the cell height in each of the drying methods decreases due to the gradual loss of

Table 5.1: Average cellular dimensions (± SD) of *A. baumannii* ACICU cells maintained in sdH2O, freeze-dried, and air-dried during the time.

***A. baumannii* ACICU cell characteristic parameters**						
Condition	**Time**	**Length (µm)**	**Width (µm)**	**Height (µm)**	**Volume (µm³)**	**Surface (µm²)**
Maintained in sdH_2O	0 hours	1.22±0.23	0.99±0.16	0.511±0.05	0.486±0.10	1.02±0.22
	6 hours	1.21±0.24	0.97±0.16	0.496±0.05	0.415±0.15	1.02±0.35
	24 hours	1.23±0.19	1.05±0.16	0.486±0.06	0.429±0.07	1.09±0.19
	2months	1.23±0.17	1.15±0.36	0.321±0.09	0.223±0.07	1.00±0.33
Freeze-dried	0 hours	1.22±0.30	0.97±0.28	0.456±0.06	0.336±0.07	0.97±0.12
	6 hours	1.20±0.27	0.98±0.25	0.437±0.04	0.275±0.05	0.96±0.25
	24 hours	1.21±0.26	0.98±0.13	0.412±0.05	0.298±0.05	0.95±0.18
	2months	1.23±0.18	1.02±0.17	0.342±0.04	0.237±0.04	0.92±0.23
Air-dried	0 hours	1.24±0.18	0.94±0.11	0.435±0.04	0.269±0.06	0.78±0.15
	6 hours	1.14±0.16	0.96±0.14	0.397±0.05	0.260±0.06	0.89±0.17
	24 hours	1.11±0.20	0.94±0.12	0.328±0.03	0.239±0.07	0.88±0.25
	2months	1.25±0.26	0.98±0.17	0.331±0.04	0.196±0.06	0.75±0.19

cellular water over two months. We also see that although hydrated cells always exhibit higher height than other cells, their height declines sharply after two months to 321nm, which is even lower than the air-dried cell height measured at 331 nm. This analysis confirms our observations regarding the morphology changes of the cells during prolonged desiccation. Another interesting result is that the cell surface parameter for each hydrated, freeze-dried, and air-dried cell does not change over time. As the cell surface remains constant, and the height of the cells decreases, the cell volume subsequently decreases over long-term desiccation as a function of these two parameters. Together, these changes lead to an increase in the surface-to-volume ratio, so that for the hydrated cells, this parameter is calculated to 2.12 μm-1 at first hours and 4.49 μm-1 after two months of desiccation, indicating a cell collapse. It is worth recalling that given our previous findings, we expect hydrated cells with the lowest surface-to-volume ratio to show the highest desiccation resistance compared to other cells, except for its cells after two months.

These observations will be examined further by cell viability assessment, but before that, we scrutinize cell volume variations as a main cellular feature that is significantly influenced by prolonged desiccation. To this aim, we calculate the percentage of volume variations for all hydrated, freeze-dried, and air-dried cells relative to their initial cell volume, as shown in Figure 5.4. A downward

trend of volume variation in all cells that can be attributed to the loss of cellular water during prolonged storage. But cell volume does not decrease for all cells with an identical ratio, which clearly shows the effect of different drying methods on cell volume.

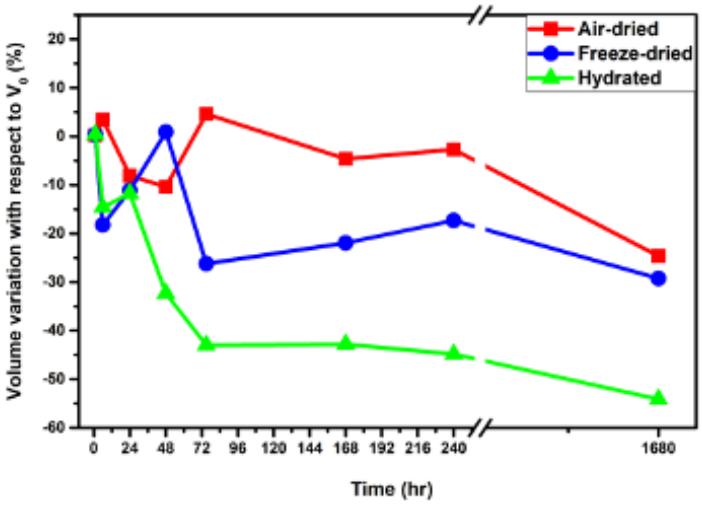

Figure 5.4: Cell volume variation of desiccated *A. baumannii* ACICU cells during two months.

Accordingly, given the data provided in the Table (4.3), the volume of hydrated, freeze-dried, and air-dried cells at the first hours of drying is 0.486 μm^3, 0.336 μm^3, and 0.269 μm^3 respectively, suggesting that the freeze-dried and in particular air-dried cells significantly lose their volume when exposed to air. Thus, the volume variations of these cells over the two months are comparatively less. Another interesting finding is that hydrated cells show the highest volume of the cells, nonetheless, we notice the largest reduction in the volume of these cells. As can be seen in Figure 5.4, the hydrated cell volume declines sharply up to 72 hours after desiccation, in which the hydrated cell volume is comparable to that of the air-dried cells, approximately 0.280 μm^3.

This result indicates that water cell maintenance leads to the preservation of cell volume for a limited number of days. Given that the main difference between hydrated and air-dried cells, in particular, in the first hour of desiccation (0 hours) is a short time that hydrated cells exposing to the air; thus,

the significant variations in their volume, which measured 0.486 μm^3 and 0.269 μm^3 respectively, implying the instant effect of desiccation on the bacterial cell.

Further analysis from Figure 5.4, reveals that each of the hydrated, freeze-dried, and air-dried cells respectively loss 54%, 29%, and 27% of their initial volume within two months of desiccation. Such findings, in the light of the AFM technique providing 3D data, indeed give us an insight into how much water the bacteria may lose during desiccation and allow us to calculate the amount of intercellular water.

A. baumannii ATCC 19606

After having discussed the impact of various degrees of desiccation on *A. baumannii* ACICU cells, we now examine the morphological response of *A. baumannii* ATCC19606 cells as laboratory strains in such environmental stresses to verify the accuracy of observations. For this purpose, similar to *A. baumannii* ACICU strain, the laboratory bacterial cells are grown in LB medium under vigorous shaking and incubated at $37°C$. The hydrated, freeze-dried, and air-dried cells of *A. baumannii* ATCC 19606 strains prepare with the same drying procedures described in section 3.2. We then store the prepared freeze-dried and air-dried samples in a sealed chamber with silica gel for humidity control (16 $\pm$4 % RH and 21$\pm$1°C) to examine the long-term desiccation effects on *A. baumannii* ATCC 19606 cells. The bacterial cell morphology is measured using the AFM peak force technique in specific time intervals of 1h, 6h, 24h, 48 h, 72h, 1week, 2week, one month, and two months. With the aim of closer inquiry into the effect of long-term desiccation in addition to the various desiccation stresses on *A. baumannii* ATCC 19606 cell morphology, we focus on the samples measured at the first hour and after two months of drying. Therefore, Figure 5.5 demonstrates the AFM height and peak force images of hydrated, freeze-dried, and air-dried cells that comparable to data presented in Figure 5.3 for *A. baumannii* ACICU cells.

Comparison of *A. baumannii* ATCC19606 cells at the first hours of drying allow us to study the effect of different drying methods on the morphology of the bacterium. At first glance, we observe that the air-dried cells have a lower height than other cells because they dried faster than freeze-dried cells and are exposed to air longer than hydrated cells. Conversely, the height of the freeze-dried and hydrated cells does not vary significantly. From the peak force images the *A. baumannii* ATCC19606 cells are typically identified as rod-shaped morphology with a length-to-width ratio of 1.78$\pm$ 0.11 (Table 4.4), whereas morphology diversity for this strain including coccus, coccobacillus,

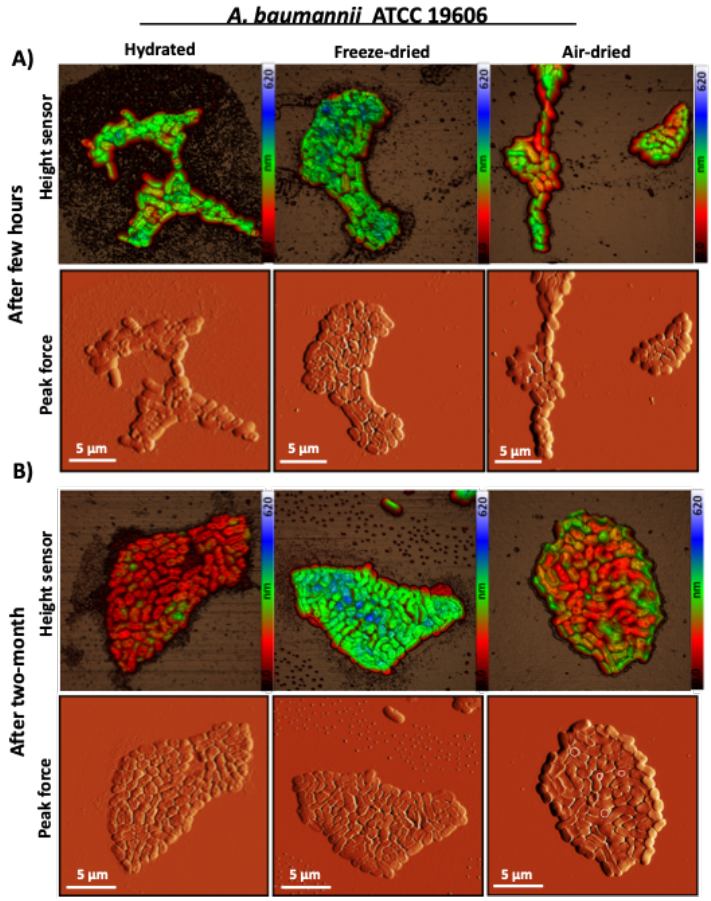

Figure 5.5: Morphological response of *A. baumannii* ATCC19606 to various degrees of desiccation.

and elongated forms is also detected in all the samples. In the case of air-dried method, the cells often deform and show an awkward shape so that the boundary between the cells is not clearly defined. Evident depressions in the cell membrane of freeze-dried cells are detectable, which may be attributed to the compression of these cells during the freezing process. Comparison of the AFM images obtained for *A. baumannii* ATCC 19606 at the first hours and

after two months of drying reveal the morphological response of the hydrated, freeze-dried, and air-dried cells to prolonged desiccation. Examination of the AFM height images display a significant decrease in the height of the hydrated and air-dried cells, while interestingly, there is no such drop in the freeze-dried cells indicating the ability of the cells to maintain their height.

Table 5.2: Average cellular dimensions (± SD) of *A. baumannii* ATCC 19606 cells maintained in sdH2O, freeze-dried, and air-dried during the time.

***A. baumannii* ATCC19606 cell characteristic parameters**

Condition	Time	Length (µm)	Width (µm)	Height (µm)	Volume (μm^3)	Surface (μm^2)
Maintained in sdH₂O	0 hours	1.78±0.42	0.89±0.12	0.288±0.03	0.298±0.06	1.25± 0.40
	6 hours	1.58±0.42	0.94±0.15	0.287±0.03	0.285±0.09	1.07±0.40
	24 hours	1.46±0.33	0.88±0.15	0.252±0.02	0.247±0.07	0.96±0.31
	2 months	1.63±0.40	0.90±0.13	0.199±0.03	0.171±0.06	1.07±0.37
Freeze-dried	0 hours	1.81±0.32	0.94±0.15	0.332±0.03	0.235±0.08	1.31±0.40
	6 hours	1.67±0.42	0.96±0.13	0.312±0.03	0.258±0.09	1.28±0.40
	24 hours	1.53±0.33	0.94±0.11	0.324±0.04	0.281±0.12	1.25±0.31
	2 months	1.67±0.46	0.95±0.12	0.351±0.05	0.273±0.11	1.07±0.37
Air-dried	0 hours	1.54±0.22	0.88±0.13	0.251±0.02	0.251±0.07	1.03±0.30
	6 hours	1.47±0.23	0.91±0.11	0.246±0.03	0.246±0.05	1.16±0.25
	24 hours	1.43±0.31	0.86±0.13	0.244±0.03	0.218±0.09	0.92±0.37
	2 months	1.86±0.77	0.96±0.15	0.227±0.03	0.238±0.04	1.31±0.28

More precisely, as reported in Table 5.2, the height of the hydrated cells decreases from 0.288± 0.03 μm at the first hours of drying to 0.199± 0.03 μm after two months. This change is equal to 0.251± 0.02 μm and 0.227± 0.03μ at the same time for the air-dried cells, respectively. Such more reduction in the height of the hydrated cells is mostly due to the osmotic stress applied to the cells when being preserved in water. In addition, the hydrated cells show a collapsed morphology characterized by the presence of intercellular material leakage around the cluster, which is very similar to our observations on *A. baumannii* ACICU hydrated samples. The effect of prolonged drying on the morphology of air-dried cells is identified by the appearance of pores on their outer cell membranes. Such pores which are indicated by white circles in the figure, suggest significant damage to the cell membranes that can be interpreted as a cell death sign. As the morphology of freeze-dried cells does not greatly change during long-term desiccation, it seems that *A. baumannii* ATCC 19606 cells are able to preserve their cellular structure under this drying method.

A closer look at Table 5.2 reveals that the cell's length, width, and surface parameters are independent of the long-term drying process, and indicate no noticeable change over time. In fact, the effect of prolonged drying is observed mainly by reducing the volume and height of cells, which is attributed to the removal of cellular water over time. These alterations subsequently result in an increase in the surface-to-volume ratio in all hydrated, freeze-dried, and air-dried samples for the *A. baumannii* ATCC 19606 species, which can contribute to cell disintegration. It should be noted that the reason that the changes in *A. baumannii* ATCC 19606 cell parameters do not exhibit a uniform trend can be related to the morphological variability identified in the measured samples.

5.4 Desiccation survival of *A. baumannii* under different environmental stresses

To clarify how desiccation stresses influence *A. baumannii* ACICU cells, besides the morphological investigation, we performed a cell viability assay by counting a viable formed colony (CFU) to examine the desiccation survival of these cells. Figure 5.6 compares the viability of hydrated (green columns), freeze-dried (blue columns), and air-dried (red columns) *A. baumannii* ACICU cells during long-term desiccation. It is clearly seen that the hydrated cells exhibit the highest ability to withstand desiccation so that the amount of CFU decreases by just half a log after two months. In comparison, the air-dried cells with a high sensitivity to drying lose their viability over one months, and practically no viable cells are observed in the second month of measurement. On the other hand, the freeze-dried cells, are able to maintain a relatively constant amount of CFU only 48h after drying; and after that time, they're losing their viability with a decreasing rate.

An unusual characteristic of these cells is that given the relative preservation of CFU up to two weeks after drying, which is more than the CFU of air-dried cells, the survival of the cells rapidly decreases so that no live cells are detected at the next measurement time point, i.e. after one-month desiccation. The effect of the stresses induced by desiccation is evident due to the different responses of the cells to drying. Within the first hours of desiccation, as air-dried cells are exposed to the air for complete drying, they lose their viability to a large degree, indicating an immediate effect of drying on cell survival. In contrast, the hydrated cells indicate a constant and highest desiccation survival and retain their viability over time, despite the significant reduction in their height after two months. Therefore, hydrated cells display inconsistency in

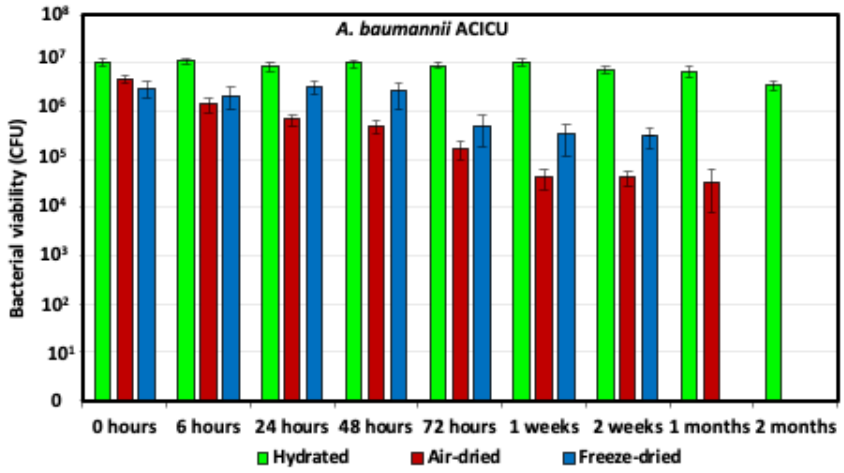

Figure 5.6: A graph of cell viability of hydrated, freeze-dried, and air-dried *A. baumannii* ACICU by counting the viable forming colony (CFU) assay.

preserving their morphological structure and corresponding viability. This may be due to the fact that long-term preservation of cells in a water solution contributes to the cell wall weakening due to osmotic pressure. Thus, as soon as the cells are exposed to air, the cell wall is unable to withstand the drying stress, resulting in cell collapse. To verify the preceding observations, we perform a cell viability assessment on *A. baumannii* ATCC 19606 cells. Figure 5.7 demonstrates a comparison of the viability of cells prepared by hydrated, freeze-dried, and air-dried methods.

At first glance, we see that the hydrated cells retain their viability for up to two months, however, they show a greater decrease compared to the *A. baumannii* ACICU cells within this period. This supports our earlier findings that preserving cells in aqueous solution contributes to longer drying cell survival. A decreasing pattern is clearly seen in the survival of air- and freeze-dried cells for up to a week, and after this time these cells lose their viability entirely. On the other hand, lower CFU levels in *A. baumannii* ATCC 19606 cells and loss of viability after two weeks suggest less desiccation resistance of these cells compared to *A. baumannii* ACICU cells, particularly for air-dried and freeze-dried cells. These results are in agreement with the findings reported in the

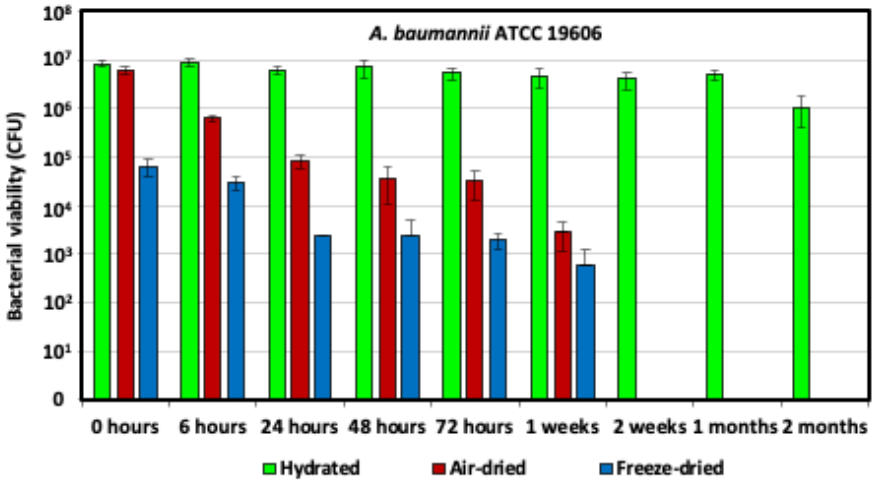

Figure 5.7: A graph of cell viability of hydrated, freeze-dried, and air-dried *A. baumannii* ATCC 19606 by counting the viable forming colony (CFU) assay.

literature. Furthermore, contrary to what is found with *A. baumannii* ACICU cells, we note that air-dried *A. baumannii* ATCC 19606 cells exhibit greater viability than freeze-dried once, suggesting that these cells are not able to survive well under freezing conditions.

5.5 Analysis of bacterial cell characteristics in single-cell form versus clustered cells.

While examining all the samples prepared by the methods described before, we found that the single-cells have a lower height than clustered cells, regardless of the sample drying procedure.

An example of this observation is given in Figure 5.8 that shows an AFM height image of hydrated ACICU bacteria in different aggregation mode including single-cells, small multicellular clusters, and large clusters.

It is clearly seen that the cells in the latter have a height of up to 650 nm which is considerably greater than single-cells whose height reaches a maximum of 350 nm. In order to find a reasonable correlation between the effect of the

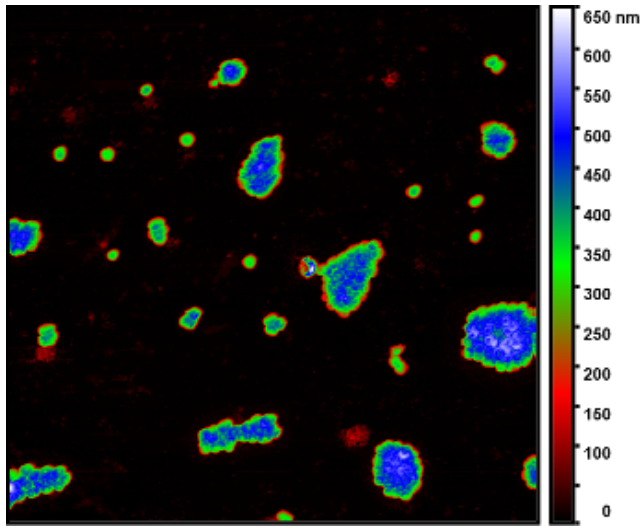

Figure 5.8: Distribution of *A. baumannii* ACICU cells in single-cell form, small and large cluster.

presence of a cell in a cluster and its corresponding cellular parameters and also to identify a general pattern of cluster-dependent cellular behavior under various environmental stresses, we perform statistical analysis on the cell surface and volume parameters for all three types of air-dried, freeze-dried and hydrated cells at two time points of 0h and 240h of desiccation.

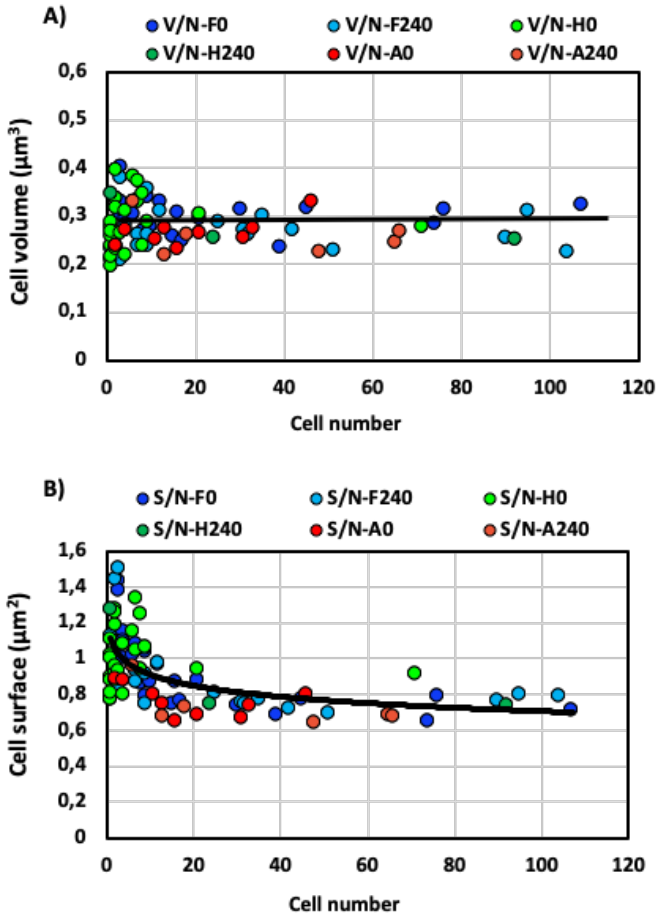

Figure 5.9: characterization of cell volume and surface depends on the size of the cluster. Panel (A) refers to the cell volume variation versus increasing the cell number in clusters, and (B) indicates the cell surface variations based on the cell number in clusters.

Figure 5.9 indicates the variations in volume (Panel A) and surface area (Panel B) of the cells as a function of the number of cells forming a cluster.

In this respect, in order to make a meaningful comparison between clusters of different sizes, we normalized the surface area and volume of each cluster by dividing them by the number of cluster cells. In these figures, the freeze-dried cells are blue, the hydrated cells are green, and the air-dried cells are red at 0h (dark colors) and after 240h (light colors) of desiccation.

According to the Figure 5.9A, it can be shown that the volume remains relatively constant with increasing numbers of cells in the cluster, indicating that the volume parameter is independent of the number of clustered cells.

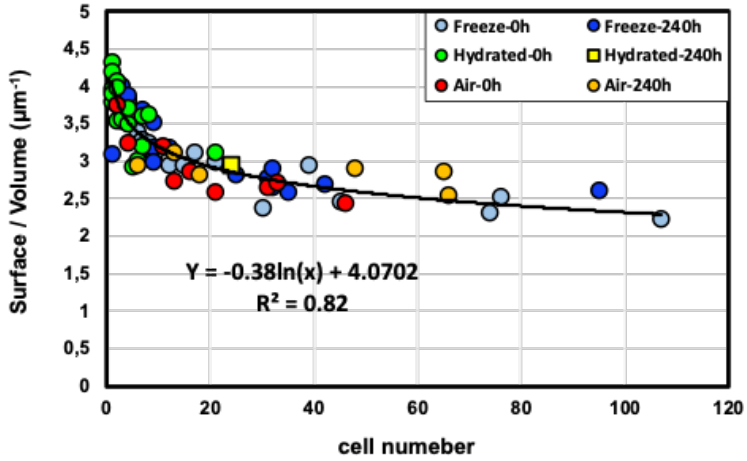

Figure 5.10: surface to volume ratio of *A. baumannii* ACICU cells from a single-cell state of an individual cell in a large cluster.

Nevertheless, volume variations are observed in small clusters (less than 10 cells aggregation) within the range of 0.2 μm^3 to 0.4μm^3, frequently associated with hydrated cells, indicating that the bulk of volume changes occur in single cells or small clusters. Figure 5.9B, on the other hand, shows cell surface changes against the number of cluster-forming cells. As shown, this parameter demonstrates a decreasing trend with increasing cell number, changing from 1.4 μm^2 for single cells to about 0.8 μm^2 for large clusters (more than 100 cells aggregation). It is worth noting that the lowest cell surface area is observed in air-dried cells with surface values of less than 1 μm^2. Such findings, consistent with work published in the literature, indicate that rapid drying of cells in the

air may contribute to their shrinkage (Potts, 1994; Lebre et al., 2017). As the cell's overall morphology depends on the simultaneous changes in surface parameters and their volume, it is, also, desirable to plot the variation of the surface-to-volume parameter as a function of cell number. The result is shown in the figure 5.10. The graph shows a gradual decrease in the ratio with the increase of cell numbers quite consistent with the variation of the cell surface (Fig 5.9 B), obviously owing to the presence of fairly constant values of cell volumes in the denominator of the surface-to-volume ratio (Fig 5.9 A).

In order to take all cellular morphological changing into account, regardless of desiccation methods, a regression analysis was used to quantitatively predict the variation of S/V versus cell numbers, yielding an exponential relationship with a determination coefficient of 0.82. The results show that the presence of cells in the cluster leads to a decrease in the cell surface-to-volume parameter as well as the cell footprint. Also, as shown in the previous sections, cells with lower footprint and surface-to-volume volume also exhibit higher drying resistance. It can, therefore, be inferred that the formation of large clusters of cells can be considered as a mechanism for cell resistance to drying

Chapter 6

The influence of storage conditions on bacterial cell changes

In addition to the long-term desiccation and different drying methods addressed in the previous sections, the condition of bacterial storage has also been documented to be a significant factor in the survival of bacteria (Jawad et al., 1996; Morgan et al., 2006; Mutlu et al., 2015). In this respect, Jawad et al. reported that the survival times for Acinetobacter strains at a higher relative humidity (31% and more) are longer than those for bacterial cells kept at a relative humidity of 10% (Jawad et al.,1996). This finding is consistent with the observed tendency of *A. baumannii* ACICU cells to survive on dry surfaces and hospital equipment, and they can be transferred under dry conditions in a hospital environment during nosocomial infection outbreaks. Most researches have therefore attempted to examine the Acinetobacter strains characteristics in a hospital condition by using either a variety of salt compounds or silica-gel for humidity control (Jawad et al., 1998; Espinal et al., 2012; Icardo et al.,2018; Zeidler and Muller, 2019). Given the importance of simulating such conditions for bacterial survival studies, in this section, we intend to explore whether long-term storage of bacteria with salt or silica for humidity control similar to hospital conditions has an impact on the bacterial structure. It is worth noticing that we implement a labeling technique named as SMSF approach allowing us to evaluate the morphology of a particular cluster over long-time storage in dry conditions.

6.1 long-term storage with salt under simulated hospital conditions

.

Studies over the past decades have provided important information on desiccation tolerance of Acinetobacter species, however, most of them suffer from poor morphological analysis of these strains over prolonged desiccation. Here, we initially examine the morphological changes of the *A. baumannii* ACICU bacterial cells, according to an instruction proposed by Jawad et al. (1998), who used salt for preserving bacterial samples to simulate hospital conditions. With this aim, the *A. baumannii* ACICU bacterial culture is prepared based on Jawad protocol (see section 3.3), and then desiccated bacterial cells are placed in the un-covered Petri dishes in an air tight transparent plastic box containing saturated salt solution ($CaCl_2 \times 6H_2O$) to maintain the humidity inside the box around 30% RH.

In order to examine the morphological changes of a specified cluster during long-term storage in dry conditions, we propose a novel approach to find, store, and re-find the same cluster at different interval time points. This approach, named SFMSF, is implemented by marking a glass slide to find an appropriate cluster in terms of size and to record the cluster distance from the substrate marks to find the intended clusters (see the material and method section 3.5).

The bacterial cluster is scanned employing the AFM Scan-Asyst mode on the air with the scan rate of 1 Hz under ambient conditions. We regularly perform the imaging process of the intended cluster over different time intervals, i.e., 1h, 6h, 24h, 48h, 72h, 1week, 2weeks, 3weeks, one month, two months, and three months after desiccation. After each measurement, the bacterial sample is stored under simulated hospital conditions in the presence of the salt for humidity control (RH 30% temperature 22°C).

Figure 6.1 shows the representative images of specified *A. baumannii* ACICU cell morphology at selected time points during three months of storage under simulated hospital conditions with salt. Based on the images obtained, the majority of *A. baumannii* ACICU cells are identified in rod-shaped morphology with a length-to-width ratio of 1.6; however, few of them appear in coccus type. The rod-shaped morphology is mainly associated with the growth conditions used to prepare the bacterial culture, highlighting the dependency of cell structure changes to growth conditions in line with our findings in the section 4.2.

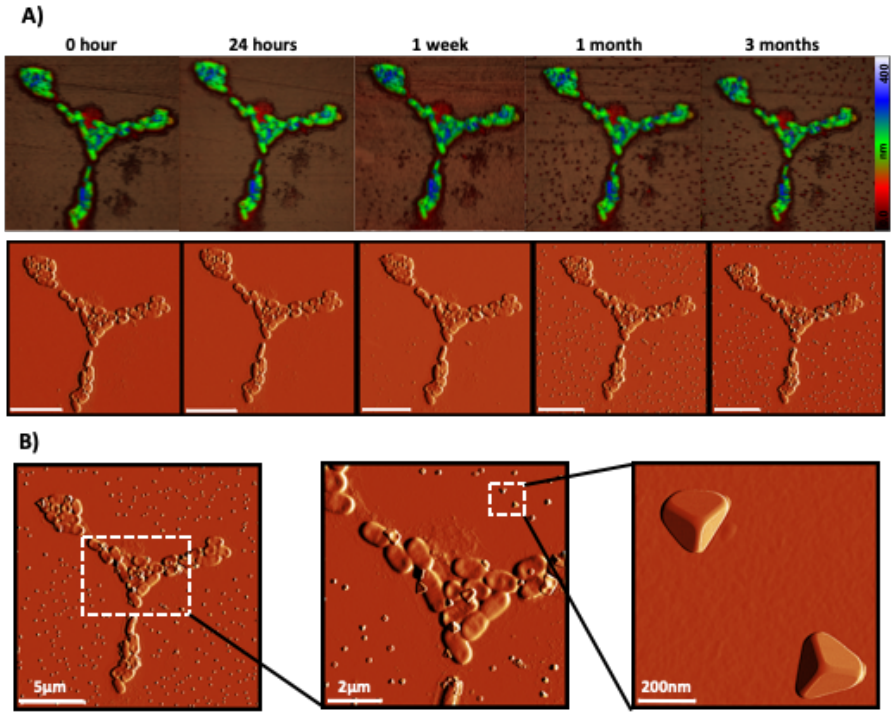

Figure 6.1: long-term desiccation of *A. baumannii* ACICU specified cluster (A) AFM height image during three months monitoring of bacterial cell. (B) Crystals form materials growing by the time and regular shapes.

Examination of AFM images reveals no significant changes in cell height over three months of measurement that may be attributed to the fact that these cells lose much of their intracellular water during the air-drying process (see section 5.1).

On the other hand, after a week, we notice the appearance of small particles on the substrate and the surface of several bacterial cells that grow over time and gradually form regular crystals. Panel B displays the high-resolution peak force images of these clustered cells after three months in which these nano-crystals decorate the surface of the bacterium by creating triangular and cubic shapes.

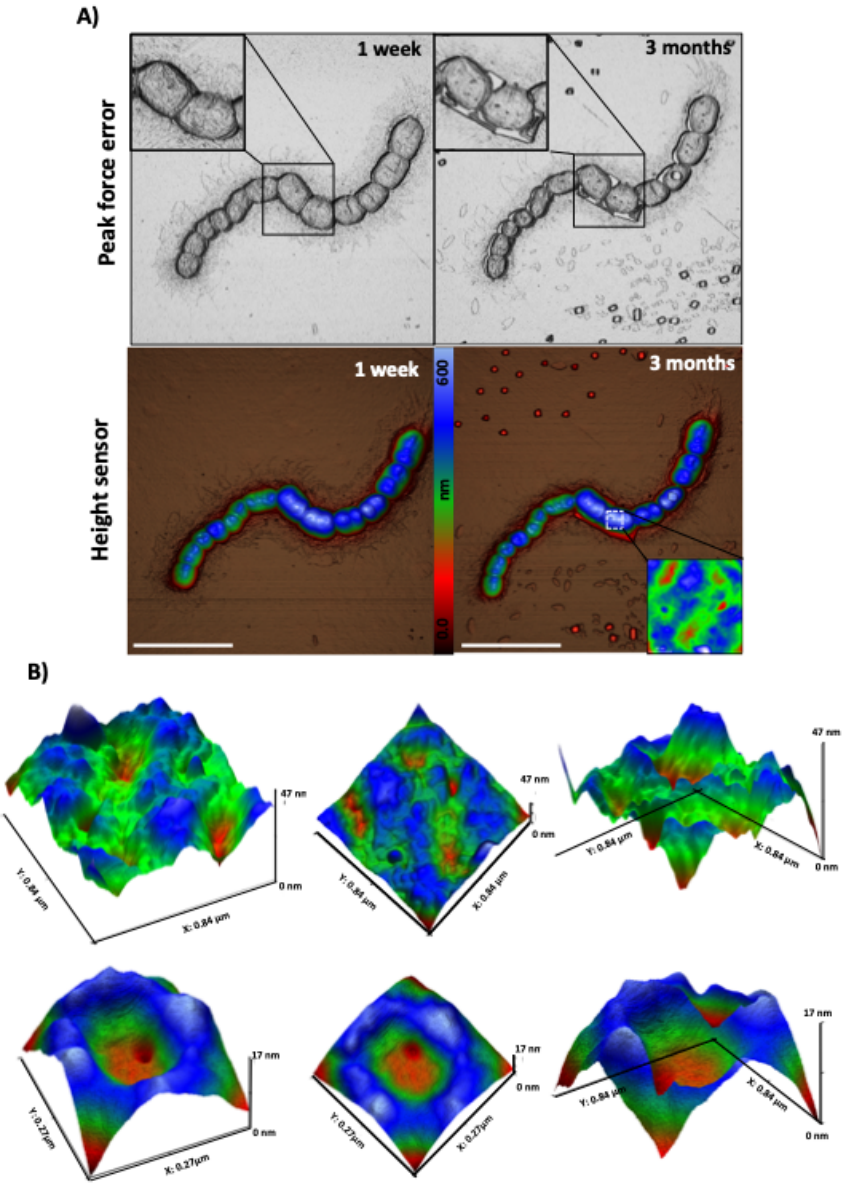

Figure 6.2: Outer cell membrane pores appearance, intracellular materials releasing and grew up the crystals on the cell surface and around the cells.

Interestingly, these crystals do not appear within a certain distance around the cluster, i.e. inside the exclusion region. As summarized in Table 6.1, these crystals can vary from diameter and height of about 40 nm and 100 nm respectively in the first week to approximately 90 nm and 300 nm after three months of storage. Moreover, a closer inspection of the images revels the presence of pores on the outer cell membranes, becoming more pronounced over time, as shown in the following figure.

It is worth noticing that, we imaged other bacterial cells under the same storage conditions to ensure the precision and repeatability of the observations, all of which represent the same results. Figure 6.2 (Panel A) shows a detailed comparison of cell surface changes for bacteria stored with saturated salt under hospital condition after one week and three months. In order to highlight the cell pores, the captured peak force images have been improved. Such pores that are detectable within the first week of storage, gradually increase in number and become more evident over time. As the pores on the cell wall appear, we also notice the leakage of intracellular material that can be associated with these cell pores, with an average depth of 30 nm, they are large enough to allow the intracellular material to be released. Panel B, in Figure 6.2, represents highly detailed magnified 3D images of cell pores corresponding to the area specified in the inset of AFM height images.

The upper row provides three-dimensional images of a very uneven cell surface including multiple pores at three different angles from the side, top, and down views; whereas the lower row, for example, specifically focuses only on one of the pores of the cell wall with a diameter of 27 and 17 nanometers, respectively. The down view image clearly shows the depressions of the pores penetrating into the cell wall with different and irregular depths. The depth of these pores can vary around 40nm from the highest part of the cell surface to 17nm compared to the cell surface around the pores. Furthermore, the pores themselves can appear as funnel-shaped (as seen in the bottom row for single pores), which can drive the protein pathway out of the cell.

Further analysis of membrane pores, reported in Table 6.1, confirms the rise in pores numbers from 7 within a first week to 25 pores number after three months, for all the cells in cluster shown in Figure 6.2, with an average depth of 30.67± 15 nm and a diameter of 63.4± 12 nm. This phenomenon, i.e. cell membrane pores increment, may also be linked to rougher cell surface over time.

Thanks to the AFM technique, we successfully identified the formation of membrane pores, as an evolutionary pathway that mediates cell death, for the intact and specified bacterial cells over time by implementing the SMSF ap-

Table 6.1: *A. baumannii* ACICU cell membrane pores and crystal dimensions.

A. *baumannii* ACICU cell membrane pores and crystal dimensions

Desiccation Time	Outer membrane pores				Crystal	
	Roughness	Number	Depth (nm)	Length (nm)	Height (nm)	Length (nm)
1-Week	21.61±5.50	7	ND	ND	152±21	40±7.8
3-Monthes	25.51±6.28	25	30.67±15	63.4±12	305±62	91±25

proach. Nevertheless, to the best of our knowledge, the emergence of membrane pores for intact bacterial cells, particularly *A. baumannii* ACICU, without any manipulation and treatment has never been reported in the literature. Taken together, all observations, suggest that the storage of samples in the presence of salt may prompt the formation of regular crystals on the substrate and cell surface, as well as the appearance of cellular pores, and leakage of intracellular materials. However, to examine whether the formation of crystals is due to the presence of the salt or can be arising from bacterial suspensions, we carried out two parallel experiments on different concentrations of bacterial suspensions stored with salt and without salt. The results (not shown here) revealed that these crystals occur only in the samples that are stored with salt and are not linked to bacterial cell suspensions. Recalling that we have previously identified cell membrane pores in rod-shaped bacteria (discussed in section 4.2), it can be argued that crystal formation and the emergence of membrane pores could be correlated to bacterial growth conditions.

6.2 The effect of long-term storage with salt and silica on bacterial cell at different growth phases

. In order to ensure that these observations are undoubtedly a consequence of the samples storage with salt and are not due to the vulnerability of the cellular structure, we design a supplementary experiment. As such, the bacterial culture will be prepared based on the optimal conditions that we have introduced in this study and harvested at different growth phases that have different abilities to withstand desiccation. Then we store the samples simultaneously in a sealed chamber containing either salt or silica-gel for humidity control, mimicking the hospital conditions. With this purpose, we have grown the bacteria

in LB medium in a flask with vigorous shaking at 37°C overnight, precisely the same as described in section 4.1. Then, the bacterial cells are harvested in logarithmic, late-logarithmic, stationary, and late-stationary growth phases. For each growth phase, we prepare two bacterial samples to store them simultaneously in a sealed chamber containing either salt or silica-gel for humidity control.

The extent of salt and silica gel is adjusted to provide the humidity below 30 % at the 22°C temperature to simulate the hospital conditions. A digital thermo-hygrometer is used to monitor RH and temperature for each storage condition. We employ the SMSF approach to image the morphological changes of the intended bacterial cells in each sample at different time points i.e. after 1h, 6h, 24h, 48h, one week, two weeks, three weeks, and one-month of storage with salt or silica.

Figure 6.3 shows the acquired peak force images from the bacterial cell at different growth phases only in two-time points, in the first hour, and after one month of storage in both conditions. As can be seen in this figure, all bacterial cells at each phase of growth are identified by coccus morphology and are distinct from those cells in the previous section. This morphological diversity is assumed to be directly related to bacterial growth conditions.

The visual examination of salt-stored samples (panel A) shows the appearance of regular nanocrystals for cells at the logarithmic phase. These crystals are indeed particles, observed within the first week of storage, grow over time and form regular crystals. Nevertheless, no particles or nanocrystals have been observed in other growth phases for salt-stored cells even after one month. We speculate that, as logarithmic phase cells have less desiccation resistance than cells from other growth phases, the appearance of crystals only in the logarithmic growth phase may be related to the weaker nature of these cells. On the other hand, panel B displays the morphological evolution of silica-stored cells at various growth phases. Surprisingly, no nanocrystalline shape is observed at any phase of growth, even in the logarithmic phase, the cells of which are weaker. By simultaneously comparing the salt and silica stored samples, and considering the absence of crystals in the logarithmic phase of silica-stored cells, it can be concluded that keeping the samples in salt causes crystals to form.

Short summary As in section 4.2, we demonstrated the coccus cells can survive desiccation better than the rod-shaped cells, or at least they are able to preserve their morphology intact without evident membrane pores. Therefore,

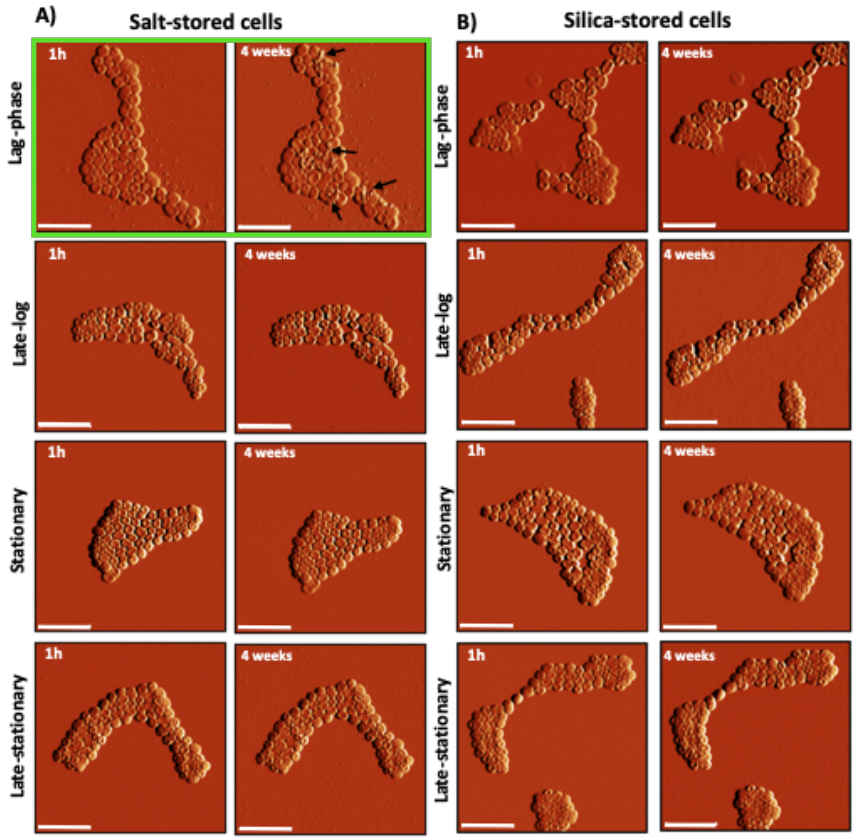

Figure 6.3: peak force AFM images of *A. baumannii* ACICU cells at a different phase of growth preserved by the salt (A) and silica gel (B) during one-month desiccation.

this phenomenon (crystals formation) could arise from the potent morphology of coccus cells compared to rod-shaped cells. On the other hand, the lack of crystals in the logarithmic phase for the silica-stored cells could be evidence of this fact that storage the bacteria with salt may enhance the formation of those crystals on bacterial cells.

Conclusions

This thesis is based on the study of the morphological changes of *Acinetobacter baumannii* ACICU under drying stress using Atomic Force Microscopy. Before systematically examining the morphological changes of the bacterium under desiccation, the intrinsic shape and structure of the *A. baumannii* cell must first be properly identified. This is essential because the bacterial cell wall is first barrier to protect the bacterium from environmental stress, and any alteration and damage to the cell wall directly affects cell survival. It has been widely reported that many factors are involved in the shape of the bacterial structure and its resistance to desiccation, including the effect of growth phase, growth conditions, and growth mediums.

In this research, we first studied the effects of each of these factors on the bacterial cell morphology and its resistance to drying. We then determined the optimal growth conditions and growth phase of the bacterium to desiccation survival, primarily concentrating upon examining maximum survival (growth rate) and highest drying resistance. Once we identified the conditions under which the bacteria were more resistant to desiccation, we then studied the effects of various degrees of drying stress on cellular structure and survival over the duration of two months, including hydrated, freeze-drying, and air-drying processes.

It is worth noting that we also examined the morphological response of the *A. baumannii* ATCC 19606 bacterium under the same drying methods and compared the results with our findings on *A. baumannii* ACICU. We tried to simulate hospital conditions in our study as the conditions of bacterial storage have been established as a factor that can significantly affect bacterial survival.

Providing hospital conditions for a bacterium requires maintaining environmental conditions at temperatures of $20°C$ and humidity below 30%. The method we employed included preservation with salt, based on instructions from Jawad et.al.1996, and silica gel.

Bacterial growth phase

We described a general morphology of *A. baumannii* ACICU cells as a coccus shape, with a length to width change rate of L/W=1.2. This structure was thoroughly maintained under the growth phase. However, in the logarithmic phase, the cells were larger and exhibited a greater height. It is noteworthy that while coccus morphology formed the dominant structure of the bacteria, the analysis of multiple larger-scale AFM images revealed the sporadic presence of some *A. baumannii* ACICU cells with a rod structure and average length of 4μm. These bacteria, which comprised only 1.2% of the total population of the studied cells, were no longer observed after entering the stationary phase.

More precisely, the observations showed that, when entering the stationary phase, the *A. baumannii* ACICU bacterium undergoes a cell contraction (i.e. becomes more coccus in form), so that the length and width of the bacterium decrease from 1.29 ± 0.15 and 1.08 ± 0.11 μm in the logarithmic phase to 0.96 ± 0.17 and 0.79 ± 0.10 μm in the stationary phase, respectively. This shrinkage, in turn, resulted in a decrease in cell height. In addition, the bacterial surface area reached its lowest value in the stationary phase of the growth process, contracting to 0.677 ± 0.17 μm^2. Nevertheless, as the bacterium went through the stationary phase, this trend was not preserved, and the surface of the bacterial cells increased, which might be a consequence of the disintegration of the cell into the death phase. Cell survival evaluation showed that the logarithmic-phase bacteria are highly susceptible to drying and lose significant viability (2 logs) upon exposure to air. In contrast, the highest desiccation resistance was observed in stationary phase cells, with no significant change in cell viability even after one week of drying.

In light of the CFU count results and given cell morphology changes, we argued that the cells that have minimal surface are associated with higher resistance to desiccation. Therefore, the shrinkage of the cells during the growth can be considered a resistance mechanism of the bacteria to survive desiccation.

Bacterial growth conditions

It is well known that several factors, such as PH, temperature, oxygen, etc., play a significant role in bacterial growth conditions. Since *A. baumannii* ACICU is an aerobic bacterium, we assessed structural changes of the cell on the basis of the amount of oxygen available during development. In this regard, we designed our experiments under two distinct conditions of flask-shaking and tube-static, in which the amount of oxygen available in the latter conditions was greater than in the former.

As mentioned earlier, during bacterial growth, most of the morphological changes occur in the logarithmic and stationary phases. Accordingly, growth curves obtained during 48 growths for both flask-shaking and tube-static conditions to collect the bacteria in these two phases. The obtained growth curves showed distinct dissimilarities for the flask-shaking and tube-static conditions. The obtained cell density for the tube-static bacteria, ca $OD_{600} = 1.5$, was $4\times$ lower than that of the flask-shaking case. Furthermore, the cells in the tube-static condition grew at a slower pace, experiencing a rather long logarithmic phase of more than 24h and reaching the stationary phase after 30 hours of growth, i.e. at a time $5\times$ longer.

Cell morphology analysis indicated that bacteria grown in flask-shaking condition appeared in both logarithmic and stationary phases with a coccus morphology that had a length-to-width ratio of 1.2, whereas bacteria grown under tube-static conditions displayed a rod morphology with a length-to-width ratio of 1.6 in both phases. The average measured height of flask-shaking bacteria was 386nm and was 238nm for tube-static bacteria. In addition, the average surface-to-volume parameter was calculated for both phases as $S/V{=}5.3\mu m^{-1}$ for tube-static rod-shaped cells and $S/V{=}3.08\mu m^{-1}$ for coccus flask-shaking cells. This result confirms that the tube-static cells have a larger footprint, which correlates well with our observation reported in the previous section that a larger cell relative footprint is linked to a lesser survival performance.

A closer inspection into cellular characteristics changes in those conditions showed that the difference in S/V is due to the larger cell surface parameter in the tube-static condition, as the volume changes in both growth conditions are not significant. Therefore, the cell surface, as a function of cell length, can be considered a representative parameter in morphological change of bacteria. By taking into account all of our observations of *A. baumannii* ACICU cell changes as a function of the growth phase and growth conditions, we determined the bacterial growth conditions, with particular attention to oxygen availability that served as a main effective factor in cell morphology alterations.

Cell viability was evaluated using CFU to analyze the conditions under which the bacteria displayed the highest drying resistance. In general, the cells that were grown in the tube always showed less resistance to drying than the flask cells; however, regardless of the growth conditions, the bacteria were found to be more susceptible to desiccation (CFU reduction of about two logs) in the logarithmic phase. The results demonstrated that the highest resistance to desiccation was associated with the *A. baumannii* ACICU cells, which were grown in flask condition and harvested during the stationary phase. Since the cells grown in the flask displayed a higher growth rate and drying resistance, and since no structural damage (pores) were found in their cell membrane, these conditions were considered in our studies to be the optimal growth conditions for *A. baumannii* ACICU cells.

We likewise examined growth medium as another factor affecting bacterial morphology. To do this, we succeeded in measuring the bacteria in various physiological environments by using the advanced AFM peak force technique. Thus, the *A. baumannii* ACICU bacteria grown under optimum conditions were suspended in liquid solutions (various media), such as LB, CAA, BSA, and 0.9%NaCl, and then compared with the sample suspended in sterile water in order to determine the role of nutrients in protecting the bacterial cell structure. Immediately after drying, we observed the formation of leaf-like structures and large salt crystals for bacteria suspended in LB and 0.9%NaCl medium, respectively.

The bacteria displayed a morphology of coccus in all media, which was often egg-shaped and without depression, while the bacteria suspended in the water, i.e., in the absence of nutrients, indicated a significant depression in their cell wall. It is notable that the bacteria suspended in the BSA not only had a morphological variation, such as coccobacillus, rod, etc., but also none of them had any cell wall damage or depression and showed untouched structures.

Different degrees of desiccation

After the flask-shaking growth conditions were identified as the optimal conditions for *A. baumannii* ACICU growth, the effects of different degrees of desiccation – that is, different types of environmental stress – were studied using various methods of maintenance in water – (hydrated), freeze-drying, and air-drying – on the cellular structure of the bacterium. For each of these three groups, morphological responses of the bacteria to a prolonged drying process were also evaluated in order to simulate the hospital environment. Thanks to the ability of AFM to produce 3D images and data, the measured volumes of

A. baumannii ACICU bacteria in the first hours of drying in hydrated, freeze-dried, and air-dried methods were equal to 0.486 ± 0.10 μm^3, 0.336 ± 0.08 μm^3 and 0.269 ± 0.06 μm^3, respectively. The latter trend was also observed with measured cell height.

These findings can be examined in various aspects. Since the hydrated bacteria were measured immediately (within 30 minutes) after evaporation of water under ambient conditions, they experienced the lowest drying stress and subsequently lost less water. This probably explains why it showed the highest volume compared with the other two conditions, i.e., air-dried and freeze-dried. The larger volume of freeze-dried than air-dried cells can also be attributed to the slow drying in the vacuum and the freezing process. On the other hand, because the air-dried cells were exposed to the air for a longer period of time to dry completely, they lost more cell water, resulting in less cell volume. Such observations and comparisons in the hydrated and air-dried cell volumes indicate the immediate effect of drying on cell volume, so that cell volume was dramatically reduced by up to 50% in the early hours of drying. The depression of bacterial cell walls is another result of varying degrees of desiccation. Analysis of cell morphology showed that hydrated cells were mostly without depression — or at around 45nm with mild depression – whereas the depressions in freeze-dried and air-dried cell membranes were measured to be 98 nm and 112 nm, respectively. The observations demonstrated that prolonged desiccation leads to a decrease in cell volume and height of *A. baumannii* ACICU cells. No significant changes were detected in other cellular characteristics, such as cell length and width. However, these changes have occurred at different rates, depending on environmental stresses imposed on bacteria when drying. A two-month analysis of the hydrated cells showed that the bacteria not only had the highest volume and height compared to the air-dried and freeze-dried cells but also had an intact morphology with low depression throughout this period. Nevertheless, after two months of storage, this intact morphology was suddenly destroyed by exposure to air, and the intercellular material leaked out and formed leaf-like structures. In contrast, air-dried and freeze-dried cells preserved their structures relatively well, and no variations in their morphology were found, except for a reduction in cell height during the prolonged desiccation.

Taken together, these findings suggest that although maintaining the cells in the water can help preserve intracellular water and apparent cell morphology, it may cause decay and weakness in the cell membrane over time due to osmotic stress in the aquatic environments. Hence, when cells are faced with atmospheric conditions, the weak cell membrane cannot withstand desiccation

stresses, resulting in a cell volume reduction over time and eventual cell collapse. The reduction of hydrated cell volume we measured over two months is somewhat surprising given the fact that these cells were maintained in water.

The cell volume analysis showed that the volume of hydrated cells after two months decreased by 54 percent with respect to the initial cell volume, whereas the freeze-dried and air-dried cells displayed a decrease in initial cell volume of 29 percent and 25 percent, respectively. It is worth noting that the analysis of cell volume undertaken here expanded our knowledge of the effect of drying methods on cell morphology and could provide an insight into cell water content. Given the cell volume reduction attributable to cell water that we measured, we can estimate the approximate content of *A. baumannii* ACICU cellular water. To validate our findings on the effect of various degrees of drying on the bacteria's cell morphology, we carried out the same experiments on *A. baumannii* ATCC 19606 strains during long-term desiccation. We identified *A. baumannii* ATCC 19606 cells as having a rod-shaped morphology and a length-to-width ratio of about L/W=1.5. The height and volume of these cells were also relatively low, leading to an increase in surface-to-volume parameters of about twice that of the *A. baumannii* ACICU cells. Accordingly, we predicted that such bacterial strains would demonstrate lower resistance to desiccation as a result of large footprints. The obtained results from the analysis of *A. baumannii* ATCC 19606 cells confirmed the association of various degrees of drying with bacterial cell volume.

In line with our previous findings, the prolonged desiccation of *A. baumannii* ATCC 19606 cells led to a decrease in cell volume and cell height over time along with an increase of the cell surface-to-volume ratio. Furthermore, the abrupt and significant reduction in the height of *A. baumannii* ATCC 19606 cells, along with the damaged cell morphology we observed after two months, provides further support for the hypothesis that maintenance of the cells in water caused erosion and weakness of the cell membrane.

After having discussed the immediate and long-term effects of various degrees of drying on the bacterial cell structure, the consequences of these environmental stresses on desiccation survival of the *A. baumannii* ACICU and ATCC 19606 were examined for two months. We performed a cell viability assessment on bacteria that were exposed to different environmental stresses in order to evaluate their desiccation survival. The hydrated cells were observed to have the highest resistance to desiccation and consistently preserved the initial CFU value for two months or more. In contrast, freeze-dried and air-dried cells showed a decreasing trend relative to initial CFU values and lost their survival after two weeks and one month, respectively. These findings

imply that environmental stresses exerted on the cells play an essential role in the desiccation survival of the bacteria. One of the interesting and important results obtained from the measurements was the inconsistency in the viability of the hydrated cells and the corresponding morphology observed after two months. We observed that although the hydrated cells display a strong volume reduction, the viability of these cells is approximately equal to their initial CFU values, demonstrating a visual incompatibility. This study is one of the first investigations to focus specifically on *A. baumannii* ACICU cell morphology alterations under different desiccation effects. Further work is therefore needed to understand the association between cell morphology and cell viability.

A similar analysis of cell viability of the *A. baumannii* ATCC 19606 species confirmed our findings of the high resistance of hydrated cells to desiccation. Indeed, these cells again consistently preserved their initial CFU value over two months. It was also noted that the air-dried *A. baumannii* ATCC 19606 cells demonstrated a higher survival rate of CFU than freeze-dried cells. However, both lost their viability after two weeks. Given that the freeze-dried and air-dried cells in *A. baumannii* ATCC 19606 species lose their viability after two weeks, despite having the low viability, our results clearly confirm that *A. baumannii* ACICU cells can better tolerate desiccation.

Storage conditions

Lastly, we examined the impact of long-term storage on *A. baumannii* ACICU cell morphology under dry conditions. To do so, we considered two different methods of controlling humidity to mimic the hospital environment. For this purpose, the bacteria were grown under optimal conditions, as previously described in this work, and harvested in different growth phases, before being kept separately in the presence of saturated salt and silica gel for two months. In a two-month study of bacteria in the presence of salt, we found that small particles emerged on the bacteria in the logarithmic growth phase after a week. These particles developed slowly over time and formed regular crystalline structures. This phenomenon was not observed in the other growth phases of bacteria in the presence of either salt or silica gel.

Further observations showed that keeping bacteria in the presence of salt would have additional consequences if the bacteria were grown in other growth conditions, such as those proposed by Jawad et al., 1996, in which the bacteria had a rod-shaped morphology. In addition to the formation and growth of regular crystals on the substrate and the bacterial surface of up to 100 nm, we detected pores with a depth of 35 nm in the cell membrane after approximately

one month, and these pores increased in number over time. As these pores arose on the cell wall, soft material appeared adjacent to the cells and gradually formed irregular structures.

It would seem that such soft material had leaked out from the cells. Taking all of the above considerations into account, it can be concluded that, if the bacteria are in the logarithmic phase or are undergoing other growth conditions that engender structural weakness, maintenance of the bacteria in the presence of salt may significantly influence cellular morphological changes during drying.

Publications

Growth phase- and desiccation- dependent Acinetobacter baumannii morphology: an atomic force microscopy investigation.

Journal:	*Langmuir*
Manuscript ID	Draft
Manuscript Type:	Article
Date Submitted by the Author:	n/a
Complete List of Authors:	Bashiri, Shadi; Roma Tre University, Dipartimento di Scienze Lucidi, Massimiliano; Roma Tre University, Dipartimento di Ingegneria Visaggio, Daniela; Roma Tre University, Dipartimento di Scienze Capecchi, Giulia; Roma Tre University, Dipartimento di Scienze Cincotti, Gabriella; Roma Tre University, Dipartimento di Ingegneria Visca, Paolo; Roma Tre University, Dipartimento di Scienze Capellini, Giovanni; Roma Tre University, Dipartimento di Scienze

TITLE: Growth phase- and desiccation- dependent *Acinetobacter baumannii* morphology: an atomic force microscopy investigation.

AUTHORS: Shadi Bashiri,[a] Massimiliano Lucidi,[b] Daniela Visaggio,[a] Giulia Capecchi,[a] Gabriella Cincotti,[b] Paolo Visca,[a] and Giovanni Capellini [a#].

AFFILIATIONS:

[a] Department of Science, University Roma Tre, viale Guglielmo Marconi 446, 00146 Rome, Italy

[b] Department of Engineering, University Roma Tre, via Vito Volterra 62, 00146 Rome, Italy

Supporting Information

ABSTRACT: *Acinetobacter baumannii* has emerged as a major bacterial pathogen during the past 3 decades. The majority *A. baumannii* infections occur in hospitals and are caused by strains endowed with high desiccation tolerance, which represents an essential feature for the adaptation to the nosocomial environment. The aim of this work is to investigate the desiccation response of the multidrug-resistant *A. baumannii* strain ACICU as a function of bacterial growth phase and oxygen availability, correlating bacterial survival on culture media with shape alterations. The morphological studies were performed by employing the atomic force microscopy (AFM) in peak force™ tapping mode. AFM images of *A. baumannii* ACICU cells revealed a prevalence of coccus morphology at all growth stages with a tendency to reduce their size in the stationary phase, accompanied by higher survival rate to air-drying. Moreover, cells harvested from logarithmic phase revealed to be more sensitive to desiccation and presented higher volume compared to the cells harvested from the later growth stages. In addition, oxygen deprivation caused a significant decrease in cellular size, formation of membrane pores and increase of membrane roughness with a parallel reduction in culturability after desiccation. Morphological plasticity and multidrug resistance may contribute to the desiccation tolerance and therefore to the persistence in the hospital setting.

KEYWORDS: *Acinetobacter*, Atomic Force Microscopy, bacteria, desiccation, morphology, nanoscopy, super-resolution microscopy.

INTRODUCTION

Bacterial species exhibit an extraordinary variability of shapes which are preserved through countless generations (1). Although, bacterial shape is genetically determined, sporadic changes in bacterial cell morphology can occur in response to environmental conditions (*i.e.*, physical and chemicals stressors, changes in osmolarity, colonization of other organisms, nutrient depletion or abundance, etc). Indeed, shape drives the interactions between a bacterial cell and its environment, and morphology modifications reflect the bacterial response to a given environmental change (2).

The ability of changing morphology in response to the stress imposed by the antimicrobials was recently described in the human pathogen, *Acinetobacter baumanni* (3, 4, 5). *A. baumannii* is an opportunistic human pathogen responsible for a variety of hospital-acquired infections, especially among severely ill- and immunocompromised-patients in intensive care units (6, 7). This bacterium has become a growing global concern in recent years due to the rapid emergence of multidrug-resistant strains (MDR), especially in hospital environments (7, 8). Among Gram-negative bacteria, *A. baumannii* is characterized by an impressive ability to tolerate long-term desiccation (9, 10, 11) and to resist to various temperatures, pH levels, and nutrient-limiting conditions, both on biotic and abiotic surfaces (12). For this peculiar feature, *A. baumannii* represents a model organism for desiccation studies in Gram-negative bacteria (13, 14, 15, 16), and to investigate the key features that promote survival and transmission of bacterial pathogens in healthcare settings (10,11). The desiccation tolerance varies among A. *baumannii* strains, in particular isolates adapted to the hospital environment appear generally more resistant than laboratory-adapted strains (11). In this work, the prototypic MDR *A. baumannii* strain ACICU (17) has been selected as clinical isolate endowed with high desiccation resistance (11), and as model organism to investigate changes in bacterial cell morphology due to desiccation.

Scanning and transmission electron microscopy have widely been used to investigate bacterial cell morphology or bacterial ultrastructure (such as pili, membrane, flagella). These techniques reach the necessary resolution to allow visualization of bacterial microdomains at the nanoscale level. However, they have several limitations, including harsh chemical procedures in sample preparation and the necessity to work under vacuum and/or cryogenic conditions. In recent years, atomic force microscopy (AFM) has brought novel molecular insights into the assembly, dynamics, and functions of bacterial cell nanostructures (18, 19). The ultrafine resolution and physical sensitivity of the technique have revealed a wealth of ultrastructural features that are invisible to traditional, diffraction-limited optical microscopy techniques or imperceptible in their true physiological state by electron microscopy (18, 19).

Several aspects of *A. baumannii* have been investigated using AFM such as the effects of antimicrobial compounds (3, 4, 20), the role of a transcriptional regulator involved in pathogenicity modulation (21), the mechanism of phage infection (22) and the bacterial adhesion and biofilm formation (23).

In the present work, AFM was employed to study the *A. baumannii* ACICU morphology in different growth phases and diverse oxygenation levels. Moreover, the *A. baumannii* ACICU cell viability was determined at each condition in order to correlate survival to desiccation with morphometric parameters measured with AFM operating in peak force mode.

EXPERIMENTAL SECTION

Growth conditions. *A. baumannii* ACICU was grown in LB liquid medium (24) for 18 h at 37°C with vigorous shaking (250 rpm), then sub-cultured (dilution 1:100) in a 15-ml tube containing 5 ml of LB or in a 350 ml flask containing 50 ml of LB and incubated at 37°C in static conditions (static tube; ST), or under vigorous aeration by rotary shaking at 250 revolutions/min (shaken flask; SF), respectively. The dissolved oxygen levels were 10% and 25% in ST and SF, respectively, as determined by using a Dissolved Oxygen Measuring System (Instech). Bacterial growth was monitored during time, measuring the absorbance at 600 nm (OD_{600}) using a BioSpectrometer® (Eppendorf) spectrophotometer.

Viable cell counts. At each time point specified in the Results section, 1 ml of bacterial culture was collected, washed twice and diluted in distilled water to reach OD_{600}=1, equivalent to *ca* $5x10^8$ CFU (Colony Forming Units) per ml. An aliquot of 20 µl of the bacterial suspension was used to determine the CFU by viable counts and a second aliquot of 20 µl was spotted on a glass coverslip (Corning® cover glasses, Sigma-Aldrich) and air-dried under the laminar flow hood for 20 minutes at room temperature. Cell viability after desiccation was determined by viable counts on LB-agar (LA) plates before and after air-drying, as previously described (11). Briefly, desiccated samples were rehydrated in 2 ml of distilled water, incubated for 15 minutes at room temperature, mixed by vigorous shaking for 30 seconds to ensure a complete detaching of bacteria from the glass coverslip, and appropriately diluted in saline (isotonic) solution to perform viable counts on LA.

Sample preparation and AFM measurements. Bacterial cells were washed twice and diluted in distilled water to OD_{600}=1. Twenty µl of the bacterial suspension were poured on a microscope glass slide (Thermo Scientific™ SuperFrost™ Microscope slides 76 x 26 mm, with 1 mm thickness) and air-dried under the laminar flow hood at room temperature for 20 minutes. AFM measurements were performed using a Dimension ICON AFM (Bruker, Santa Barbara, USA) set to Peak Force Tapping mode equipped with a ScanAsyst-Air Bruker silicon probe featuring a cantilever elastic constant of 0.4 Nm^{-1} and a tip with a nominal radius of 2 nm. The AFM images were recorded at a temperature ranged from 20–24 °C. The oscillation frequency and oscillation amplitude of the cantilever were set to 1 kHz and 150 nm, respectively.

For each measurement, height sensor and peak force error images were recorded simultaneously. The AFM images were analyzed and processed with the Gwyddion software (http://gwyddion.net). All images were first-order flattened and set to the constant value of height to facilitate their comparison. After leveling, to measure the biophysical parameters of cells, a metrological analysis was performed on at least 30 different, randomly selected cells. Briefly, cellular length (L) and width (W) were referred to elongated and short horizontal axes, respectively. The cross-section of the cell was graphically portrayed as cell height (H). Cell volume (V) was interpreted as a set of curves, each belonging to one pixel in the XY plane. The depth of the cell-membrane pores was considered from the highest protruding rim relative to the lowest concave edge. Surface roughness was obtained by measuring the root mean square deviation of flattened images, in the area of 400 nm × 400 nm of the cells, by an average of at least ten different cell areas.

RESULTS AND DISCUSSION

Growth phase influences desiccation tolerance and cell morphology.

Previous findings demonstrated that desiccation tolerance in *A. baumannii* ATCC19606^T type strain is a growth phase-dependent phenomenon, in that cells harvested during the logarithmic growth phase were more sensitive to dehydration than stationary phase cells (25, 15, 16, 26). We wondered whether also *A. baumannii* ACICU shows a growth phase-dependent susceptibility to desiccation and whether a correlation exists between growth phase, bacterial survival and cell morphology. *A. baumannii* ACICU was cultured in LB medium and bacterial growth was monitored for up to 48 h in shaken flask (SF condition), in order to define the time intervals of the different growth phases. By measuring the absorbance at 600 nm during time, the following growth phases were defined: lag (t_{growth}<1 h), early logarithmic (1 h<t_{growth}<4 h), late logarithmic (4 h<t_{growth}<6 h), stationary (6 h<t_{growth}<32 h), and death (t_{growth}>32 h) phase (Figure 1A). Concurrently, at 3, 6, 14, 24 and 48 h of growth (corresponding to early logarithmic, late logarithmic, stationary, late stationary and death phase, respectively), bacterial cells were washed and normalized to OD_{600}=1. The bacterial survival rates, were determined before and after air-drying, and expressed as viable counts (CFU; Figure 1B). During incubation of bacteria at 37° in LB medium, one CFU log reduction was observed only at 48 h, confirming the predicted death phase, while no reduction in bacterial viability was observed in earlier growth stages. As expected, desiccation of *A. baumannii* ACICU cells taken from the early logarithmic phase caused a significant decrease (P=0.0024) in survival compared with cells harvested from late logarithmic (P= 0.0326), stationary (P= 0.055) or death (P=0.75) phases.

In order to evaluate whether the desiccation effect on cell viability correlates with an alteration of cell morphology, AFM was used to image *A. baumannii* ACICU cells at each growth phase (Figure 1C). In all the investigated samples, a tendency of the bacteria to condensate in clusters was observed, with only few sparse individual cells, probably due to the driving force of the evaporating water which cause the so-called “coffee-stain” effect (27). Interestingly, the height of *A. baumannii* ACICU cells in early-logarithmic growth phase was higher than the other growth phases (Figure 1C). To gain insight into the cell dimensions, length, width, height, volume, and surface/volume ratio were calculated on more than 30 desiccated cells for each growth phase (Table1).

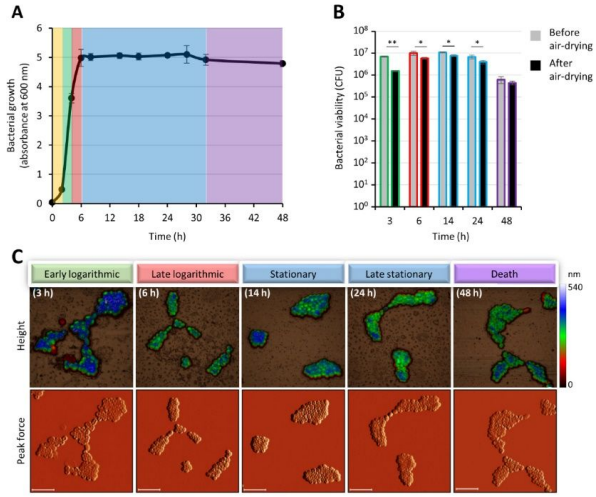

Figure 1. Growth, cell viability, and morphology of *A. baumannii* ACICU during growth in shaken flasks (SF). (A) Growth plot of *A. baumannii* ACICU cultured in LB at 37°C under vigorous shaking. At the indicated time points, bacterial growth was measured as absorbance at 600 nm (OD_{600}). The colour boxes yellow, green, red, cyan, and violet indicate lag, logarithmic, late logarithmic, stationary, and death phase, respectively. (B) CFU at different growth phases determined by viable counts on LA plates before and after air-drying. Colours of the histogram bars outline correspond to the growth phases shown in panel A. (C) *A. baumannii* ACICU cells imaged with AFM. All images were first-order flattened and set to the same range of height (0-540 nm) to facilitate comparison between conditions. Scale bar: 5 µm. Statistical analysis was performed with the software GraphPad Instat (GraphPad Software, Inc., La Jolla, CA), using One-Way Analysis of Variance (ANOVA). Asterisks indicate statistically significant differences between before and after air-drying conditions (* P <0.05; ** P <0.01).

Table 1. Cellular dimensions at different growth phases of *A. baumannii* ACICU cultured in shaken flask (SF).

Growth phase	Cellular dimensions				
	Length (µm)	Width (µm)	Height (µm)	Volume ($µm^3$)	Surface/Volume ($µm^{-1}$)
Logarithmic	**1.29 ± 0.15**	**1.08 ± 0.11**	**0.397 ± 0.11**	**0.350 ± 0.06**	**3.14± 0.40**
Late logarithmic	**1.06 ± 0.14**	**0.90 ± 0.11**	**0.335 ± 0.04**	**0.201 ± 0.03**	**3.79± 0.61**
Stationary	**0.96 ± 0.17**	**0.79 ± 0.10**	**0.325 ± 0.04**	**0.226 ± 0.06**	**3.02± 0.31**
Late stationary	**1.06 ± 0.18**	**0.88 ± 0.12**	**0.308 ± 0.06**	**0.203 ± 0.05**	**3.86± 0.63**
Death	**1.15 ± 0.18**	**0.96 ± 0.13**	**0.316 ± 0.04**	**0.260 ± 0.04**	**4.01± 1.12**

At all the investigated time points, *A. baumannii* ACICU cells displayed a coccus morphology, with an oval surface projection featuring an average length-to-width ratio of L/W=1.2 ± 0.02, suggesting that the shape of *A. baumannii* ACICU is not influenced by growth-phase in the tested experimental condition. Although the overall cell morphology did not change, the height and the volume of cells in the early-logarithmic phase were higher than those in the late logarithmic, stationary, late stationary, and death phase. Interestingly, *A. baumannii* ACICU cells in stationary phase showed the lowest surface to volume ratio and were also the most resistant to desiccation compared with cells in the other growth phases.

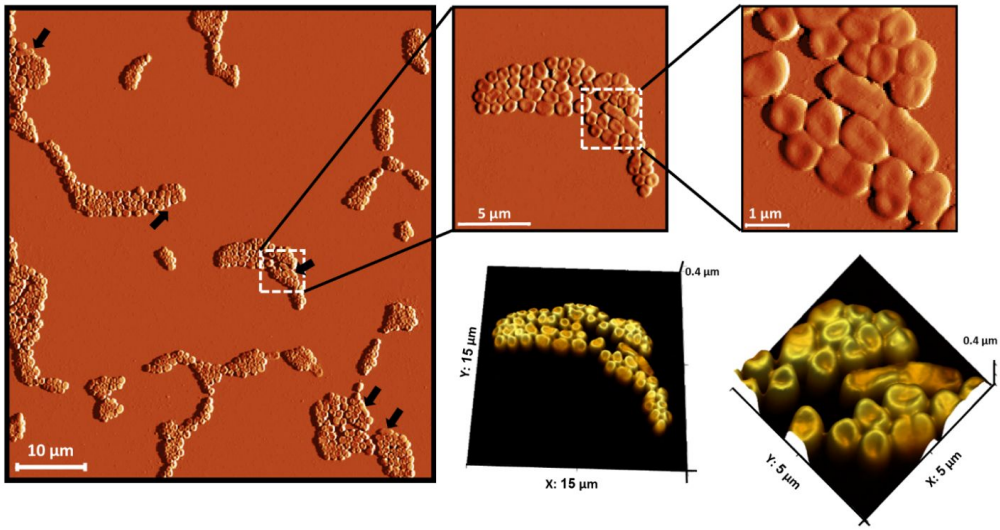

Figure 2. Morphology of *A. baumannii* ACICU cells. Bacillary and rod shape of *A. baumannii* ACICU grown for 14 h in flask at 37°C with shaking. Bacterial cells were harvested, washed twice and diluted to OD_{600}=1 in distilled water. An aliquot of 20 µl of the bacterial suspension was deposited on a microscope glass slide and air-dried for 20 minutes at room temperature before imaging with AFM. Black arrows indicate elongated cells. Relative insets of a bacillary-shaped cell and the corresponding 3D projections were shown.

Then, we speculated that cells with lesser surface are endowed with higher desiccation resistance. This observation is in line with a previous study of Madigan and coworkers, suggesting that smaller cells can tolerate adverse conditions better than the large cells (28, 29).

Of note, albeit AFM analysis indicates that *A. baumannii* ACICU had coccus shape, sporadic 4 µm-long rod-shaped cells were detected in the logarithmic-phase (Figure 2), in agreement with previous studies reporting a bacillus-like morphology for cells in the logarithmic growth phase (30). From the high magnification 3D rendering of a rod-shaped cell (inset of Figure 2), it was possible to observe a sizeable lower heights and a larger footprint compared to the surrounding coccus cells. The abundance of elongated-cells observed in the early-logarithmic growth phase was <0.3%, but increased to ~1.5% in the late-logarithmic growth phase. Interestingly, rod-shaped cells were not detected in samples collected at > 6 h incubation, following examination of > 300 cells.

Oxygen deprivation influences desiccation tolerance and cell morphology

Bacterial cell morphology can be influenced by a number of factors like temperature, light, pH, relative humidity, salt concentration and oxygenation (31, 32). Although *A. baumannii* is a strictly aerobic bacterium (33), it can occasionally be faced with low oxygen concentrations, *e.g.* during biofilm-mode growth *in vivo* (34). Therefore, we wondered whether microaerophilic cultural conditions could influence *A. baumannii* cell survivability to desiccation and/or morphologically. To this aim, the effects of oxygen deprivation on the growth of *A. baumannii* ACICU has been mimed by inoculating cells in a tube containing 1/3 atmospheric oxygen/cultural medium volume ratio and incubated in static conditions. Since *A. baumannii* is a non-motile bacterium, the static condition causes the bacteria to settle at the bottom of the tube, minimizing oxygen availability (35). The effect of static tube (ST) growth on *A. baumannii* ACICU desiccation tolerance and morphology was then compared with those determined for aerated (SF) cultures. To this purpose, *A. baumannii* ACICU growth in ST was monitored for up to 48 h (Figure 3A), and compared with the SF condition (Figure 1A). Cultivation in ST produced an overall slowdown of growth rate, with a clear delay of all growth phases: lag (t_{growth}<3 h), early logarithmic (3 h<t_{growth}<24 h), late logarithmic (24 h<t_{growth}<26 h), stationary (26 h<t_{growth}<32 h), and death (t_{growth}>32 h) phases. Moreover, the maximum of cell density reached under ST conditions was *ca.* fivefold lower than that reached in SF (OD_{600}= 1.0 *vs*. OD_{600}= 5.0, respectively). Furthermore, the logarithmic growth phase duration was fivefold longer in ST than in SF. Then, the impact of oxygen availability on *A. baumannii* ACICU desiccation resistance was investigated by comparing the bacterial viability before and after drying between SF and ST cultures (Figure 3B). An overall increased susceptibility to desiccation was observed for ST cells, compared with SF cells, and this effect was evident irrespective of the growth stage (exponential or stationary; Figure 3B).

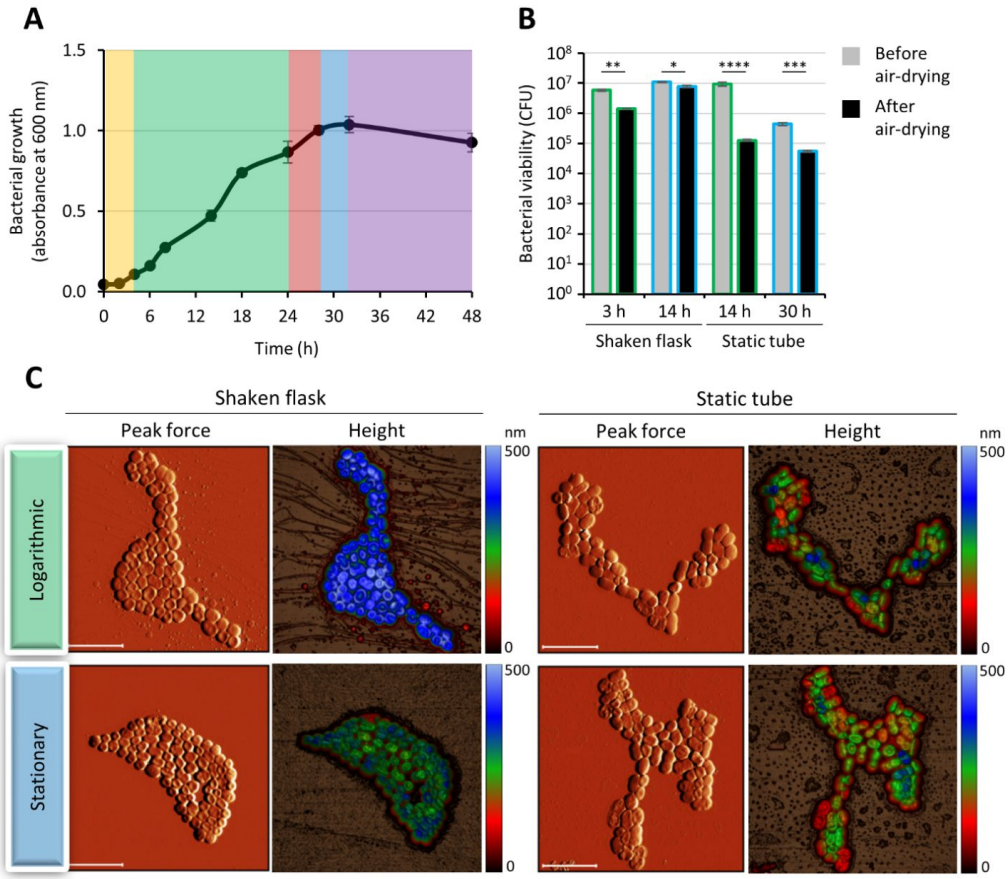

Figure 3. Comparison of growth, cell viability and morphology of *A. baumannii* ACICU during growth in shaken flasks (SF) and static tube (ST). (A) Growth plot of *A. baumannii* ACICU cultured in LB at 37°C in static condition. At the indicated time points, bacterial growth was measured as absorbance at 600 nm (OD_{600}). The colour boxes yellow, green, red, cyan, and violet indicate lag, logarithmic, late logarithmic, stationary, and death phase, respectively. (B) CFU of *A. baumannii* ACICU grown in shaking and in static condition. The CFUs were determined before and after air-drying. Colours of the histogram bars outline correspond to the growth phases shown in panel A. (C) AFM imaging of *A. baumannii* ACICU grown in static and shaking conditions. All of the images were first-order flattened and set to the same range of height (0-500 nm) to facilitate comparison between conditions. Scale bar: 5 µm. Statistical analysis was performed with the software GraphPad Instat (GraphPad Software, Inc., La Jolla, CA), using One-Way Analysis of Variance (ANOVA). Asterisks indicate statistically significant differences between before and after air-drying conditions (* P <0.05; ** P <0.01; *** P <0.001; **** P <0.0001).

At the exponential phase, the extent of desiccation-dependent cell death was *ca.* two log reduction in ST and < one log in SF. Likewise, desiccation had nearly no effect on SF cell at the stationary phase, while it caused one log reduction of ST cells. These results indicate that low oxygen availability increases the susceptibility to desiccation of *A. baumannii* ACICU. To extend the investigation of the effect of oxygen availability on cell morphology, *A. baumannii* ACICU cells from SF and ST conditions were imaged by AFM during the logarithmic and stationary growth phases (Figure 3C). AFM investigations revealed that cells grown in a low-oxygen condition (ST) displayed reduced height than SF cells (Figure 3C). To better characterize *A. baumannii* ACICU cells grown in ST, the length, width, height, volume and surface/volume ratio were calculated for more than 30 air-dried cells harvested from logarithmic and stationary growth phases (Table 2). ST cells showed a ~1.6 L/W ratio in both logarithmic and stationary phases. Moreover, no significant differences for all the calculated parameters were observed between ST cells from logarithmic and stationary phase.

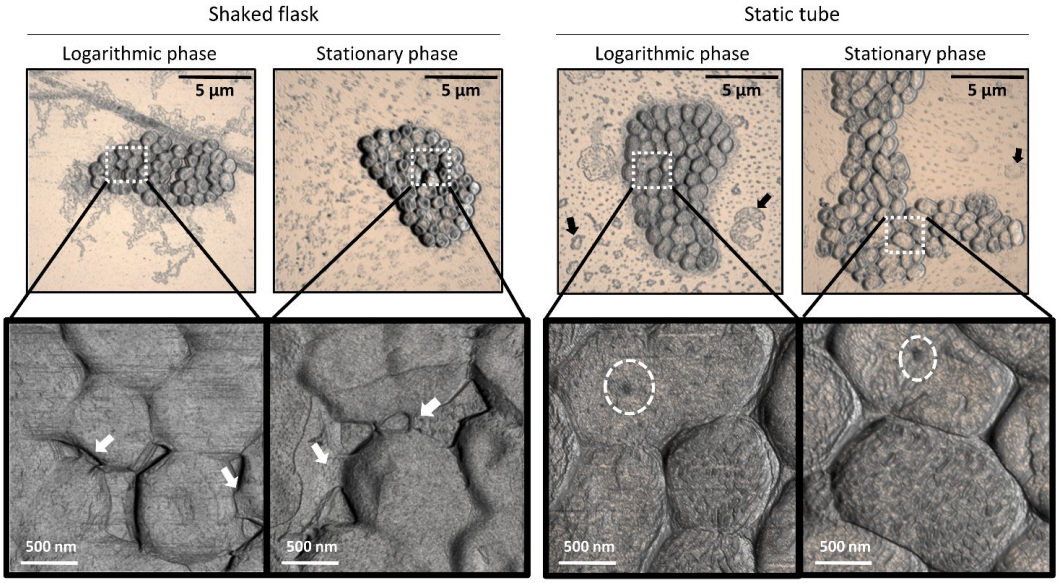

Figure 4. Surface morphology of *A. baumannii* ACICU cells after growth under static and shaked conditions. *A. baumannii* ACICU cells were imaged by AFM after desiccation. White and black arrows denote the presence of an exopolysaccharidic layer on the cell surface and the release of DNA, respectively. White dot circles denote membrane pores.

Table 2. Cellular dimensions of *A. baumannii* ACICU grown in static tube (ST).

Growth phase	Cellular dimensions				
	Length (µm)	Width (µm)	Height (µm)	Volume (µm^3)	Surface/Volume (µm^{-1})
Logarithmic	1.73±0.22	1.11±0.13	0.244±0.31	0.275±0.04	5.091±0.63
Stationary	1.67±0.30	1.05±0.12	0.232±0.25	0.263±0.05	5.498±1.28

Of note, ST cells grown under oxygen-deprivation condition appeared to be *ca* 1.5-fold longer and 0.7-fold thinner than those cultured in SF (Table 1). It must be pointed out that nearly all the measured ST cells should be considered dead, given the dramatic reduction of cell viability observed after desiccation (Figure 3B). Interestingly, ST cells had a larger footprint and surface to volume ratio compared with SF cells, corroborating our observations that a larger cell relative footprint is related with a decrease in viability. Since morphological differences were observed depending on the oxygenation level, AFM comparative analysis at higher resolution was performed on SF and ST cells (Figure 4). To this aim, 3x3 µm field of views were acquired, revealing the presence of a smooth layer covering the SF bacteria (Figure 4, white arrows). This layer, which is absent in ST bacteria, could be composed by exopolysaccharides that could play an osmoprotectant role by retaining water in the local microenvironment, protecting bacterial cells from dehydration and enhancing the survival in harsh environments (25, 36). On the other hand, ST cells were characterized by more irregular surface with visible ripples and relatively large pores (Figure 4, see dashed circles). These pores were likely generated by major alterations in membrane integrity caused by desiccation. The pore average depth and diameter measured 20-30 nm. These holes were large enough to allow the leakage of intracellular material, including that observed on the glass slide in the neighborhood of some cell clusters (Figure 4, black arrows). The presence of a putative exopolysaccharide layer covering SF cells impeded a scan topography of their surface. Thus, root mean squared (RMS) roughness analysis of the cell membrane was carried out on at least twenty different ST cells. Nearly identical surface roughness of 1.2 ± 0.3 nm and 1.1 ± 0.2 nm was observed for the logarithmic and stationary phase, respectively (Figure S1). This finding is in line with an earlier study on the *A. baumannii* type strain ATCC19606^T, showing that the RMS roughness was invariant for cells across all growth phases (3).

CONCLUSIONS

The peculiar capacity of *A. baumannii* to overcome the desiccation stress certainly contributes to the adaptive success of this bacterium in the nosocomial environment. While *A. baumannii* is endowed with a formidable desiccation resistance compared with other Gram-negative bacteria, some intra-species differences exist, resulting some strains more resistant than others (11). This has led us to gain more insights into the functional and morphological effects of desiccation on *A. baumannii* ACICU, a strain regarded to as the prototype of epidemic strains causing large outbreaks around the world (13,17). In the present work, we demonstrated that desiccation tolerance and cellular dimension are strongly influenced by the growth phases and by oxygen availability. *A. baumannii* ACICU cells presented a predominant coccoidal morphology at all growth phases, although rare rod-shaped elements were detected in the logarithmic phase. Moreover, *A. baumannii* ACICU cells in early-logarithmic phase appeared more susceptible to desiccation than those in stationary phase. Intriguingly the *A. baumannii* cells in stationary phase display the smallest surface/volume ratio, indicating a possible correlation between cell dimension and desiccation resistance. As to the effect of oxygen on cell shape and desiccation resistance, a significant decrease in cell height and volume, together with a significant reduction of survival rates, were observed for *A. baumannii* cells cultured in a microaerobic environment (ST condition). Moreover, growth under microaerobic conditions resulted in the formation of membrane pores (likely responsible of intracellular material leakage) and an increase of surface RMS roughness, which represent novel identified cellular markers of environmental fitness decline, after exposure to dry conditions. In conclusion, this pioneering work provides a preliminary description of some functional and morphological changes occurring in *A. baumannii* during desiccation under condition mimicking those encountered in the hospital environment, and paves the way for the use of AFM as a tool for the investigation of the adaptive response to dehydration, or other environmental stresses.

■ ACKNOWLEDGMENT

This work was supported by the Excellence Departments grant from the Italian Ministry of Education, University and Research (MIUR, Italy) (Art. 1, commi 314-337 Legge 232/2016) to the Department of Science, Roma Tre University, and by the PRIN 2017 grant protocol 20177J5Y3P from MIUR to F.I. and P.V. We acknowledge the technical support of the LIME laboratory at Roma Tre University.

■ ASSOCIATED CONTENT

Supporting Information. Surface characterization (normal distribution and histogram of surface roughness) for ST cells in both logarithmic and stationary growth phases.

■ AUTHOR INFORMATION

Corresponding Author
Email: giovanni.capellini@uniroma3.it

Notes

The authors declare no conflict of interest

■ REFERENCES

(1) Van Teeseling, M. C. F.; de Pedro, M. A.; Cava, F. Determinants of Bacterial Morphology: From Fundamentals to Possibilities for Antimicrobial Targeting. *Front. Microbiol.* **2017**, 8. https://doi.org/10.3389/fmicb.2017.01264.

(2) Yang, D. C.; Blair, K. M.; Salama, N. R. Staying in Shape: The Impact of Cell Shape on Bacterial Survival in Diverse Environments. *Microbiol. Mol. Biol.* Rev. **2016**, 80 (1), 187–203. https://doi.org/10.1128/MMBR.00031-15.

(3) Soon, R. L.; Nation, R. L.; Hartley, P. G.; Larson, I.; Li, J. Atomic Force Microscopy Investigation of the Morphology and Topography of Colistin-Heteroresistant *Acinetobacter baumannii* Strains as a Function of Growth Phase and in Response to Colistin Treatment. *Antimicrobial Agents and Chemotherapy* **2009**, 53 (12), 4979–4986. https://doi.org/10.1128/AAC.00497-09.

(4) Soon, R. L.; Nation, R. L.; Harper, M.; Adler, B.; Boyce, J. D.; Tan, C.-H.; Li, J.; Larson, I. Effect of Colistin Exposure and Growth Phase on the Surface Properties of Live *Acinetobacter baumannii* Cells Examined by Atomic Force Microscopy. *International Journal of Antimicrobial Agents* **2011**, 38 (6), 493–501. https://doi.org/10.1016/j.ijantimicag.2011.07.014.

(5) Htoo, H. H.; Brumage, L.; Chaikeeratisak, V.; Tsunemoto, H.; Sugie, J.; Tribuddharat, C.; Pogliano, J.; Nonejuie, P. Bacterial Cytological Profiling as a Tool To Study Mechanisms of Action of Antibiotics That Are Active against *Acinetobacter baumannii*. Antimicrobial Agents and *Chemotherapy* **2019**, 63 (4). https://doi.org/10.1128/AAC.02310-18.

(6) Dijkshoorn, L.; Nemec, A.; Seifert, H. An Increasing Threat in Hospitals: Multidrug-Resistant *Acinetobacter baumannii*. *Nat. Rev. Microbiol.* **2007**, *5* (12), 939–951. https://doi.org/10.1038/nrmicro1789.

(7) Peleg, A. Y.; Seifert, H.; Paterson, D. L. *Acinetobacter baumannii*: Emergence of a Successful Pathogen. *Clinical microbiology reviews* **2008**. https://doi.org/10.1128/CMR.00058-07.

(8) Rice, L. B. Federal Funding for the Study of Antimicrobial Resistance in Nosocomial Pathogens: No ESKAPE. *J. Infect. Dis.* **2008**, *197* (8), 1079–1081. https://doi.org/10.1086/533452.

(9) Wendt, C.; Dietze, B.; Dietz, E.; Ruden, H. Survival of *Acinetobacter baumannii* on Dry Surfaces. *J. Clin. Microbiol.* **1997**, *35* (6), 1394–1397.

(10) Jawad, A.; Seifert, H.; Snelling, A. M.; Heritage, J.; Hawkey, P. M. Survival of *Acinetobacter baumannii* on Dry Surfaces: Comparison of Outbreak and Sporadic Isolates. *J. Clin. Microbiol.* **1998**, *36* (7), 1938–1941.

(11) Giannouli, M.; Antunes, L. C. S.; Marchetti, V.; Triassi, M.; Visca, P.; Zarrilli, R. Virulence-Related Traits of Epidemic *Acinetobacter baumannii* Strains Belonging to the International Clonal Lineages I-III and to the Emerging Genotypes ST25 and ST78. *BMC Infect. Dis.* **2013**, 13, 282. https://doi.org/10.1186/1471-2334-13-282.

(12) Bergogne-Berezin, E.; Towner, K. J. *Acinetobacter* Spp. as Nosocomial Pathogens: Microbiological, Clinical, and Epidemiological Features. *Clin. Microbiol. Rev.* **1996**, *9* (2), 148–165.

(13) Antunes, L. C. S.; Visca, P.; Towner, K. J. *Acinetobacter baumannii*: Evolution of a Global Pathogen. *Pathog Dis* **2014**, *71* (3), 292–301. https://doi.org/10.1111/2049-632X.12125.

(14) Harding, C. M.; Hennon, S. W.; Feldman, M. F. Uncovering the Mechanisms of *Acinetobacter baumannii* Virulence. *Nat. Rev. Microbiol.* **2018**, *16* (2), 91–102. https://doi.org/10.1038/nrmicro.2017.148.

(15) Zeidler, S.; Muller, V. The Role of Compatible Solutes in Desiccation Resistance of *Acinetobacter baumannii*. *Microbiologyopen* **2019**, 8 (5), e00740. https://doi.org/10.1002/mbo3.740.

(16) Zeidler, S.; Muller, V. Coping with Low Water Activities and Osmotic Stress in *Acinetobacter baumannii*: Significance, Current Status and Perspectives. Environ. Microbiol. 2019, 21 (7), 2212–2230. https://doi.org/10.1111/1462-2920.14565.

(17) Iacono, M.; Villa, L.; Fortini, D.; Bordoni, R.; Imperi, F.; Bonnal, R. J. P.; Sicheritz-Ponten, T.; De Bellis, G.; Visca, P.;

Cassone, A.; et al. Whole-Genome Pyrosequencing of an Epidemic Multidrug-Resistant *Acinetobacter baumannii* Strain Belonging to the European Clone II Group. *Antimicrob. Agents Chemother.* **2008**, 52 (7), 2616–2625. https://doi.org/10.1128/AAC.01643-07.

(18) Scheuring, S.; Dufrene, Y. F. Atomic Force Microscopy: Probing the Spatial Organization, Interactions and Elasticity of Microbial Cell Envelopes at Molecular Resolution. *Mol. Microbiol.* **2010**, *75* (6), 1327–1336. https://doi.org/10.1111/j.1365-2958.2010.07064.x.

(19) Viljoen, A.; Foster, S. J.; Fantner, G. E.; Hobbs, J. K.; Dufrêne, Y. F. Scratching the Surface: Bacterial Cell Envelopes at the Nanoscale. *mBio* **2020**, *11* (1). https://doi.org/10.1128/mBio.03020-19.

(20) Deliorman, M.; Gordesli Duatepe, F. P.; Davenport, E. K.; Fransson, B. A.; Call, D. R.; Beyenal, H.; Abu-Lail, N. I. Responses of *Acinetobacter baumannii* Bound and Loose Extracellular Polymeric Substances to Hyperosmotic Agents Combined with or without Tobramycin: An Atomic Force Microscopy Study. *Langmuir* **2019**, *35* (27), 9071–9083. https://doi.org/10.1021/acs.langmuir.9b01227.

(21) Kuo, H.-Y.; Chao, H.-H.; Liao, P.-C.; Hsu, L.; Chang, K.-C.; Tung, C.-H.; Chen, C.-H.; Liou, M.-L. Functional Characterization of *Acinetobacter baumannii* Lacking the RNA Chaperone Hfq. *Front. Microbiol.* **2017**, *8*. https://doi.org/10.3389/fmicb.2017.02068.

(22) Dubrovin, E. V.; Popova, A. V.; Kraevskiy, S. V.; Ignatov, S. G.; Ignatyuk, T. E.; Yaminsky, I. V.; Volozhantsev, N. V. Atomic Force Microscopy Analysis of the *Acinetobacter baumannii* Bacteriophage AP22 Lytic Cycle. *PLoS One* **2012**, *7* (10). https://doi.org/10.1371/journal.pone.0047348.

(23) James, S. A.; Hilal, N.; Wright, C. J. Atomic Force Microscopy Studies of Bioprocess Engineering Surfaces - Imaging, Interactions and Mechanical Properties Mediating Bacterial Adhesion. *Biotechnol J* **2017**, *12* (7). https://doi.org/10.1002/biot.201600698.

(24) Bertani G. Lysogeny at mid-twentieth century: P1, P2, and other experimental systems. *J. Bacteriol.* **2004**, 186:595-600. doi: 10.1128/jb.186.3.595-600.2004.

(25) Farrow, J. M.; Wells, G.; Pesci, E. C. Desiccation Tolerance in *Acinetobacter baumannii* Is Mediated by the Two-Component Response Regulator BfmR. *PLoS ONE* **2018**, 13 (10), e0205638. https://doi.org/10.1371/journal.pone.0205638.

(26) Kysela, D. T.; Randich, A. M.; Caccamo, P. D.; Brun, Y. V. Diversity Takes Shape: Understanding the Mechanistic and Adaptive Basis of Bacterial Morphology. *PLOS Biology* **2016**, 14 (10), e1002565. https://doi.org/10.1371/journal.pbio.1002565.

(27) Mampallil, D.; Eral, H. B. A Review on Suppression and Utilization of the Coffee-Ring Effect. *Adv Colloid Interface Sci* **2018**, 252, 38–54. https://doi.org/10.1016/j.cis.2017.12.008.

(28) Madigan, M., Martinko, J. & Parker, J. (1997) Brock Biology of Microorganisms (Prentice Hall, Upper Saddle River, NJ).

(29) Nystrom, T. Stationary-Phase Physiology. *Annu. Rev. Microbiol.* **2004**, 58, 161–181. https://doi.org/10.1146/annurev.micro.58.030603.123818.

(30) Navarro Llorens, J. M.; Tormo, A.; Martinez-Garcia, E. Stationary Phase in Gram-Negative Bacteria. *FEMS Microbiol Rev* **2010**, 34 (4), 476–495. https://doi.org/10.1111/j.1574-6976.2010.00213.x.

(31) Wilkinson, J. F.; Duguid, J. P. The Influence of Cultural Conditions on Bacterial Cytology. In International Review of Cytology;
Bourne, G. H., Danielli, J. F., Eds.; *Academic Press*, **1960**; Vol. 9, pp 1–76. https://doi.org/10.1016/S0074-7696(08)62744-8.

(32) Donelli, G.; Matarrese, P.; Fiorentini, C.; Dainelli, B.; Taraborelli, T.; Di Campli, E.; Di Bartolomeo, S.; Cellini, L. The Effect of Oxygen on the Growth and Cell Morphology of *Helicobacter pylori*. FEMS *Microbiol. Lett*. **1998**, 168 (1), 9–15. https://doi.org/10.1111/j.1574-6968.1998.tb13248.x.

(33) Howard, A.; O'Donoghue, M.; Feeney, A.; Sleator, R. D. *Acinetobacter baumannii*. *Virulence* **2012**, 3 (3), 243–250. https://doi.org/10.4161/viru.19700.

(34) Eze, E. C., Chenia, H. Y., & El Zowalaty, M. E. *Acinetobacter baumannii* biofilms: effects of physicochemical factors, virulence, antibiotic resistance determinants, gene regulation, and future antimicrobial treatments. *Infection and drug resistance*, **2018**, 11, 2277–2299. https://doi.org/10.2147/IDR.S169894

(35) Somerville, G. A.; Proctor, R. A. Cultivation Conditions and the Diffusion of Oxygen into Culture Media: The Rationale for the Flask-to-Medium Ratio in Microbiology. *BMC Microbiol* **2013**, 13, 9. https://doi.org/10.1186/1471-2180-13-9.

(36) Chang, W.-S.; van de Mortel, M.; Nielsen, L.; Nino de Guzman, G.; Li, X.; Halverson, L. J. Alginate Production by *Pseudomonas putida* Creates a Hydrated Microenvironment and Contributes to Biofilm Architecture and Stress Tolerance under Water-Limiting Conditions. *J. Bacteriol*. **2007**, 189 (22), 8290–8299. https://doi.org/10.1128/JB.00727-07.

Table of Contents/Abstract Graphic

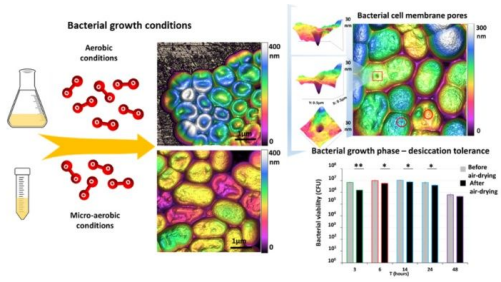

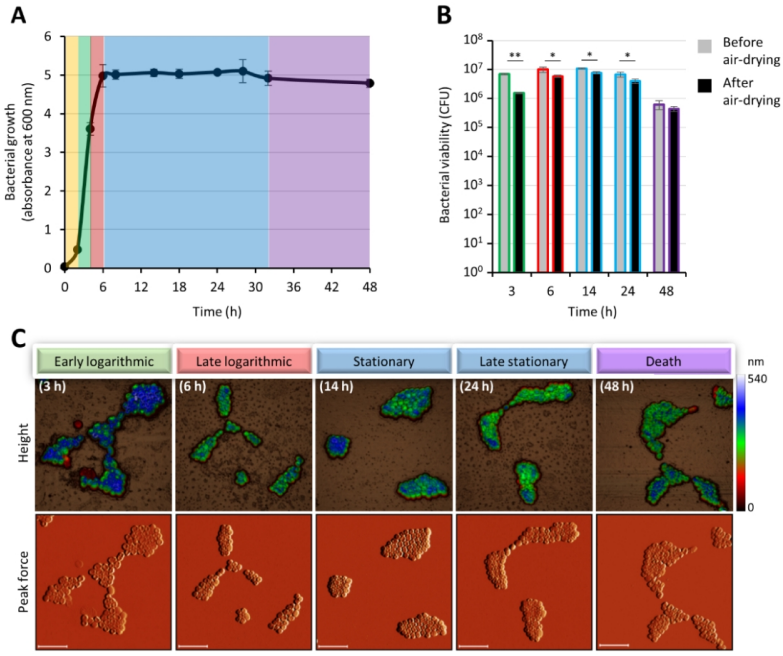

Growth, cell viability, and morphology of A. baumannii ACICU during growth in shaken flasks (SF). (A) Growth plot of A. bau-mannii ACICU cultured in LB at 37°C under vigorous shaking. At the indicated time points, bacterial growth was measured as ab-sorbance at 600 nm (OD600). The colour boxes yellow, green, red, cyan, and violet indicate lag, logarithmic, late logarithmic, station-ary, and death phase, respectively. (B) CFU at different growth phases determined by viable counts on LA plates before and after air-drying. Colours of the histogram bars outline correspond to the growth phases shown in panel A. (C) A. baumannii ACICU cells im-aged with AFM. All images were first-order flattened and set to the same range of height (0-540 nm) to facilitate comparison between conditions. Scale bar: 5 µm. Statistical analysis was performed with the software GraphPad Instat (GraphPad Software, Inc., La Jolla, CA), using One-Way Analysis of Variance (ANOVA). Asterisks indicate statistically significant differences between before and after air-drying conditions (* P <0.05; ** P <0.01).

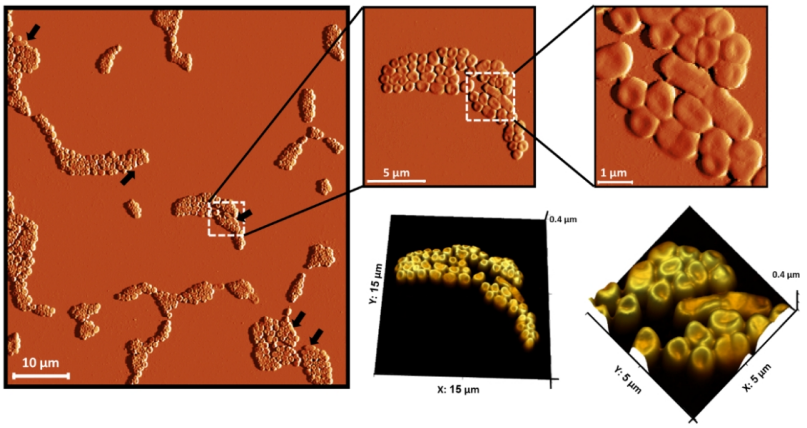

Morphology of A. baumannii ACICU cells. Bacillary and rod shape of A. baumannii ACICU grown for 14 h in flask at 37°C with shaking. Bacterial cells were harvested, washed twice and diluted to OD600=1 in distilled water. An aliquot of 20 µl of the bacterial suspension was deposited on a microscope glass slide and air-dried for 20 minutes at room temperature before imaging with AFM. Black arrows indicate elongated cells. Relative insets of a bacillary-shaped cell and the corresponding 3D projections were shown.

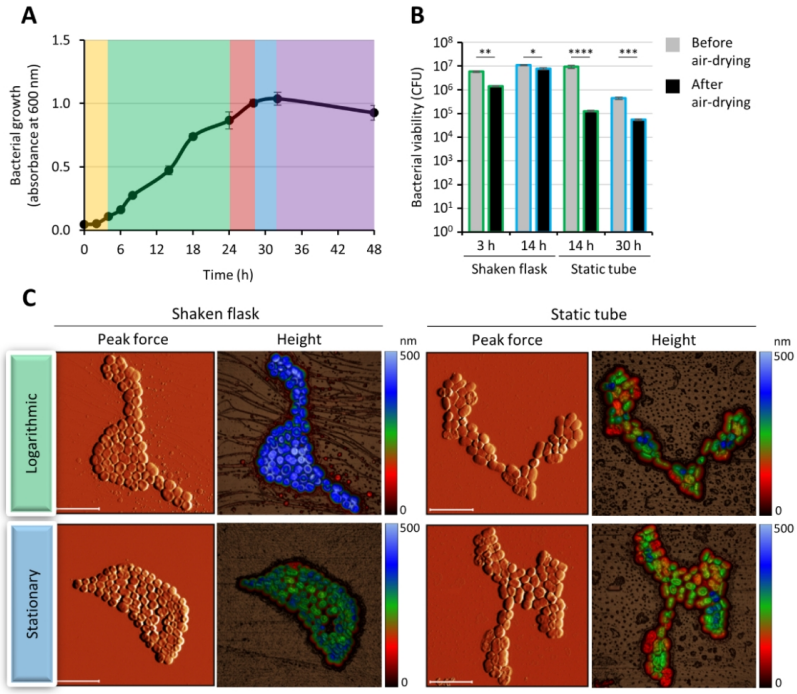

Comparison of growth, cell viability and morphology of A. baumannii ACICU during growth in shaken flasks (SF) and static tube (ST). (A) Growth plot of A. baumannii ACICU cultured in LB at 37°C in static condition. At the indicated time points, bacterial growth was measured as absorbance at 600 nm (OD600). The colour boxes yellow, green, red, cyan, and violet indicate lag, logarith-mic, late logarithmic, stationary, and death phase, respectively. (B) CFU of A. baumannii ACICU grown in shaking and in static con-dition. The CFUs were determined before and after air-drying. Colours of the histogram bars outline correspond to the growth phases shown in panel A. (C) AFM imaging of A. baumannii ACICU grown in static and shaking conditions. All of the images were first-order flattened and set to the same range of height (0-500 nm) to facilitate comparison between conditions. Scale bar: 5 µm. Statistical analysis was performed with the software GraphPad Instat (GraphPad Software, Inc., La Jolla, CA), using One-Way Analysis of Vari-ance (ANOVA). Asterisks indicate statistically significant differences between before and after air-drying conditions (* P <0.05; ** P <0.01; *** P <0.001; **** P <0.0001).

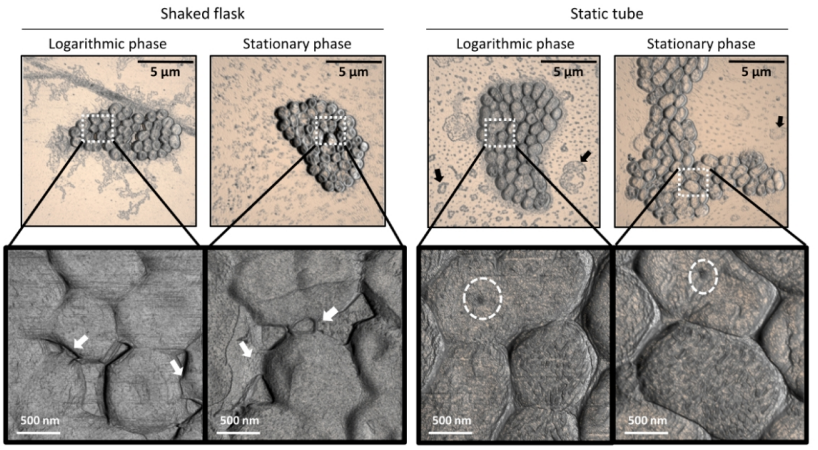

Surface morphology of A. baumannii ACICU cells after growth under static and shaked conditions. A. baumannii ACICU cells were imaged by AFM after desiccation. White and black arrows denote the presence of an exopolysaccharidic layer on the cell surface and the release of DNA, respectively. White dot circles denote membrane pores.

Bibliography

[1] A-hassan, Emad, William F Heinz, Matthew D Antonik, Neill P D Costa, Soni Nageswaran, Cora-ann Schoenenberger, and Jan H Hoh. "Relative Microelastic Mapping of Living Cells by Atomic Force Microscopy." Biophysical Journal 74, no. 3 (1998): 1564–78.

[2] Abramovitch, Daniel Y, Sean B Andersson, Lucy Y Pao, and Georg Schitter. "A Tutorial on the Mechanisms, Dynamics, and Control of Atomic Force Microscopes." Proceedings of the American Control Conference, 2007, 3488–3502.

[3] Adamcik, Jozef, Alexandre Berquand, and Raffaele Mezzenga. "Single-Step Direct Meas-urement of Amyloid Fibrils Stiffness by Peak Force Quantitative Nanomechanical Atom-ic Force Microscopy." Applied Physics Letters 98, no. 19 (2011): 1–4.

[4] Ahmad, Irfan, Nabil Karah, Aftab Nadeem, Sun Nyunt Wai, Bernt Eric, and Uhlin Id. "Analysis of Colony Phase Variation Switch in *Acinetobacter baumannii* Clinical Iso-lates," 2019, 1–13.

[5] Almasaudi, Saad B. "Acinetobacter Spp. as Nosocomial Pathogens: Epidemiology and Resistance Features." Saudi Journal of Biological Sciences 25, no. 3 (2018): 586–96.

[6] Alsteens, David, Vincent Dupres, Sami Yunus, Jean-paul Latge, Ju J Heinisch, and Yves F Dufre. "High-Resolution Imaging of Chemical and Biological Sites on Living Cells Us-ing Peak Force Tapping Atomic Force Microscopy," 2012.

[7] Alsteens, David, Hermann E Gaub, Richard Newton, and Moritz Pfreundschuh. "Atom-ic Force Microscopy-Based Characterization and Design of Biointerfaces." Nature Pub-lishing Group 2 (2017): 1–16.

[8] Alvarez, Hector M, Roxana A Silva, Ana C Cesari, Ana L Zamit, Silvia R Peressutti, Ru-dolf Reichelt, Ulrike Keller, et al. "Physiological and Morphological Responses of the Soil Bacterium Rhodococcus Opacus Strain PD630 to Water Stress." FEMS Microbiol-ogy Ecology 50, no. 2 (2004): 75–86.

[9] Amaya-villar, Rosario, and Ana Dı. "Optimum Treatment Strategies for Carbapenem- Resistant *Acinetobacter baumannii* Bacteremia," 2015.

[10] Anderson, Kimberly L, Ethel E Apolinario, and Kevin R Sowers. "Desiccation as a Long-Term Survival Mechanism for the Archaeon Methanosarcina Barkeri." Applied and Environmental Microbiology 78, no. 5 (2012): 1473–79.

[11] Antunes, C S, Francesco Imperi, Alessandra Carattoli, and Paolo Visca. "Deci-phering the Multifactorial Nature of *Acinetobacter baumannii* Pathogenicity" 6, no. 8 (2011).

[12] Aranda, Jesus, Carlota Bardina, Alejandro Beceiro, Soraya Rumbo, Maria P Ca-bral, Jordi Barbe, and German Bou. "*Acinetobacter baumannii* Reca Protein in Repair of DNA Damage, Antimicrobial Resistance, General Stress Response, and Virulence." Journal of Bacteriology 193, no. 15 (2011): 3740–47.

[13] Koch, A. L., and S. Woeste. 1992. Elasticity of the sacculus of Escherichia coli. J. Bacteriol. 174:4811–4819.

[14] Atrouni, Ahmad Al, Marie Laure Joly-Guillou, Monzer Hamze, and Marie Kempf. "Reservoirs of Non-Baumannii Acinetobacter Species." Frontiers in Microbiolo-gy 7, no. FEB (2016): 1–12.

[15] Auerbach, Ilene D, Cody Sorensen, Helen G Hansma, and Patricia A Holden. "Physical Morphology and Surface Properties of Unsaturated Pseudomonas Putida Bio-films." Journal of Bacteriology 182, no. 13 (2000): 3809–15.

[16] Baidamshina, Diana R, Elena Y Trizna, Marina G Holyavka, Mikhail I Bo-gachev, Valeriy G Artyukhov, Farida S Akhato, Elvira V Rozhina, and Rawil F Fakhrullin. "Targeting Microbial Biofilms Using Ficin , a Nonspecific Plant Protease," no. September 2016 (2017).

[17] Bardina, Carlota, Alejandro Beceiro, Soraya Rumbo, Maria P Cabral, Jordi Barbe, Departament De Gene, Cerdanyola Valle, Hospital Son, Espasesuniversitat De Illes, and Instituto Universitario De. "*Acinetobacter baumannii* RecA Protein in Repair of DNA Damage, Antimicrobial Resistance, General Stress Response, and Virulence" 193, no. 15 (2011): 3740–47.

[18] Bassetti, Matteo, and Elda Righi. "New Antibiotics and Antimicrobial Combina-tion Therapy for the Treatment of Gram-Negative Bacterial Infec-

tions." Current Opinion in Critical Care 21, no. 5 (2015): 402–11.

[19] Berquand, Alexandre, Charles Roduit, Sandor Kasas, Andreas Holloschi, Leslie Ponce, and Mathias Hafner. "Atomic Force Microscopy Imaging of Living Cells." Mi-croscopy Today 18, no. 6 (2010): 8–14.

[20] Beveridge, T J. "Use of the Gram Stain in Microbiology." Biotechnic and Histo-chemistry 76, no. 3 (2001): 111–18. Beveridge, T J, and L L Graham. "Surface Layers of Bacteria." Microbiological Reviews 55, no. 4 (1991): 684–705.

[21] Beveridge, Terry J. "MINIREVIEW Structures of Gram-Negative Cell Walls and Their Derived Membrane Vesicles" 181, no. 16 (1999): 4725–33.

[22] Blair, Kris M, and Nina R Salama. "Staying in Shape: The Impact of Cell Shape on Bacterial Survival in Diverse Environments" 80, no. 1 (2016): 187–203.

[23] Boll, Joseph M, Ashley T Tucker, Dustin R Klein, Alexander M Beltran, Jennifer S Brodbelt, Bryan W Davies, and M Stephen Trent. "Reinforcing Lipid a Acylation on the Cell Surface of *Acinetobacter baumannii* Promotes Cationic Antimicrobial Peptide Resistance and Desiccation Survival." mBio 6, no. 3 (2015): 1–11.

[24] Brown, Geoffrey R, Iain C Sutcliffe, David Bendell, and Stephen P Cummings. "The Modification of the Membrane of Oceanomonas Baumannii When Subjected to Both Osmotic and Organic Solvent Stress." FEMS Microbiology Letters 189, no. 2 (2000): 149–54.

[25] Cabeen, Matthew T, and Christine Jacobs-Wagner. "Bacterial Cell Shape." Na-ture Reviews Microbiology 3, no. 8 (2005): 601–10.

[26] Carvalho, A S, J Silva, P Ho, P Teixeira, F X Malcata, and P Gibbs. "Effect of Various Growth Media upon Survival during Storage of Freeze-Dried Enterococcus Fae-calis and Enterococcus Durans," 2003, 947–52.

[27] Carvalho, Ana S, Joana Silva, Peter Ho, Paula Teixeira, F Xavier Malcata, and Paul Gibbs. "Relevant Factors for the Preparation of Freeze-Dried Lactic Acid Bacteria" 14 (2004): 835–47.

[28] F. Eghiaian, A. Rigato, S. Scheuring, Structural, mechanical, and dynamical vari-ability of the actin cortex in living cells. Biophys. J. 108, 1330–1340 (2015

[29] Chaibenjawong, Plykaeow, and Simon J Foster. "Desiccation Tolerance in Staph-ylococcus Aureus." Archives of Microbiology 193, no. 2 (2011): 125–35.

[30] Chien, An Chun, Norbert S Hill, and Petra Anne Levin. "Cell Size Control in Bacteria." Current Biology 22, no. 9 (2012): R340–R349.

[31] Costa, E, J Usall, N Teixido, N Garcia, and I Vin. “Effect of Protective Agents , Rehydration Media and Initial Cell Concentration on Viability of Pantoea Agglomerans Strain CPA-2 Subjected to Freeze-Drying,” no. Rhodes 1993 (2000): 793–800.

[32] Diancourt, Laure, Virginie Passet, Alexandr Nemec, Lenie Dijkshoorn, and Syl-vain Brisse. “The Population Structure of *Acinetobacter baumannii*: Expanding Multire-sistant Clones from an Ancestral Susceptible Genetic Pool” 5, no. 4 (2010).

[33] Dijkshoorn, Lenie, Alexandr Nemec, and Harald Seifert. "An Increasing Threat in Hospitals: Baumannii" 5, no. december (2007).

[34] Seltmann, Guntram, and Otto Holst. The Bacterial Cell Wall. Berlin: Springer, 2001.

[35] Du, Han, Sumant Puri, Andrew McCall, Hannah L Norris, Thomas Russo, and Mira Edgerton. “Human Salivary Protein Histatin 5 Has Potent Bactericidal Activity against ESKAPE Pathogens.” Frontiers in Cellular and Infection Microbiology 7, no. FEB (2017): 1–12.

[36] Dufrene, Yves F, Toshio Ando, Ricardo Garcia, David Alsteens, David Martinez-martin, Andreas Engel, Christoph Gerber, and Daniel J Muller. “Imaging Modes of Atomic Force Microscopy for Application in Molecular and Cell Biology.” Nature Pub-lishing Group 12, no. 4 (2017): 295–307.

[37] Eaton, Peter, Joao C Fernandes, Eulalia Pereira, Manuela E Pintado, and F Xa-vier Malcata. “Atomic Force Microscopy Study of the Antibacterial Effects of Chitosans on Escherichia Coli and Staphylococcus Aureus.” Ultramicroscopy 108, no. 10 (2008): 1128–34.

[38] Eghiaian, Frederic, Felix Rico, Adai Colom, Ignacio Casuso, and Simon Scheu-ring. “High-Speed Atomic Force Microscopy: Imaging and Force Spectroscopy” 588 (2014): 3631–38.

[39] Environments, Diverse. “Diverse Environments.” Ieee Software 80, no. August (2000): 187–203.

[40] Espinal, P, S Marti, and J Vila. “Effect of Biofilm Formation on the Survival of *Acinetobacter baumannii* on Dry Surfaces.” Journal of Hospital Infection 80, no. 1 (2012): 56–60.

[41] Farrow, John M, I I I Id, Greg Wells, and Everett C Pesci Id. “Desiccation Tol-erance in *Acinetobacter baumannii* Is Mediated by the Two-Component Response Regu-lator BfmR,” 2018, 1–25.

[42] Feltin, Nicolas, Sebastien Ducourtieux, Loic Crouzier, Alexandra Delvallee, Kai Dirscherl, and Guanghong Zeng. Scanning Probe Microscopy (SPM). Characterization of Nanoparticles: Measurement Processes for Nanoparticles, 2019.

[43] Feng, Lu, R J Roughley, and Les Copeland. "Morphological Changes of Rhizobia in Peat Cultures These Include: Morphological Changes of Rhizobia in Peat Cultures." Applied and Environmental Microbiology 68, no. 3 (2002): 1064–70.

[44] Fishbain, Joel, and Anton Y Peleg. "Treatment of Acinetobacter Infections." Clin-ical Infectious Diseases 51, no. 1 (2010): 79–84.

[45] Flemming, Hans-Curt, Jost Wingender, Ulrich Szewzyk, Peter Steinberg, Scott A Rice, and Staffan Kjelleberg. "Biofilms: An Emergent Form of Bacterial Life." Nature Reviews Microbiology 14, no. 9 (2016): 563–75.

[46] Fournier, P E, H Richet, and R A Weinstein. "The Epidemiology and Control of *Acinetobacter baumannii* in Health Care Facilities." Clinical Infectious Diseases 42, no. 5 (2006): 692–99.

[47] Francey, Thierry, Frederic Gaschen, Jacques Nicolet, and Andre P Burnens. "The Role of *Acinetobacter baumannii* as a Nosocomial Pathogen for Dogs and Cats in an Intensive Care Unit." Journal of Veterinary Internal Medicine / American College of Veterinary Internal Medicine 14, no. 2 (2000): 177–83.

[48] Frca, Ken Inweregbu, and Alison Pittard Frca. "Nosocomial Infections." Contin-uing Education in Anaesthesia Critical Care & Pain 5, no. 1 (2005): 14–17.

[49] Garnacho-Montero, Jose, Rosario Amaya-Villar, Carmen Ferrandiz-Millon, Ana Diaz-Martin, Jose Maria Lopez-Sanchez, and Antonio Gutierrez-Pizarraya. "Optimum Treatment Strategies for Carbapenem-Resistant *Acinetobacter baumannii* Bacteremia." Expert Review of Anti-Infective Therapy 13, no. 6 (2015): 769–77.

[50] Gayoso, Carmen M, Jesus Mateos, Jose A Mendez, Patricia Fernandez-Puente, Carlos Rumbo, Maria Tomas, Oskar Martinez De Ilarduya, and German Bou. "Molecu-lar Mechanisms Involved in the Response to Desiccation Stress and Persistence in Aci-netobacter Baumannii." Journal of Proteome Research 13, no. 2 (2014).

[51] Gerber, Christoph, and Hans Peter Lang. "How the Doors to the Nanoworld Were Opened." Nature Nanotechnology 1, no. 1 (2006).

[52] Giamarellou, Helen, Anastasia Antoniadou, and Kyriaki Kanellakopoulou. "Aci-netobacter Baumannii: A Universal Threat to Public Health" 32 (2008): 106–19.

[53] Giannouli, Maria, Luisa C S Antunes, Veronica Marchetti, Maria Triassi, Paolo Visca, and Raffaele Zarrilli. "Virulence-Related Traits of Epidemic Acinetobacter Bau-mannii Strains Belonging to the International Clonal Lineages I-III and to the Emerging Genotypes ST25 and ST78." BMC Infectious Diseases 13, no. 1 (2013)

[54] Gupta, R S. "Protein Phylogenies and Signature Sequences: A Reappraisal of Evolutionary Relationships among Archaebacteria, Eubacteria, and Eukaryotes." Micro-biology and Molecular Biology Reviews: MMBR 62, no. 4 (1998): 1435–91.

[55] Hardij, Julie, Francesca Cecchet, Alexandre Berquand, Damien Gheldof, Chris-tian Chatelain, François Mullier, Bernard Chatelain, and Jean Michel Dogné. "Character-isation of Tissue Factor-Bearing Extracellular Vesicles with AFM: Comparison of Air-Tapping-Mode AFM and Liquid Peak Force AFM." Journal of Extracellular Vesicles 2, no. 1 (2013)

[56] Harding, Christian M, Seth W Hennon, and Mario F Feldman. "Uncovering the Mechanisms of *Acinetobacter baumannii* Virulence." Nature Publishing Group, 2017.

[57] Heu, Celine, Alexandre Berquand, Celine Elie-Caille, and Laurence Nicod. "Glyphosate-Induced Stiffening of HaCaT Keratinocytes, a Peak Force Tapping Study on Living Cells." Journal of Structural Biology 178, no. 1 (2012): 1–7.

[58] Simon J. Foster, Georg E. Fantner, Jamie K. Hobbs, Yves F. Dufrene, Scratching the Surface: Bacterial Cell Envelopes at the Nanoscale Albertus Viljoen, mBio Feb 2020, 11 (1) e03020.

[59] Houang, Elizabeth T S, Raija T Sormunen, Luisau Lai, C Y Chan, and Anthony S Y Leong. "Effect of Desiccation on the Ultrastructural Appearances of *Acinetobacter baumannii* and Acinetobacter Lwoffii." Journal of Clinical Pathology 51, no. 10 (1998): 786–88.

[60] Howard, Aoife, Michael O'Donoghue, Audrey Feeney, and Roy D Sleator. "Aci-netobacter Baumannii An Emerging Opportunistic Pathogen." Virulence 3, no. 3 (2012).

[61] Hu, Jun, Yi Zhang, Haibin Gao, Minqian Li, and Uwe Hartmann. "Artificial DNA Patterns by Mechanical Nanomanipulation," 2002.

[62] Huang, Qiaoyun, Huayong Wu, Peng Cai, Jeremy B Fein, and Wenli Chen. "Atomic Force Microscopy Measurements of Bacterial Adhesion and Biofilm Formation onto Clay-Sized Particles." Nature Publishing Group, no. October (2015).

[63] Iacono, M., L. Villa, D. Fortini, R. Bordoni, F. Imperi, R. J. Bonnal, T.Sicheritz-Ponten, G. De Bellis, P. Visca, A. Cassone, and A. Carattoli. 2008. Whole-genome pyrosequencing of an epidemic multidrug-resistant Acineto-bacter baumannii strain belonging to the European clone II group. Antimicrob. Agents Chemother. 52:2616–2625.

[64] Chapartegui-Gonzalez, I., Lázaro-Díez, M., Bravo, Z.,Navas, J., Icardo, J.M., and Ramos-Vivas, J. (2018) Aci-netobacter baumannii maintains its vir-

ulence after long-time starvation. PLoS One 13: e0201961.

[65] Inweregbu, Ken, Jayshree Dave, and Alison Pittard. "Nosocomial Infections." Continuing Education in Anaesthesia, Critical Care and Pain 5, no. 1 (2005): 14–17.

[66] Jacobs, Anna C, Khalid Sayood, Stephen B Olmsted, Catlyn E Blanchard, Steven Hinrichs, David Russell, Paul M Dunman, and Correspondence Paul M Dunman. "Characterization of the *Acinetobacter baumannii* Growth Phase-Dependent and Serum Responsive Transcriptomes" 64 (2012): 403–12.

[67] James, G A, D R Korber, and D E Caldwell. "Digital Image Analysis of Growth and Starvation Responses of a Surface-Colonizing Acinetobacter Sp ." 177, no. 4 (1995): 907–15.

[68] Janning, Birgit, P H.in t. Veld, S Notermans, and J Krämer. "Resistance of Bac-terial Strains to Dry Conditions: Use of Anhydrous Silica Gel in a Desiccation Model Sys-tem." Journal of Applied Bacteriology 77, no. 3 (1994): 319–24.

[69] Jawad, A, J Heritage, A M Snelling, D M Gascoyne-Binzi, and P M Hawkey. "In-fluence of Relative Humidity and Suspending Menstrua on Survival of Acinetobacter Spp. on Dry Surfaces." Journal of Clinical Microbiology 34, no. 12 (1996): 2881–87.

[70] Jawad, A, H Seifert, A M Snelling, and J Heritage. "Survival of *Acinetobacter baumannii* on Dry Surfaces: Comparison of Outbreak and Sporadic Isolates" 36, no. 7 (1998): 1938–41.

[71] Jones, Stuart E, and Jay T Lennon. "Dormancy Contributes to the Maintenance of Microbial Diversity." Proceedings of the National Academy of Sciences of the United States of America 107, no. 13 (2010): 5881–86.

[72] Justice, Sheryl S, Alistair Harrison, Brian Becknell, and Kevin M Mason. "Bacte-rial Differentiation, Development, and Disease: Mechanisms for Survival." FEMS Mi-crobiology Letters 360, no. 1 (2014): 1–8.

[73] Kirby, Andrew R, A Patrick Gunning, Victor J Morris, and Michael J Ridout. "Observation of the Helical Structure of the Bacterial Polysaccharide Acetan by Atomic Force Microscopy." Biophysical Journal 68, no. 1 (1995): 360–63.

[74] Kleanthous, Colin, and Judith P Armitage. "The Bacterial Cell Envelope." Philo-sophical Transactions of the Royal Society B: Biological Sciences 370, no. 1679 (2015): 1–17.

[75] Koch, A L, and S Woeste. "Elasticity of the Sacculus of Escherichia Coli." Jour-nal of Bacteriology 174, no. 14 (1992): 4811–19.

[76] Kranner, Ilse, and Simona Birtic. "A Modulating Role for Antioxidants in Desic-cation Tolerance." Integrative and Comparative Biology 45, no. 5

(2005)

[77] Kuznetsov YG, McPherson A. 2011. Atomic force microscopy in imaging of vi-ruses and virus-infected cells. Microbiol Mol Biol Rev 75(2):268–285.

[78] Lebre, Pedro H, Pieter De Maayer, and Don A Cowan. "Xerotolerant Bacteria: Surviving through a Dry Spell." Nature Reviews Microbiology 15, no. 5 (2017)

[79] Liu, Shaobin, Keong Ng, Rong Xu, Jun Wei, Ming Tan, and Yuan Chen. "Anti-bacterial Action of Dispersed Single-Walled Carbon Nanotubes on Escherichia Coli and Bacillus Subtilis Investigated by Atomic Force Microscopy," 2010, 2744–50.

[80] Liu, Yuying, Tianzhen Zhang, Yabo Zhou, Jiping Li, Xiaoyu Liang, Nannan Zhou, Jiadi Lv, Jing Xie, Feiran Cheng, and Yiliang Fang. "Visualization of Perforin / Gasdermin / Complement-Formed Pores in Real Cell Membranes Using Atomic Force Microscopy." Cellular & Molecular Immunology, no. August (2018): 1–10.

[81] Gu J, Valdevit A, Chou T-M, Libera M. Substrate effects on cell-envelope defor-mation during early-stageStaphylococcus aureus biofilm formation. Soft Matter 2017; 13:2967–76.

[82] Soon RL, Nation RL, Harper M, Adler B, Boyce JD, Tan CH, Li J,Larson I. 2011. Effect of colistin exposure and growth phase on the surfaceproperties of live Aci-netobacter baumannii cells examined by atomic force microscopy. Int. J. Antimicrob. Agents 38:493–501.

[83] Rittershaus ES, Baek SH, Sassetti CM (2013) The normalcy of dormancy: Common themes in microbial quiescence. Cell Host Microbe 13(6):643–651.

[84] Marchetti, M, G J L Wuite, and W H Roos. "ScienceDirect Atomic Force Mi-croscopy Observation and Characterization of Single Virions and Virus-like Particles by Nano-Indentation." Current Opinion in Virology 18 (2016): 82–88.

[85] Gayoso CM, Mateos J, Mendez JA, Fernandez-Puente P, Rumbo C,Tomas M, Martinez de Ilarduya O, Bou G. 2014. Molecular mechanisms involved in the response to desiccation stress and persistence in *Acinetobacter baumannii*. J Proteome Res 13:460–476.

[86] Medalsy, Izhar, Ulf Hensen, and Daniel J Muller. "Imaging and Quantifying Chemical and Physical Properties of Native Proteins at Molecular Resolution by Force-Volume AFM." Angewandte Chemie - International Edition 50, no. 50 (2011): 12103–8.

[87] Michalopoulos, Argyris, and Matthew E Falagas. "Treatment of Acinetobacter In-fections," 2010, 779–88.

[88] B. Voigtlander, Scanning Probe Microscopy- Atomic Force Microscopy and Scanning Tunneling Microscopy, Springer Berlin Heidelberg, Berlin Heidelberg 2015.

[89] Mitochondria, Did. "Protein Phylogenies and Signature Sequences: A Reappraisal of Evolutionary Relationships among Archaebacteria , Eubacteria , and Eukaryotes" 62, no. 4 (1998): 1435–91.

[90] C.A. Morgan, N. Herman, P.A. White, G. Vesey. Preservation of microorganisms by drying: A review Journal of Microbiological Methods, 66 (2006), pp. 183-193

[91] S. Morita, Roadmap of Scanning Probe Microscopy, Nanoscience and Technol-ogy (Springer, Berlin, 2007), p. 201.

[92] Mortel, Martijn Van De, and Larry J Halverson. "Cell Envelope Components Contributing to Biofilm Growth and Survival of Pseudomonas Putida in Low-Water-Content Habitats." Molecular Microbiology 52, no. 3 (2004): 735–50.

[93] Mortezaei, Narges, Bhupender Singh, Johan Zakrisson, Esther Bullitt, and Mag-nus Andersson. "Article Biomechanical and Structural Features of CS2 Fimbriae of En-terotoxigenic Escherichia Coli." Biophysj 109, no. 1 (2015): 49–56.

[94] Moultrie, Denise, Jeremy Hawker, and Shannon Cole. "Factors Associated with Multidrug-Resistant Acinetobacter Transmission: An Integrative Review of the Litera-ture." AORN Journal 94, no. 1 (2011): 27–36.

[95] Muller DJ, Dufrene YF (2008) Atomic force microscopy as a multifunctional molecular toolbox in nanobiotechnology. Nat Nanotechnol 3:261–269.

[96] Mutlu, Baris R, Katie Hirschey, Lawrence P Wackett, and Alptekin Aksan. "Long-Term Preservation of Silica Gel-Encapsulated Bacterial Biocatalysts by Desicca-tion." Journal of Sol-Gel Science and Technology 74, no. 3 (2015): 823–33.

[97] Nemec, Alexandr, Lenka Krizova, Martina Maixnerova, Tanny J K van der Reijden, Pieter Deschaght, Virginie Passet, Mario Vaneechoutte, Sylvain Brisse, and Le-nie Dijkshoorn. "Genotypic and Phenotypic Characterization of the Acinetobacter Calco-aceticus-*Acinetobacter baumannii* Complex with the Proposal of Acinetobacter Pittii Sp. Nov. (Formerly Acinetobacter Genomic Species 3) and Acinetobacter Nosocomialis Sp. Nov. (Formerly Acinetobacter Genomic Species 13TU)." Research in Microbiology 162, no. 4 (2011): 393–404.

[98] Dijkshoorn L, Nemec A, Seifert H. 2007. An increasing threat in hospitals: mul-tidrug-resistant *Acinetobacter baumannii*. Nat Rev Microbiol 5:939–951.

[99] Neonakis, Ioannis K, Demetrios A Spandidos, and Efthimia Petinaki. "Interna-tional Journal of Antimicrobial Agents Confronting Multidrug-Resistant Acinetobacter Baumannii: A Review." International Journal of Antimicrobial Agents 37, no. 2 (2011): 102–9.

[100] Francey, T., F. Gaschen, J. Nicolet, and A. P. Burnens. 2000. The role of Aci-netobacter baumannii as a nosocomial pathogen for dogs and cats in an intensive care unit. J. Vet. Intern. Med. 14:177–183.

[101] Van Niel, C.B.: The culture, general physiology, morphology, and classification of non-sulfur purple and brown bacteria. Bact. Rev. 8, 1-118 (1944)

[102] Nielsen, Lindsey, Xiaohong Li, and Larry J Halverson. "Cell-Cell and Cell-Surface Interactions Mediated by Cellulose and a Novel Exopolysaccharide Contribute to Pseudomonas Putida Biofilm Formation and Fitness under Water-Limiting Conditions." Environmental Microbiology 13, no. 5 (2011): 1342–56.

[103] Nikaido, H. 1992. Porins and specific channels of bacterial outer membranes. Mol. Microbiol. 6:435–442.

[104] Nocker, Andreas, Priscilla Sossa Fernandez, Roy Montijn, and Frank Schuren. "Effect of Air Drying on Bacterial Viability: A Multiparameter Viability Assessment." Journal of Microbiological Methods 90, no. 2 (2012): 86–95.

[105] Orsinger-Jacobsen, Samantha J, Shenan S Patel, Ernestine M Vellozzi, Phillip Gialanella, Leonardo Nimrichter, Kildare Miranda, and Luis R Martinez. "Use of a Stainless-Steel Washer Platform to Study *Acinetobacter baumannii* Adhesion and Bio-film Formation on Abiotic Surfaces." Microbiology (United Kingdom) 159, no. PART 12 (2013): 2594–2604.

[106] Otter, J A, K Vickery, J T Walker, E deLancey Pulcini, P Stoodley, S D Gold-enberg, J A G Salkeld, J Chewins, S Yezli, and J D Edgeworth. "Surface-Attached Cells, Biofilms and Biocide Susceptibility: Implications for Hospital Cleaning Anddisinfection." Journal of Hospital Infection 89, no. 1 (2015): 16–27.

[107] WongD, NielsenTB, BonomoRA, PantapalangkoorP, LunaB,Spellberg B. 2017. Clinical and pathophysiological overview of Acinetobacter infections: a century of chal-lenges. Clin Microbiol Rev 30:409–447.

[108] Paterson, David L. "The Epidemiological Profile of Infections with Multidrug-Resistant Pseudomonas Aeruginosa and Acinetobacter Species." Clinical Infectious Dis-eases 43, no. Supplement-2 (2006): S43–S48.

[109] Peleg, Anton Y, Harald Seifert, and David L Paterson. "Acinetobacter Bau-mannii: Emergence of a Successful Pathogen" 21, no. 3 (2008): 538–82.

[110] L.S. Dorobantu, M.R. GrayApplication of atomic force microscopy in bacterial research Scanning, 32 (2010), pp. 74-96.

[111] Pillet, Flavien, Louise Chopinet, Cécile Formosa, and Étienne Dague. "Bio-chimica et Biophysica Acta Atomic Force Microscopy and Pharmacology: From Micro-biology to Cancerology." BBA - General Subjects 1840, no. 3 (2014): 1028–50.

[112] Pintado, Manuela E, F Xavier Malcata, C Fernandes, and Peter Eaton. "Ultra-microscopy Atomic Force Microscopy Study of the Antibacterial Effects of Chitosans on Escherichia Coli and Staphylococcus Aureus" 108 (2008): 1128–34.

[113] Pletikapic, Galja, Vera zutic, Ivana Vinković Vrček, and Vesna Svetličić. "Atomic Force Microscopy Characterization of Silver Nanoparticles Interactions with Marine Dia-tom Cells and Extracellular Polymeric Substance." Journal of Molecular Recognition 25, no. 5 (2012): 309–17.

[114] OINDEXTER, 1964. And J. S. Biological properties classification of the Cau-lobacter group. Bacteriol. . Rev. 28:231-295.

[115] P. Eaton, J.C. Fernandes, E. Pereira, M.E. Pintado, F.X. Malcata Atomic force microscopy study of the antibacterial effects of chitosans on Escherichia coli and Staphylococcus aureus Ultramicroscopy, 108 (2008), pp. 1128-1134

[116] Popova, Anastasia, Sergei Ignatov, Evgeniy V Dubrovin, Anastasia V Popova, Sergey V Kraevskiy, and Sergei G Ignatov. "Atomic Force Microscopy Analysis of the *Acinetobacter baumannii* Bacteriophage AP22 Lytic Cycle Atomic Force Microscopy Analysis of the *Acinetobacter baumannii* Bacteriophage AP22 Lytic Cycle," no. October 2012 (2017).

[117] Potts, Malcolm. "Desiccation Tolerance of Prokaryotes." Microbiological Re-views 58, no. 4 (1994): 755–805.

[118] Potts, Malcolm, Stephen M Slaughter, Frank U Hunneke, James F Garst, and Richard F Helm. "Desiccation Tolerance of Prokaryotes: Application of Principles to Human Cells." Integrative and Comparative Biology 45, no. 5 (2005): 800–809.

[119] Raetz, Christian R H, and Chris Whitfield. "Ipopolysaccharide Ndotoxins," 2002, 635–700.biochem.71.110601.135414. "Lipopolysaccharide Endotoxins." Annual Review of Biochemistry 71, no. 1 (2002): 635–700.

[120] Ricci, Claudia, Giulio Melone, Nadia Santo, and Manuela Caprioli. "Morpholog-ical Response of a Bdelloid Rotifer to Desiccation." Journal of Morphology 257, no. 2 (2003): 246–53.

[121] Rice, Louis B. "Federal Funding for the Study of Antimicrobial Resistance in Nosocomial Pathogens: No ESKAPE" 197 (2008): 1079–81.

[122] Rittershaus, Emily, Seung-hun Baek, and Christopher Sassetti. "The Normalcy of Dormancy." Cell Host Microbe 13, no. 6 (2013): 643–51.

[123] Roca, Ignasi, Paula Espinal, Xavier Vila-farrés, and Jordi Vila. "The Acinetobac-ter Baumannii Oxymoron: Commensal Hospital Dweller Turned Pan-Drug-Resistant Menace" 3, no. April (2012): 1–30.

[124] Rodr, Guillermo, Antonio Lama, Ana Jime, Juan Ferna, and Rafael Guille. "Ol-ive Stone an Attractive Source of Bioactive and Valuable Compounds" 99 (2008): 5261–69.

[125] Rodríguez, Guillermo, Antonio Lama, Rocío Rodríguez, Ana Jiménez, Rafael Guillen, and Juan Fernández-Bolaños. "Olive Stone an Attractive Source of Bioactive and Valuable Compounds." Bioresource Technology 99, no. 13 (2008): 5261–69.

[126] Ross, Peter, Raphael Mayer, and Moshe Benziman. "Cellulose Biosynthesis and Function in Bacteria" 55, no. 1 (1991): 35–58.

[127] Santos, Helena, and Milton S Costa. "3Haloarchae.Pdf" 4 (2002): 501–9. "Mini-review Compatible Solutes of Organisms That Live in Hot Saline Environments" 4 (2002): 501–9.

[128] Saun, Tomas J, Alan D Rogers, Jerome A Leis, and Robert Cartotto. "The Use of Intravenous and Inhaled Colistin Therapy during a Burn Center Outbreak of Multidrug-Resistant *Acinetobacter baumannii*." Journal of Burn Care and Research 39, no. 6 (2018): 1029–36.

[129] Saun, Tomas J, Alan D Rogers, F C Plast Surg, Jerome A Leis, and Robert Cartotto. "The Use of Intravenous and Inhaled Colistin Therapy During a Burn Center Outbreak of Multidrug-Resistant *Acinetobacter baumannii*," 2017, 1–8.

[130] Scheuring, Simon. "Manipulating and Imaging Individual Membrane Proteins by AFM Rui Pedro Gon Calves," 2006, 1413–18.

[131] Scheuring, Simon, and Yves F Dufrene. "Atomic Force Microscopy: Probing the Spatial Organization, Interactions and Elasticity of Microbial Cell Envelopes at Molecu-lar Resolution." Molecular Microbiology 75, no. 6 (2010): 1327–36.

[132] "Micro Review Atomic Force Microscopy: Probing the Spatial Organization , In-teractions and Elasticity of Microbial Cell Envelopes at Molecular Resolution" 75, no. February (2010): 1327–36.

[133] Schillers, Hermann, Izhar Medalsy, Shuiqing Hu, Andrea L Slade, and James E Shaw. "PeakForce Tapping Resolves Individual Microvilli on Living Cells," no. Septem-ber 2015 (2016): 95–101.

[134] Scoffoni, Christine, Christine Vuong, Steven Diep, Herve Cochard, and Lawren Sack. "Leaf Shrinkage with Dehydration: Coordination with Hydraulic

Vulnerability and Drought Tolerance." Plant Physiology 164, no. 4 (2014): 1772–88.

[135] Scola, Bernard La, and Didier Raoult. "A *Acinetobacter baumannii* in Human Body Louse." Emerging Infectious Diseases 10, no. 9 (2004): 1671–73.

[136] Silhavy, Thomas J, Daniel Kahne, and Suzanne Walker. "The Bacterial Cell En-velope," 2010, 1–17.

[137] Soon, Rachel L, Roger L Nation, Marina Harper, Ben Adler, John D Boyce, Chun-hong Tan, Jian Li, and Ian Larson. "International Journal of Antimicrobial Agents Effect of Colistin Exposure and Growth Phase on the Surface Properties of Live Acineto-bacter Baumannii Cells Examined by Atomic Force Microscopy" 38 (2011): 493–501.

[138] Soon, Rachel L, Roger L Nation, Patrick G Hartley, Ian Larson, and Jian Li. "Atomic Force Microscopy Investigation of the Morphology and Topography of Colistin-Heteroresistant *Acinetobacter baumannii* Strains as a Function of Growth Phase and in Response to Colistin Treatment" 53, no. 12 (2009): 4979–86.

[139] Stirland, R M, Valerie F Hillier, and M G Steyger. "Analysis of Hospital Bacteri-ological Data." Journal of Clinical Pathology S2-3, no. 1 (1969): 82–86.

[140] Su, Hai-nan, Zhi-hua Chen, Sheng-bo Liu, Li-ping Qiao, Xiu-lan Chen, Hai-lun He, Xian Zhao, Bai-cheng Zhou, and Yu-zhong Zhang. "Characterization of Bacterial Polysaccharide Capsules and Detection in the Presence of Deliquescent Water by Atomic Force Microscopy," 2012, 3476–79.

[141] Surface, Cell. "Pathogenic Acinetobacter: From the Cell Surface to Infinity and Beyond" 198, no. 6 (2016): 880–87.

[142] Sutcliffe, Iain C. "A Phylum Level Perspective on Bacterial Cell Envelope Archi-tecture" 18, no. 10 (2010). "A Phylum Level Perspective on Bacterial Cell Envelope Ar-chitecture." Trends in Microbiology 18, no. 10 (2010): 464–70.

[143] Sutherland, I A N W. "Bacterial Surface Polysaccharides: Structure and Func-tion" 113 (188).

[144] Tang, Yi-wei, Nicole M Ellis, Marlene K Hopkins, Douglas H Smith, Deborah E Dodge, and David H Persing. "Comparison of Phenotypic and Genotypic Techniques for Identification of Unusual Aerobic Pathogenic Gram-Negative Bacilli" 36, no. 12 (1998): 3674–79.

[145] Tech, Virginia. "Desiccation Tolerance of Prokaryotes: Application of Principles to Human Cells 1" 809, no. January (2018): 800–809.

[146] Teeseling, Muriel C F van, Miguel A de Pedro, and Felipe Cava. "Determinants of Bacterial Morphology: From Fundamentals to Possibilities

for Antimicrobial Target-ing." Frontiers in Microbiology 8, no. JUL (2017).

[147] Tomaras, Andrew P, Michael J Flagler, Caleb W Dorsey, Jennifer A Gaddy, and Luis A Actis. "Characterization of a Two-Component Regulatory System from Acineto-bacter Baumannii That Controls Biofilm Formation and Cellular Morphology." Micro-biology 154, no. 11 (2008): 3398–3409.

[148] "Characterization of a Two-Component Regulatory System from *Acinetobacter baumannii* That Controls Biofilm Formation and Cellular Morphology," no. 2008 (2019): 3398–3409.

[149] Touhami, Ahmed, Manfred H Jericho, and Terry J Beveridge. "Atomic Force Microscopy of Cell Growth and Division in Staphylococcus Aureus." Journal of Bacteri-ology 186, no. 11 (2004): 3286–95. https://doi.org/10.1128/JB.186.11.3286-3295.2004. [150] Ulehlova, B. Micro-Organisms. Natural Grasslands, 1992.

[151] Vaneechoutte, M, L A Devriese, L Dijkshoorn, B Lamote, P Deprez, G Verschraegen, and F Haesebrouck. "*Acinetobacter baumannii*-Infected Vascular Cathe-ters Collected from Horses in an Equine Clinic." Journal of Clinical Microbiology 38, no. 11 (2000): 4280–81.

[152] Viljoen, Albertus, Simon J Foster, Georg E Fantner, Jamie K Hobbs, and Yves F Dufrêne. "Scratching the Surface: Bacterial Cell Envelopes at the Nanoscale." mBio 11, no. 1 (2020): 1–12. [153] Wang, Xun, M Stephen Trent, and Bryan W Davies. "Desiccation Tolerance Assays for "*Acinetobacter baumannii*" 1946 (2019): 189–94 . [154] Weber, Brent S, Christian M Harding, and Mario F Feldman. "Pathogenic Aci-netobacter: From the Cell Surface to Infinity and beyond Recommended Citation Patho-genic Acinetobacter: From the Cell Surface to Infinity and Beyond." Journal of Bacteriol-ogy 1986, no. 6 (2016): 880–87.

[155] Weber, David J, William A Rutala, Melissa B Miller, Kirk Huslage, and Emily Sickbert-Bennett. "Role of Hospital Surfaces in the Transmission of Emerging Health Care-Associated Pathogens: Norovirus, Clostridium Difficile, and Acinetobacter Species." American Journal of Infection Control 38, no. 5 SUPPL. (2010): S25–S33.

[156] Wendt, C, B Dietze, E Dietz, and H Ruden. "Survival of Acinetobacter Bau-mannii on Dry Surfaces." J. Clin. Microbiol. 35, no. 6 (1997): 1394–97.

[157] Wolfe, Joe, and Gary Bryant. "Article ID Cryo." Cryobiology 39 (1999): 103–29 "Freezing, Drying , and / or Vitrification of Membrane – Solute – Water Systems" 129 (1999): 103–29. [158] Xu, Ke, Weihang Sun, Yongjian Shao, Fanan Wei, Xiaoxian Zhang, Wei Wang, and Peng Li. "Recent Development of PeakForce Tapping Mode Atomic Force Microscopy and Its Applications on Nanoscience" 7, no. 6 (2018): 605–21.

[159] Yang, Chin-hao, Yi-cheng Chen, Shih-yi Peng, Andy Po-yi Tsai, and Tony Jer-fu Lee. "An Engineered Arginine-Rich α -Helical Antimicrobial Peptide Exhibits Broad-Spectrum Bactericidal Activity against Pathogenic Bacteria and Reduces Bacterial Infec-tions in Mice." Scientific Reports, no. April (2018): 1–14.

[160] Young, Kevin D. "Bacterial Morphology: Why Have Different Shapes?" 10, no. 6 (2008): 596–600. "The Selective Value of Bacterial Shape" 70, no. 3 (2006): 660–703.

[161] Zarrilli, Raffaele, Maria Giannouli, Federica Tomasone, and Maria Triassi. "Re-view Article Carbapenem Resistance in "*Acinetobacter baumannii*: The Molecular Epi-demic Features of an Emerging Problem in Health Care Facilities,"

[162] Zarrilli, Raffaele, Maria Giannouli, Federica Tomasone, Maria Triassi, and Ath-anassios Tsakris. "Carbapenem Resistance in "*Acinetobacter baumannii*: The Molecular Epidemic Features of an Emerging Problem in Health Care Facilities." Journal of Infec-tion in Developing Countries 3, no. 5 (2009): 335–41.

[163] Zeidler, Sabine, and Volker Muller. "The Role of Compatible Solutes in Desicca-tion Resistance of "*Acinetobacter baumannii*," no. August (2018).

[164] Zeng, Guanghong, Brian S Vad, Morten S Dueholm, Gunna Christiansen, Mar-tin Nilsson, Tim Tolker-nielsen, Per H Nielsen, and Rikke L Meyer. "Functional Bacte-rial Amyloid Increases Pseudomonas Biofilm Hydrophobicity and Stiffness" 6, no. Oc-tober (2015): 1–14.